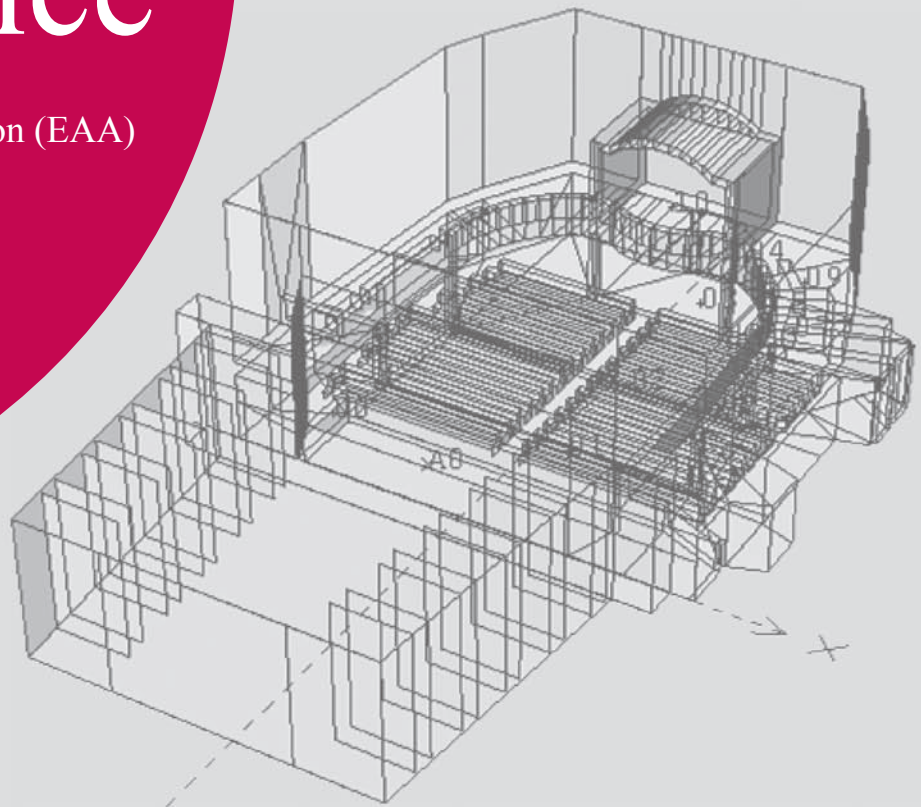


Acoustics in Practice

International e-Journal of the
European Acoustics Association (EAA)

Vol. 2 • No. 2 • December 2014





Acoustics in Practice®

International e-Journal of the
European Acoustics Association (EAA)

Vol. 2 • No. 2 • December 2014

SUMMARY

P. 3

Letter from the Editor

P. 5

**Models to predict the railway vibrations:
preliminary results and comparison
with experimental measurements**

Salvatore Curcuruto, Delio Atzori, Rinaldo Betti, Giuseppe Marsico
and Enrico Mazzocchi, Ernesto Monaco, Francesco Amoroso and
Vincenzo Limone, Giuseppe Loprencipe

P. 13

**Comparison of Two Baroque Theatres
from Acoustical Point of View**

Monika Rychtáriková, Jana Dolejší, Gerrit Vermeir,
Jan Dolejší, Ladislav Pouzar

P. 21

**Acoustic sound insulation measurements
for the direct and flanking transmission
of typical swiss timber constructions**

Amabel Melián Hernández, Christoph Geyer,
Andreas Müller, Ali Sanavi

P. 29

**Localization Experiments with two Different
Configurations in an Artificial Water Depository**

Panagiotis Papadakis I., George Piperakis S.

P. 37

**Defining the Acoustic Environment
of (semi-)open Plan Offices**

Sara Vellenga-Persoon, ir. Theodoor Höngens

P. 43

**The ballistic wave, from rifle bullet to Apollo
command module**

Jean Varnier and Frédéric Sourgen

editor in chief

Colin English

editorial assistant

Monika Rychtarikova

editing coordinator

Miguel Ausejo

edited by

European Acoustics Association (EAA)

secretary@european-acoustics.net • office@european-acoustics.net

www.euracoustics.org

c/o. Sociedad Española de Acústica (SEA)

Serrano, 144, ES-28006 Madrid, Spain

Legal Deposit: M-21922-2013 • ISSN: 2308-1813

Key title: Acoustics in practice

Abbreviated key title: Acoust. pract.

Printing by DiScript Preimpresión, S. L.



www.euracoustics.org

All rights reserved. Use by third parties of the contents
of this journal without the prior written consent of the
copyright holder may constitute a criminal offence
under intellectual property law.

Letter from the Editor

It is my pleasure to welcome to the fourth edition of Acoustics in Practice. This journal serves the many practitioners members of the European Acoustics Association's member societies who work in the many areas of applied acoustics including consultancy, policy making, regulation and manufacturing. The journal provides web-based platform for authors throughout Europe to disseminate their work.

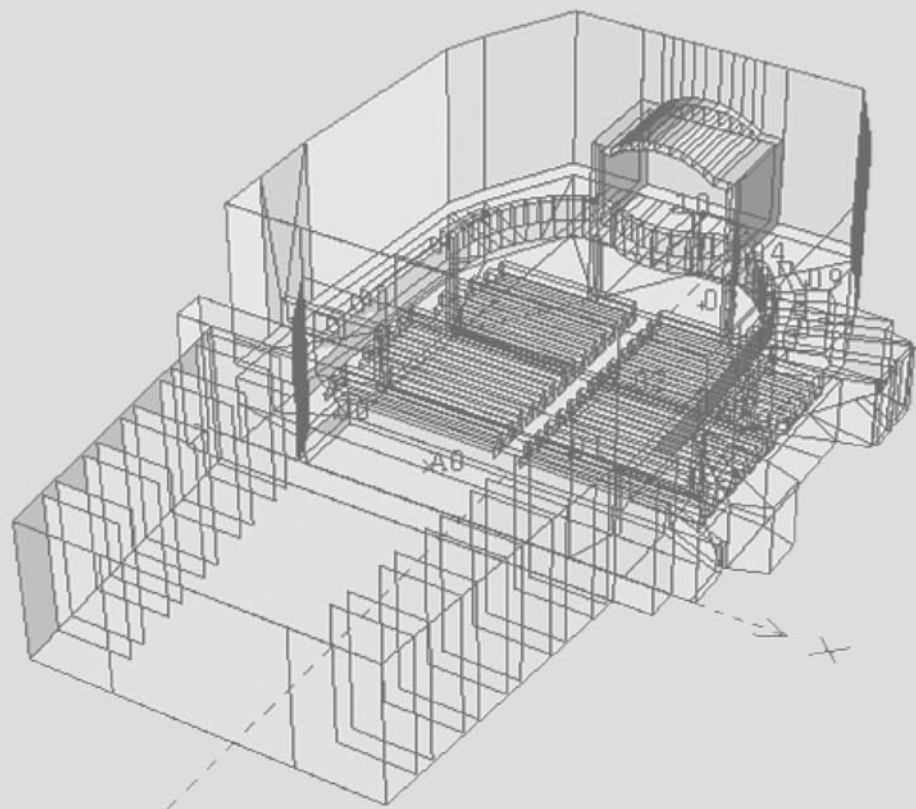
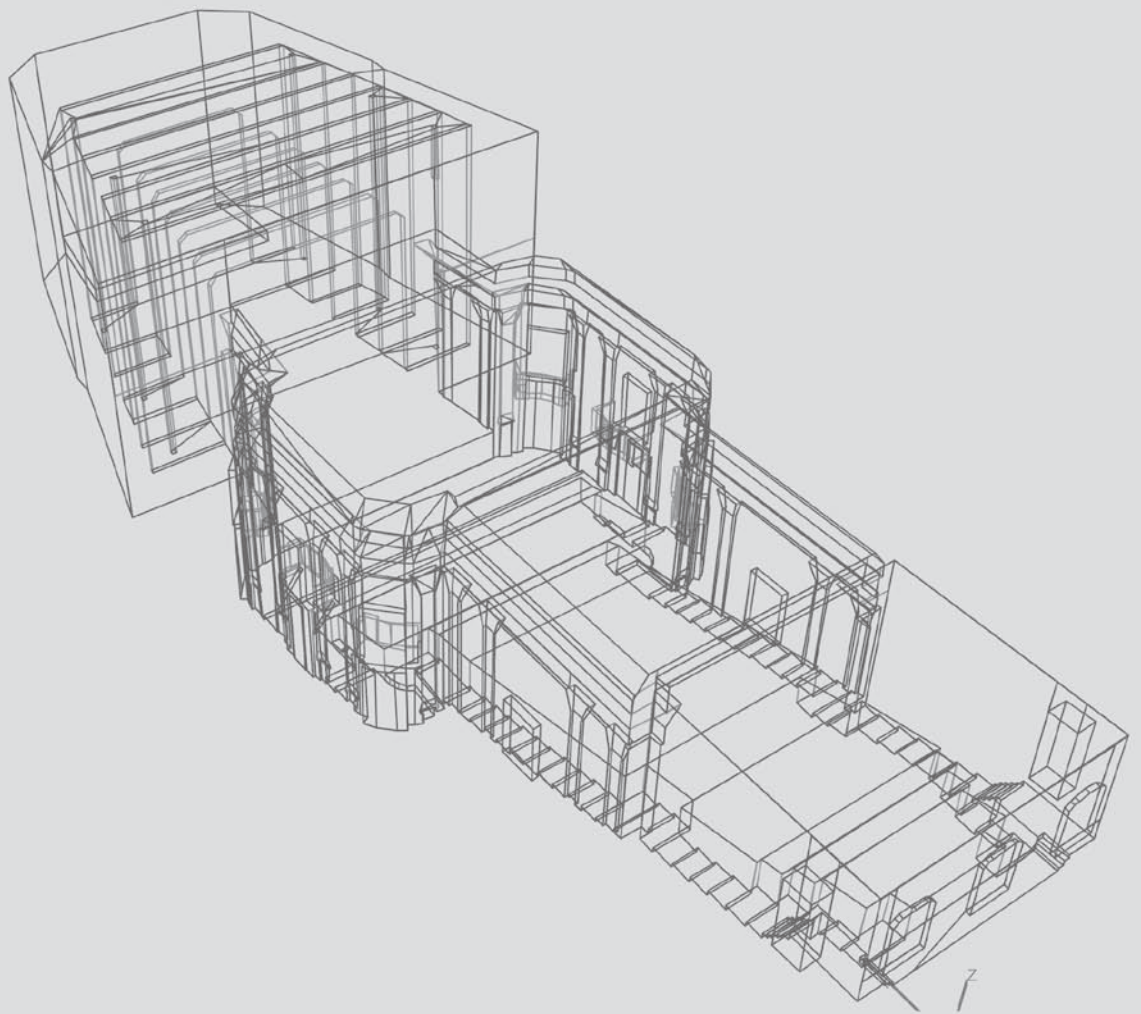
The ambition of the journal is to publish papers on the widest spectrum of topics and to engage members of all societies in the EAA. With four editions now published it is a suitable time to reflect on our progress. Just under half of the papers published are on room and building acoustics, with the remainder covering topics as diverse as noise mapping to musical acoustics, transportation noise to audio acoustics. The authors are drawn from ten European countries, together with a co-author from the USA. An objective for the journal was to publish original work and also provide a permanent web presence for papers presented at local and national conferences and congresses which may otherwise not be readily available to practitioners working in other countries. We have achieved this goal, but I would like to take this opportunity to encourage you to consider publishing your new work in Acoustics in Practice. If you have recently presented a paper at a local conference, please consider bringing it to a wider readership through our journal.

We recently received confirmation of the Journal's permanent registration of our International Standard Serial Number which is ISSN 2308-1813 and the journal's official abbreviation is Acoust. pract. for referencing purposes.

The editorial board can be found in this issue immediately after the technical papers. Offers from anyone wishing to join the editorial board would be most welcome. We would like the board to cover all areas of acoustics, but also represent as many as possible of the EAA member societies.



Colin English
(AiP Editor in Chief)



Models to predict the railway vibrations: preliminary results and comparison with experimental measurements

Salvatore Curcuruto, Delio Atzori, Rinaldo Betti, Giuseppe Marsico and Enrico Mazzocchi

ISPRA – Italian Institute for Environmental Protection and Research, Italy

Ernesto Monaco, Francesco Amoroso and Vincenzo Limone

Sonora S.r.l., Italy

Giuseppe Loprencipe

DICEA – Dept. of Civil, Building and Environmental Engineering, Sapienza University of Rome, Italy

Corresponding author: salvatore.curcuruto@isprambiente.it

PACS: 43.40.-r

ABSTRACT

In recent years, the topic of vibrations in homes and workplaces has grown in importance. In order to reduce the vibrations due to road and rail traffic, several actions can be implemented, some of which are economically very expensive. As a consequence, before implementing any mitigation measures, the availability of appropriate simulation tools able to characterize the effectiveness of the chosen solutions becomes more and more relevant. As part of this work, the development of a predictive software has been addressed, combined with experimental measurements, in order to assess with acceptable accuracy the vibration levels caused by low speed rail transport.

Predictions are obtained by characterizing waves propagation through the ground.

1. INTRODUCTION

Recently, the problem of vibrations induced into homes and workplaces has achieved a relevant importance, related to the various types of buildings —varying greatly by moving from city centres to new residential neighbourhoods of the cities— and also because of the increase of vibratory sources that has provided more sensitivity to this environmental component. As a consequence, more frequently than in the past, the assessment of the impact due to vibrations is carried out.

In order to reduce the vibrations induced by road and rail traffic and mitigations costs, it is very important to make a previsional study for vibration levels assessment at the receivers. Nevertheless, to correctly determine the vibration levels, it is necessary to study the dynamic characteristics of sources —spectral content, levels of excitation, energy etc.—, as well as the waves propagation. That is a considerably complex matter, since characteristics and geological structure of a soil can be difficult to determine.

The implementation of calculation methods has been addressed, in order to predict the vibration levels induced by rail transport systems. The aim of this work is to develop a software tool based on predictive models from the scientific literature of recent years that —combined with accurate measurement techniques and characterization of the vibrational waves in the soil under consideration— can allow end-users and infrastructure designers to assess the vibration impact in a with a sufficient accuracy. In this paper we present also the results achieved and the future potential of this activity.

2. EXPERIMENTAL MEASUREMENTS

2.1. Simplified attenuation model

The transit of trains generates both body waves (compression and shear) and surface waves (Rayleigh and Love), to a different extensions in relation to the type of infrastructure. In particular, the equation used to calculate the attenuation of vibrations, expressed in dB, along their propagation path is:

$$L = 20\log\left[10^{\frac{L_c}{20}} + 10^{\frac{L_t}{20}} + 10^{\frac{L_s}{20}}\right] \quad (1)$$

where L_c , L_t , L_s —respectively the levels in dB transmitted through compression, shear and surface waves— are given by the following relations:

$$L_c = L_0 + 20\log(\beta_c) - k_c \log\left(\frac{R}{R_0}\right) - \alpha_c(R - R_0)\frac{f}{V_c} \quad (1.a)$$

$$L_t = L_0 + 20\log(\beta_t) - k_t \log\left(\frac{R}{R_0}\right) - \alpha_t(R - R_0)\frac{f}{V_t} \quad (1.b)$$

$$L_s = L_0 + 20\log(\beta_s) - k_s \log\left(\frac{R}{R_0}\right) - \alpha_s(R - R_0)\frac{f}{V_s} \quad (1.c)$$

in which:

- L_0 , L : vibration levels in dB respectively at the source and at the receiver;
- R : distance of receiver from the line axis;
- R_0 : distance of source from the line axis (reference point);
- V_c : speed of compression waves;
- V_t : speed of shear waves;
- V_s : speed of surface waves,
- α : attenuation factor;
- β : factors taking into account of the relative importance among the different kinds of wave propagations into the soil;
- k : geometric attenuation coefficient;
- c , t , s : indexes referred respectively to compression, shear and surface waves.

Values of the above mentioned ground factors are available in the literature [4,5]. Furthermore, it can be noted that the simplified model, described by Eq. (1), implements a kind of attenuation as following:

$$L = a(R - R_0)f + b\log\frac{R}{R_0} \quad (2)$$

where f is the central frequency band.

2.2 Vibrations induced by tramways: attenuation factor independent of frequency

Experimental measurements have been carried out aimed at characterization of the vibration source as well as at validation and verification of the propagation model in the soil. Actually, the measurement positions have been chosen either in the vicinity of the source and in a point located at a given distance; the simultaneously acquisition of accelerations at the two points allows to assess the reduction trend of vibration as a function of frequency and distance. The choice of

such two points is due to a right balance between the available space in the urban area indentified for the measurements and the need of a measurement significance.

Attention has been drawn to vibrations induced by urban railway lines (tramways), having a flat configuration, considered as low-speed trains. They represent an important source, crossing the historic centres of cities where the sensitivity to vibrations —for both inhabitants and buildings— can be very relevant, as the architectural heritage should be preserved and monitored.

Below an analysis is reported about the vibration levels measured in the city of Rome on a tramway line advised as critical by Municipality. The data analysis has been divided into the following steps:

- 1) Events detecting from the time-history
- 2) Application of a 1/3-octave band filter to the signal acquired along the three measurement axes
- 3) Calculating the acceleration levels for each frequency band and for each axis
- 4) Calculating the overall acceleration values (provided by the contribution of the three components along the 3 axes) for each frequency band.

The identification of the events has been performed only along the vertical direction to the line linking the measurement point to the source. The beginning and the end of an event have been established by evaluating the difference from the maximum peak; points 2, 3 and 4 have been performed for both the measuring positions. The final result of the analysis consists of determining the spectrum in amplitude for the acceleration vector, at source and receiver, for each event.

The measurement point at the source was placed at about 0.7 m from the outer rail of the line (i.e. 1.4 m from the line axis), while the point at the receiver was fixed at 7.15 m from the point source, at 8.55 m from line axis.

The different events identified (Figure 1) have acceleration levels as a function of frequency in a range of a few dB, and only some events have a deviation from the average value of about ± 5 dB. This trend is the same for all the events and at the receiver point they are very close to the average value.

From both the average spectra at the source and at the receiver, it is possible to determine the attenuation in the frequency domain.

There are semi-empirical models in the literature [1,2,3,4] used in the determination of vibration levels caused by rail transport. According to this approach, the vibrational

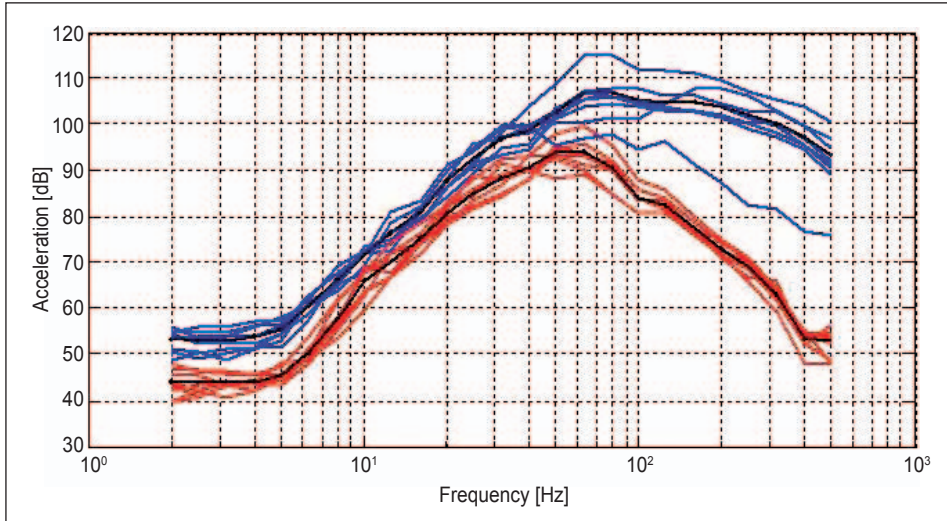


Figure 1. Acceleration amplitude at the source (blue) and at the receiver (red) for all events – in black the average value of the acceleration amplitude.

annoyance at the receivers, evaluated in the frequency domain, depends on the different kind of wave propagation and attenuation (or amplification) along the transmission path: source of the disturbance, railway infrastructure, type of soil to cross, building’s structural type, physiological sensitivity of the people etc.

It is possible to calculate the curve best-fitting the attenuation in frequency, measured at a given distance. Since the simplified model implements a linear frequency dependence as shown in Eq. (2), a linear interpolation has been used, where $(R - R_0)$ and (R/R_0) are known parameters. This provides an experimental procedure useful to determine the input attenuation parameters of the soil for the simplified model. In this case, Eq. (2) gives this formula:

$$L = 0.125f + 5.09 \tag{3}$$

Figure 2 shows the average attenuation calculated by using the measured data and the best-fitting linear frequency interpolation given by Eq. (3).

Figure 3 reports a comparison between the measured data and those calculated with the software tool developed to implement the simplified model given in Eq. (1). As input data for the tool, the following literature [4,5] values have been assigned:

- Typology of source: linear
- Layout of track: flat
- Distance from the receiver point: 8.5 m
- Typology of soil: clay
- $k_c = 10$
- $k_t = 10$
- $k_s = 0$
- $\beta_c = 0.20$

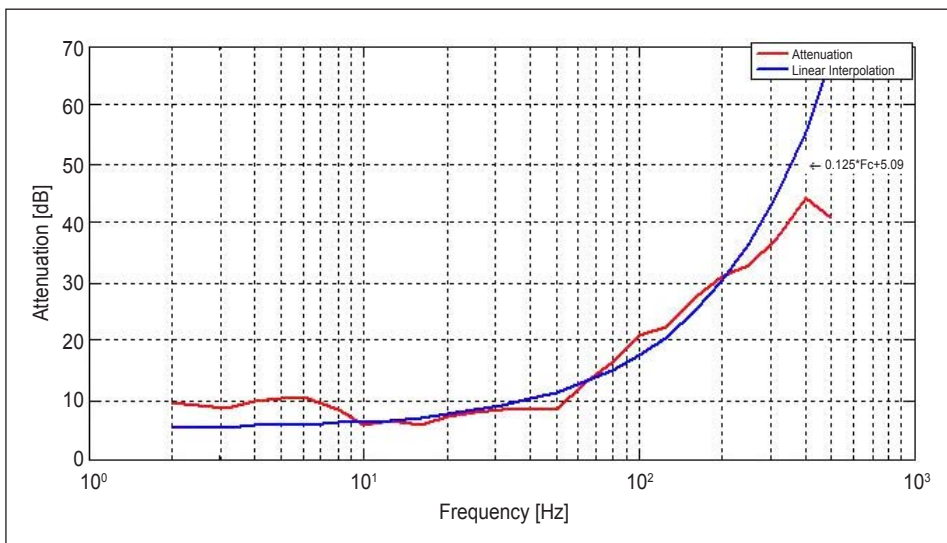


Figure 2. Assessing the attenuation parameters using best-fitting interpolation.

- $\beta_t = 0.20$
- $\beta_s = 0.60$
- $\alpha_c = 3.5 \text{ dB}$
- $\alpha_t = 3.5 \text{ dB}$
- $\alpha_s = 3.5 \text{ dB}$
- $V_c = 700 \text{ m/s}$
- $V_t = 150 \text{ m/s}$
- $V_s = 120 \text{ m/s}$

The superficial waves is the most relevant type up to 80÷100 Hz, because at high frequency the contribution to the attenuation due to the last term of Eq. (1.c) – superficial waves attenuation - becomes significant.

The software tool also implements the possibility to insert a different attenuation – constant, linear, quadratic and cubic vs. frequency. A new linear frequency attenuation, as that of the Eq. (2), has been

chosen by means of a best-fit curve obtained by the data calculated with the simplified model: $R=8.5$, $R_0=1.4$, $a=0.0174$ and $b=6.44$.

Figure 4 shows a comparison between the data measured and those related to the calculations carried out by the software tool, implementing the new linear frequency attenuation. It should be noted the good concordance between measured and calculated values.

Furthermore, it should be pointed out that a and b values thus calculated, though quite different from the those of Eq. (3), leads to a better concordance between measurements and previsions, especially at low frequency, because they allow to reduce the uncertainty related to the mere application of the simplified method.

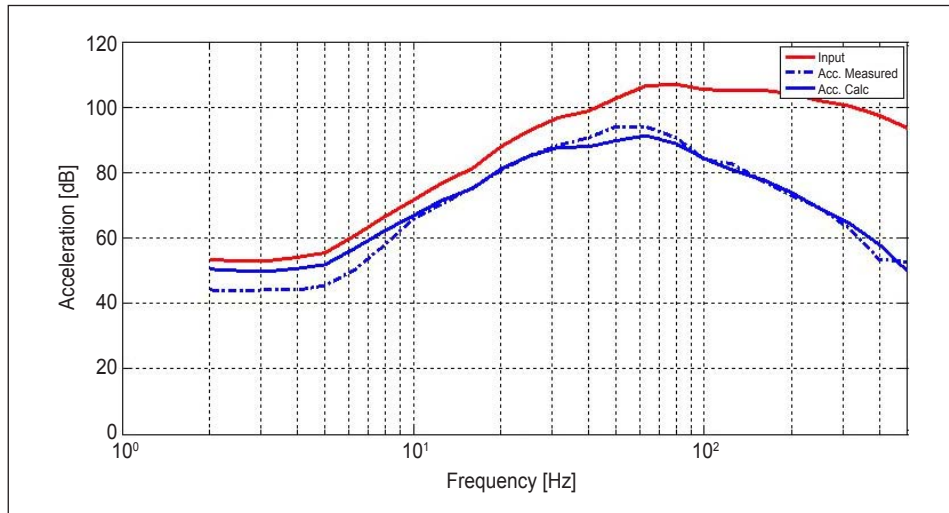


Figure 3. Excitation spectrum and comparison of numerical and experimental acceleration levels at the receiver – using of the simplified model.

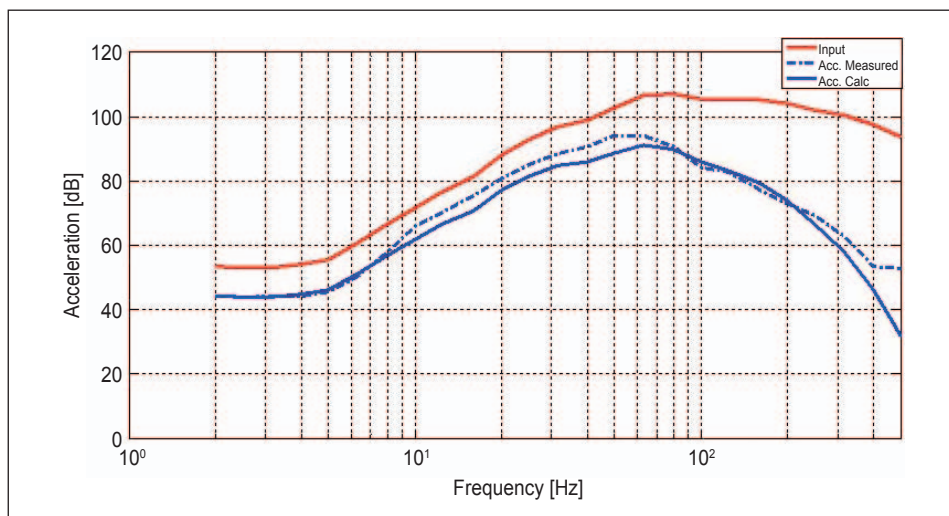


Figure 4. Excitation spectrum and comparison of numerical and experimental acceleration levels at the receiver – attenuation.

Regarding Figures 3 and 4, attenuation can be deduced from acceleration values. In fact, the difference in dB between measured and calculated attenuation is the same of that expressed by the difference between acceleration levels. Furthermore, it is much more interesting to set out the final results provided by the numerical calculation method in terms of acceleration levels instead of attenuation.

2.3. Vibrations induced by a high-speed train running at low-speed: frequency dependent attenuation factor

The second case considered is related to the study of vibration produced by high-speed trains running at low speed (about 50 km/h). Vibration measurements have been carried out close to a flat railway and at a receiver placed at 12 m from the source [8].

The comparison of the spectra obtained from the measurements has allowed to calculate the transfer function representative of the attenuation along the source-receiver path (Figure 5).

In the literature a model for the estimation of vibrations for frequency dependent cases is not available yet. For this reason, the measurement values do not allow to discuss about their dependence on the physical parameters of the ground but should be got as an experimental investigation of vibration levels noticed as high speed train going into urban areas.

The shape of the transfer function obtained suggests to bring back the study to the previous case as discussed for tramways. Two frequency bands have been considered separately, the first ranging from 1 Hz up to 25.4 Hz and second from 32 Hz up to 250 Hz, as shown in Figure 6. For both the frequency bands, a linear curve fit has been found out by calculating a and b parameters of Eq. (2).

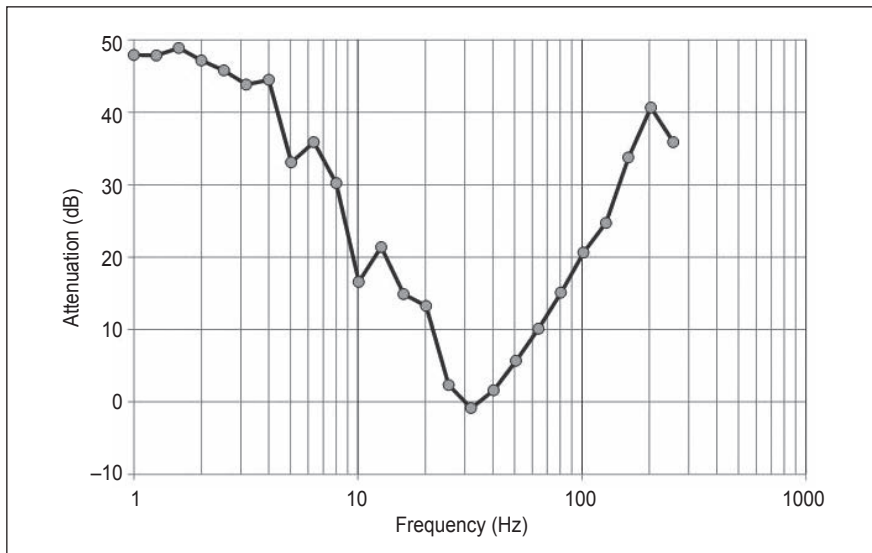


Figure 5. Frequency transfer function.

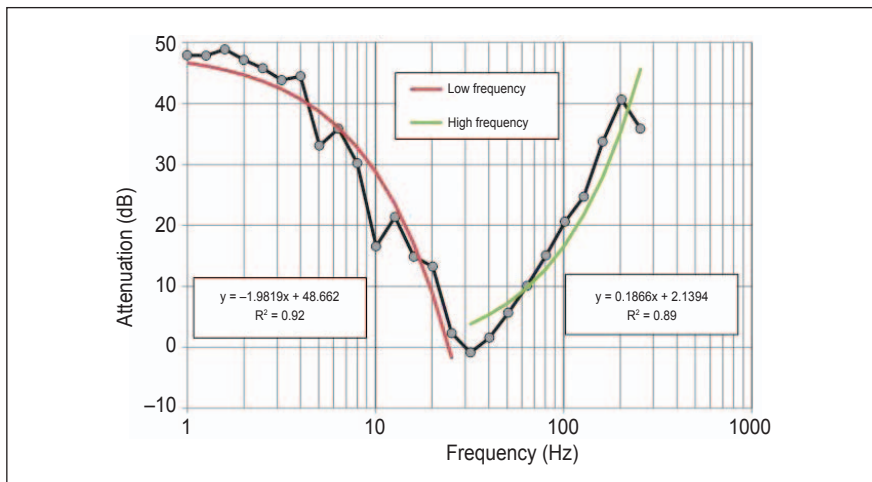


Figure 6. Transfer function for the two separate frequency bands.

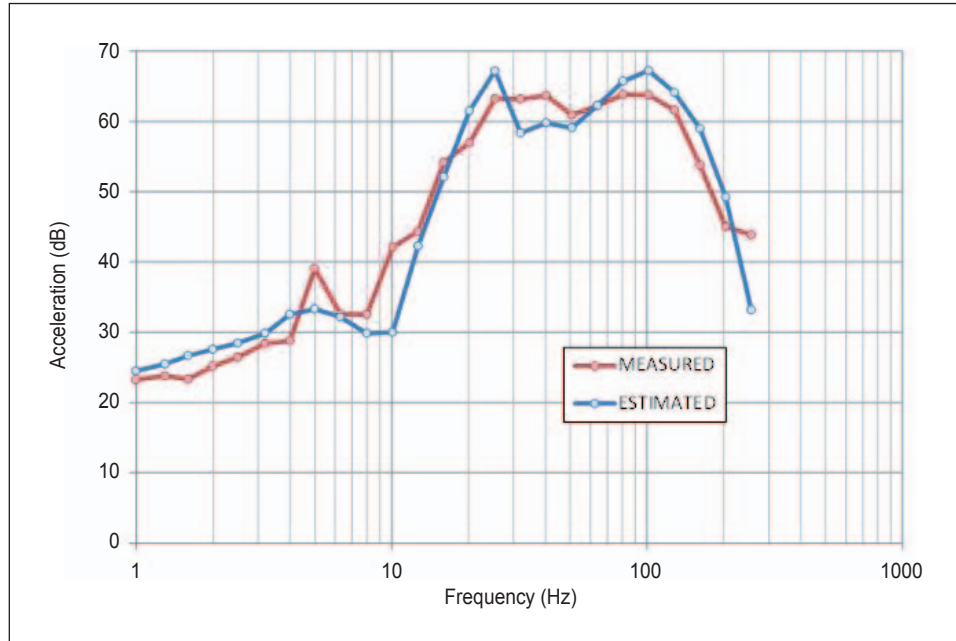


Figure 7. Comparison between estimated (blue) vs measured (red) vibrational level.

Nevertheless, as this procedure aims to fit the curve in Figure 5, the a and b values calculated vary between the two frequency bands. Finally, it should be noticed that the vibration at the receiver is almost equal to that on the source in the 31.5 Hz frequency band, because of a ground resonance phenomenon.

Figure 7 shows the comparison between the measured data and those calculated with the soft-ware tool applied for the two ranges of frequencies.

The curves are quite close to each other and this seems to confirm the overall reliability of the model, but the model cannot explain other effects that depend on particular situations (track parametric excitation, rail corrugation, rolling stock characteristics, etc.). For example, in this case the peak in the measured acceleration at 5 Hz was not detected by the model committing an error in the estimation of more than 5 dB.

3. CONCLUSIONS AND FUTURE DEVELOPMENTS

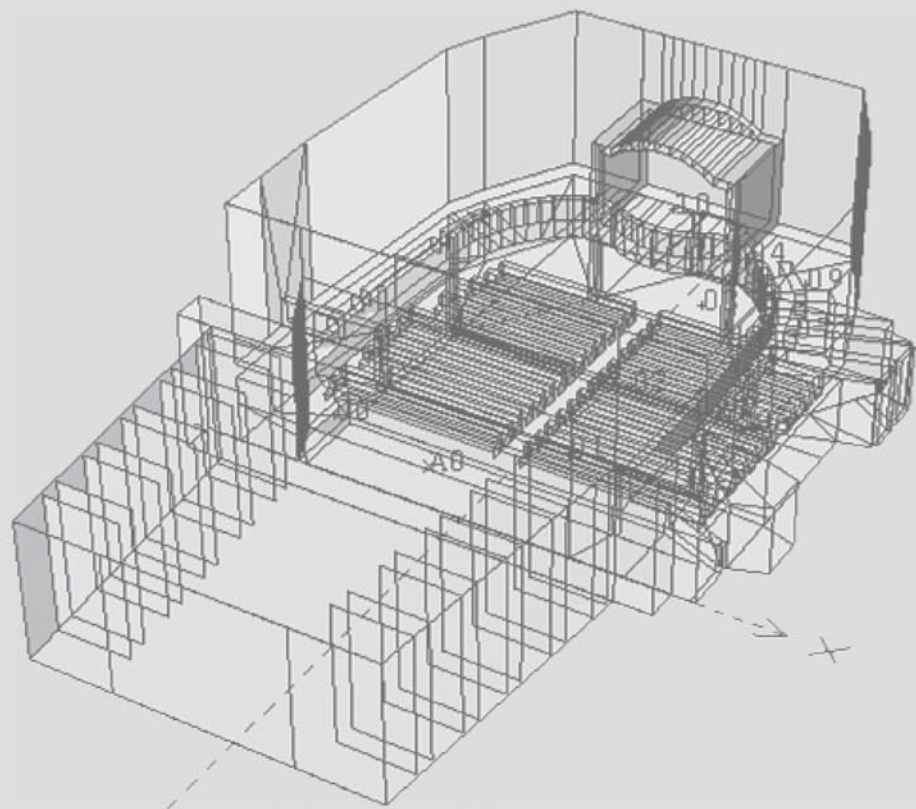
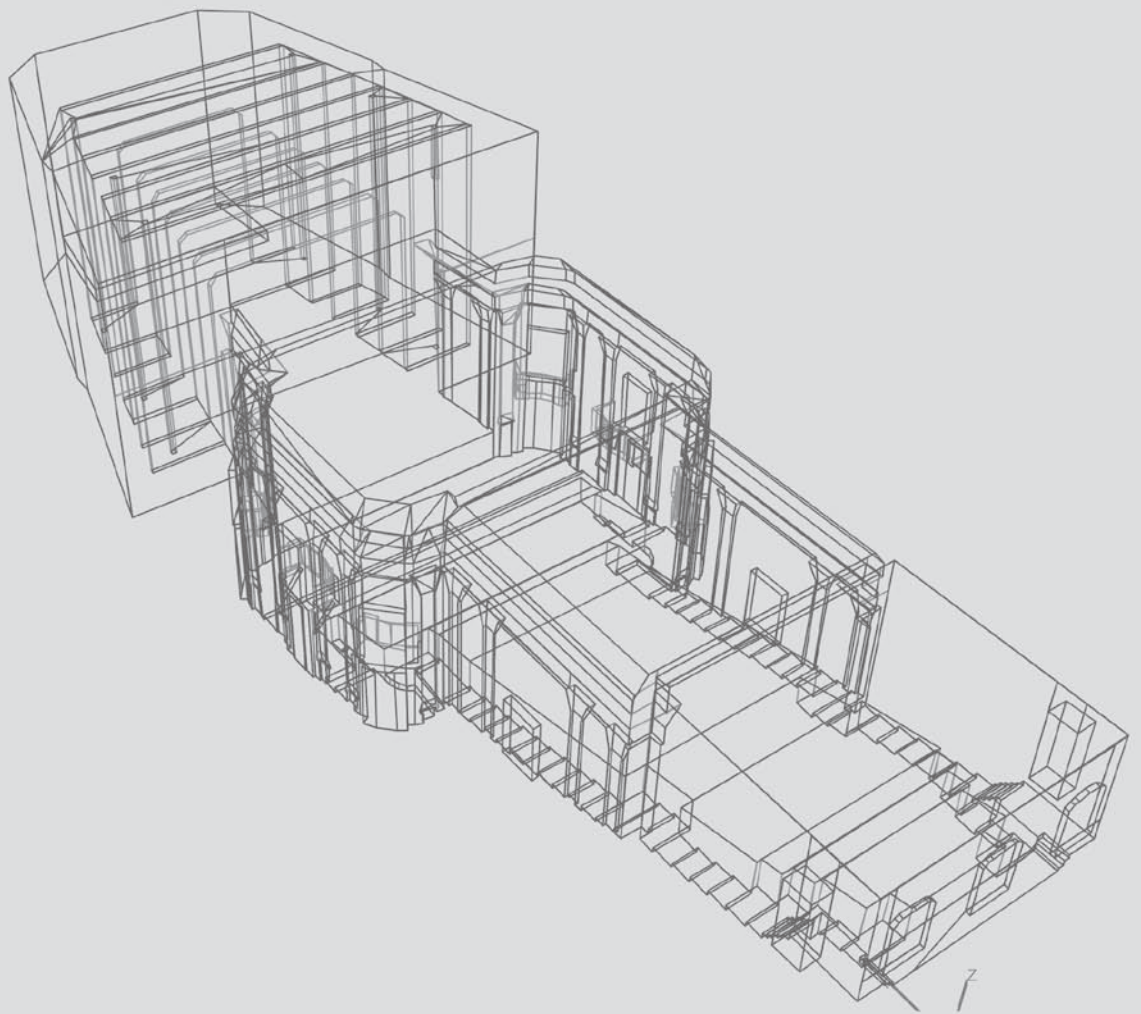
From the measurements made and the numerical comparison-experimental it is possible to conclude that, regarding to the simplified model used for the prediction of the vibrational levels relative to low-speed sources, frequency attenuation can be considered validated. Actually, the value of the coefficient to be calculated experimentally in the examined cases allows the calculation of the level at the receiver in a manner known fairly accurate and based on the average spectrum of the vibration levels to the source.

Regarding to high-speed trains, the phenomenology is completely different to the previous case, resulting very complex as reported in the literature [7,9].

REFERENCES

- [1] C.M. Harris, *Shock and Vibration Handbook*, McGraw Hill (1988).
- [2] H.J. Saurenman, J.T. Nelson, G.P. Wilson, *Handbook of urban rail noise and vibration control*, U.S. Department of Transportation, Washington D.C. (1982).
- [3] H. Miller, *Transit Noise and Vibration. Impact assessment*, U.S. Department of Transportation, Washington D.C. (1995).
- [4] P. Pezzoli, *Le vibrazioni indotte dal traffico su rotaia e tecniche di previsione*, Estratto, Ingegneria Ferroviaria n°. IF – VI – 2004, pp. 521 ÷ 545, Rome, Italy (2004).
- [5] CEB n. 209, *Vibration problems in structures – Practical guidelines*, Losanne, Switzerland (1991)
- [6] H. Xia, Y.M. Cao, G. DeRoock, *Theoretical modelling and characteristic analysis of moving-train induced ground vibrations*, Journal of Sound and Vibration 329, pp. 819–832 (2010).
- [7] V.V. Krylov, “Vibrational impact of high-speed trains. I. Effect of track dynamics”, J. Acoust. Soc. Am. 100 (5), (1996).
- [8] A. D’Andrea, G. Loprencipe, E. Xhixha, “Vibration induced by rail traffic: evaluation of attenuation properties in a bituminous sub-ballast layer”. 5th Int. SIIV Congress.

- Procedia: Social & Behavioral Sciences October 29–31, Rome, Italy. (2012).
- [9] G. Marsico, S. Curcuruto, E. Mazzocchi, D. Atzori, R. Betti, E. Monaco, F. Amoroso, V. Limone, G. Loprencipe, F. De Felice, “*Propagation of Vibrations Induced on Track: Implementation of Provisional Models for Low and High Speed Trains and Comparison with Experimental Measurements*”. 19th International Congress on Sound and Vibration. July 8–12, Vilnius, Lithuania (2012).



Comparison of Two Baroque Theatres from Acoustical Point of View

Monika Rychtáriková^{1,3}, Jana Dolejší², Gerrit Vermeir¹, Jan Dolejší², Ladislav Pouzar²

¹ Laboratory of Acoustics, Soft Matter and Biophysics, KU Leuven, Belgium

² Studio D-akustika s.r.o., České Budějovice, Czech Rep.,

⁴ KKPS, STU Bratislava, Bratislava, Slovak Rep.

Corresponding author: monika.rychtarikova@kuleuven.be

PACS: 43.55.-n

ABSTRACT

Two baroque castle theatres, i.e. theatre in the state castle in Český Krumlov (Czechia) and the theatre in the Swedish royal palace in Drottningholm (Sweden) are compared from acoustical point of view. The two places belong to unique historical sites in Europe, which represent valuable examples of theatres with baroque scenes from the late 18th century. Both theatres are preserved with exceptional completeness and authenticity since they have never burned, and were modernized only in relation to their functionality. Measurements and simulations in Odeon software[®] have been performed in both spaces and many similarities have been found, including almost identical values of reverberation time.

Keywords: baroque theatre, architectural and room acoustics, acoustical measurement and computer simulation

1. INTRODUCTION

The beginning of the baroque architectural style date to late 16th century in Italy from where it has been spread to Europe (17th and 18th century). This period must be understood as a time when many methods of expression had to act in harmony and the individual elements had to complement each other to be interconnected to produce an effective unit. During this period many private court theatres have been built. Theatres in general have got some typical features such as refinement of the proscenium stage in detail and orchestra positioned in a pit in front of the stage, below the stage level. The stage floor has been enlarged to accommodate rich scenery, dancing actors and sophisticated equipment. Other typical characteristics lay in strong relations between the architecture, contemporary scene lighting, intensity of contours and colored areas, the illusive paintings of the interior which can be observed only under specific illumination level, perspectives and proportions, room acoustic properties, contemporary musical interpretations and vocal techniques and other elements acting in global harmony.

Music in this context relates to development of musical instruments that has reached the top level for string instruments such as violins, violas or cellos. Contrabass hasn't existed yet and the wind instruments were still changing their shapes and mechanics. Almost all wooden wind instruments existed except of the clarinet. Organs, and few harpsichords, had already at least two keyboards. Baroque music is often characterized by a main melody with a bass line or by different kinds of polyphonic music where composers were often leaving some space for improvisation to an artist, since they often wrote out just a main melody and harmony and musician could chose his own arrangements or ornamental notes. Baroque period has thus touched and interconnected many different fields and presumed that individual elements complement each other to produce an effective unit.

2. HISTORICAL BACKGROUND

2.1. Baroque Theatre in the State Castle in Český Krumlov

The baroque theater in Český Krumlov is a part of the fifth courtyard of the castle situated in the historical town of Český Krumlov that belong to UNESCO's list. Theatre has never burned out and during the last two centuries it hasn't been modernized. In this circumstances

it has been preserved with all its completeness and authenticity. The first construction of the theatre was built in 1680 under the leadership of Johann Kristian, the duke of Eggenberg, since the size of the old theater hall inside the castle has no longer been large enough to accommodate typical amount of invited people.

The main architect of the theatre design is unfortunately not known but information has been kept about the Italian builders Giacomo Antonio de Maggi, Giovanni Maria Spinetti and Giovanni Canevalle. The sixteen scene decorations have been painted by Martin Schaumberger from Salzburg and carpentry work on the roof of the building and construction of the theater machinery have been carried out by Laurentius Khuenmihlner.

The theatre has been renovated in 1762 during the reign of prince Josef I. Adam of Schwarzenberg according to Andrea Altomonte's plans and most of the

works including the construction itself have been finished before 1768. Johann Wetschel and Leo Merkhel from Vienna have painted the fresco artworks around the stage in the auditorium as well as collection of decorations.

During the 17th and 18th centuries more than two thousand librettos for dramas, comedies, operas and ballets were collected in the castle library. In the 19th century theatre became the centre of interest for travelling companies. In the year 1898 the theatre was closed down because of unsafe conditions.

In the beginning of the 20th century theater has been used only occasionally and almost never for social events or broad public. In the year 1947 this property of Schwarzenberg family was taken by state and in 1950 became a property of Czechoslovakian republic. In the second half of twentieth century a concept of



Figure 1. View on a castle in Český Krumlov in 20th century [4].

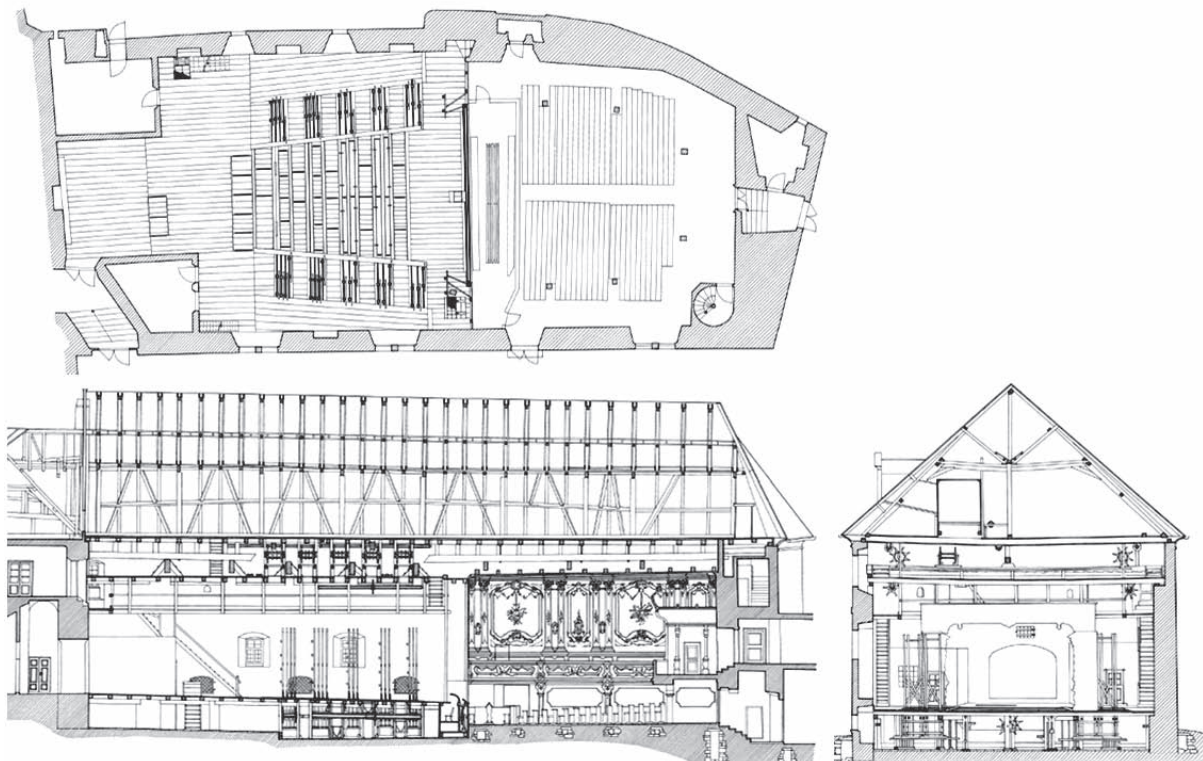


Figure 2. Ground plan and cross-sections of the theatre.

renovation and restoration based on technical and artistic principles became a topic of discussions. Nowadays, the aim of restoration work is to keep maximum authenticity and originality.

In Europe there is only one theatre that is comparable with Český Krumlov, the Baroque Theatre in the Swedish Royal Palace in Drottningholm.

2.2. Baroque Theatre in the Swedish Royal Palace in Drottningholm

Swedish Royal Palace in Drottningholm is situated on Island Lovön very close to Stockholm and is also on UNESCO's World Heritage list. A construction of the palace, that includes also baroque theatre, has started in 17th century under architect Tessin the elder and his son, both pointed by Hedviga Eleonora, the widow of Swedish king Karl X. The palace has been first designed in a French style, but later on queen Lovisa Ulrika let the palace rebuild. In 1762 the theatre has burn out and in 1766 a new baroque theatre has been constructed according to design of the architect Carl Frederik Adelcrantz and is preserved almost unchanged until today. Theatre in Drottningholm achieved great times in the years 1777 - 1792 thanks to the Swedish king Gustav III., who made it a new cultural centre of the country. Performances usually took place during summer time when the royal family moved to royal palace. Similar to other baroque theatres, moving scenery induces the illusion of different places, such as a rural cottage, a wild forest, a city or the Rome ancient

palace. Different devices are placed behind the scenes to evoke the atmosphere of a storm or a strong wind, or other natural phenomena by faithful imitation of sounds.

During the 19th century, the palace was not used and some of the buildings were even damaged and abandoned, since the king Charles XIV John of Sweden has perceived this castle as symbol of the old dynasty. The theatre was reopened in the first half of 20th century thanks to historian Agne Beijer, who made it electrified.

Nowadays, the theatre is used during summer time and performances are given in historical costumes using contemporary stage equipment and technology. Instruments in the orchestra that accompanies the musical performances are copies of period instruments or directly contemporary originals.

3. COMPARISON OF THE THEATRES

Impulse response measurements have been performed in both theatres where omnidirectional sound source was located in the stage and several microphone positions placed in the audience area. Estimation of the reverberation time and other acoustical parameters have followed. Later 3D computer models of the two theatres have been virtually constructed and calibrated according the measurements. Simulated results have been compared with a respect to the spatial distribution of acoustical parameters.

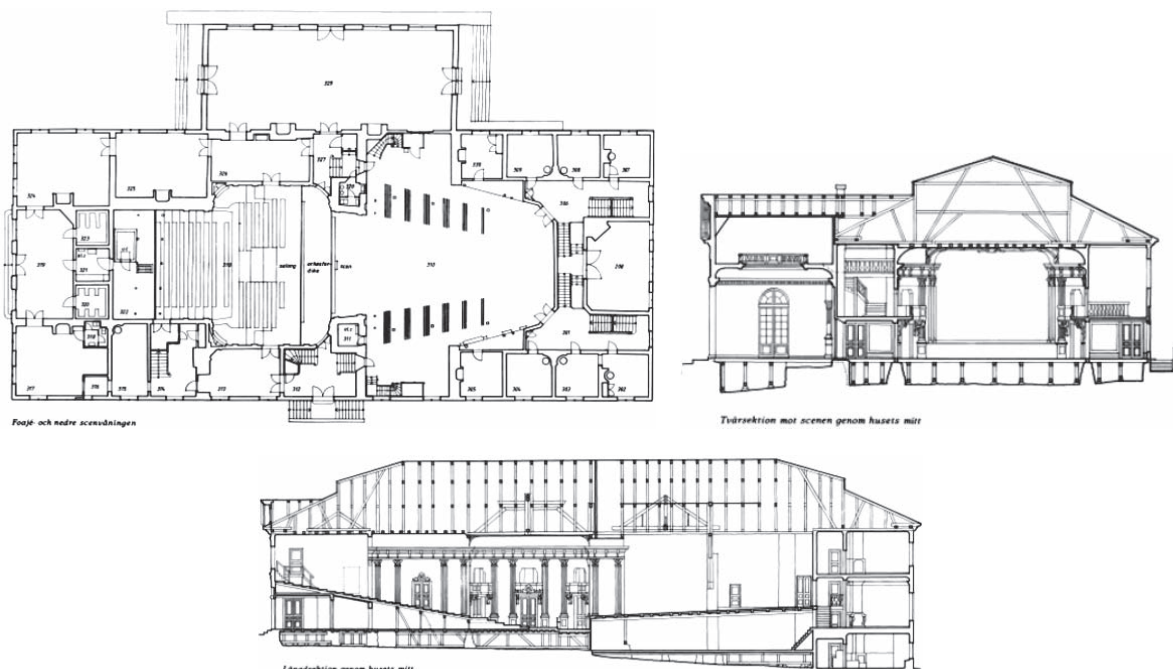


Figure 3. Ground plan of the theatre (left) and its cross section (right).

Theatre in Český Krumlov has a volume of 3200 m³ and Drottningholm around 4000 m³. Figure 4 shows the interior of the two case studies. Illustrations on the walls in both theatres give impression, that walls are finished by 3D ornament surfaces, whereas all the walls are completely smooth and flat. This is very important information when speaking about the acoustics in relation to sound diffusion in the space. In a first look, walls look also rather hard such as plastered surfaces with almost no sound absorption. However, walls in the theatre have acoustically rather interesting structure, since they are constructed as wooden plates hanged on the masonry wall, decorated by paintings directly on wooden surface. Careful investigation of these wooden plates result in a hypothesis that these can work as sound absorbers at low frequencies, since their connection with masonry wall is not completely rigid. As they are slightly “loose” they can act as membranes, which absorb sound.

Seats in Český Krumlov are simple wooden benches on wooden floor, whereas in Drottningholm the seats are slightly upholstered and floor is partially covered by carpet.

In Krumlov, the floor is flat and benches with increasing level form a slope. Theatre also contains balconies on the side and back wall. Swedish theatre has sloped audience area and contains only two small balconies in front that were in the past used by royal family.

3.1. Reverberation time

Measured reverberation time (RT) was calculated as an average from several positions in the theatres and is shown in the figure 5 right. It is interesting that the two evaluated theatres have almost the same values of this parameter. Except of the octave band 125 Hz is the RT almost identical. But RT is not the only parameter that describes the acoustical comfort in the room. The two investigated theatres have rather different geometry. Theatre in Drottningholm is in comparison with Český Krumlov much longer and narrower. The audience area part have in the Swedish theatre ground floor dimensions around 27 x 9-14m (Fig. 3) and in the Czech theatre 19 x 17m (Fig. 2). These differences have almost no influence on RT but might influence other acoustical parameters. As already mentioned, measurements of impulse responses were performed on several positions,



Figure 4. Interior of the theatre in Český Krumlov (left) and Drottningholm (right).

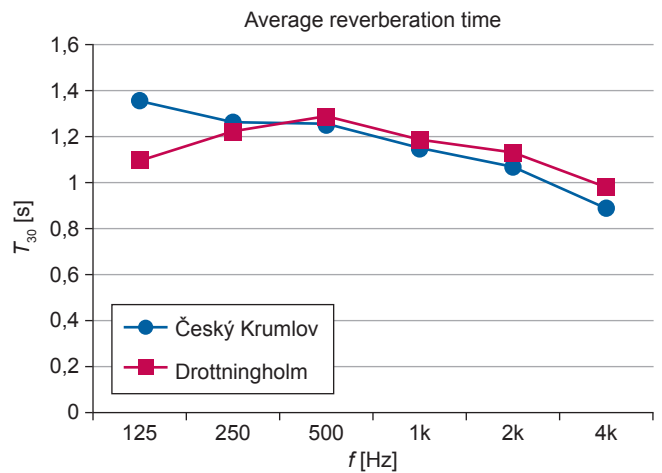


Figure 5. comparison of the reverberation time measured in two theatres (right) and picture from the measurements in situ (left).

however for the better overview of data and distribution of values in audience area, plots from acoustical simulations are more complete.

reverberation time in situ. Several acoustical parameters were calculated from simulation and a few of them have been chosen for comparisons in this paper.

3.2. Simulations

3.2.1. Computer model

Computer 3D models (Figure 6) of the Český Krumlov has been prepared in the software CATT acoustics® v.8.0e and the Drottningholm theatre in the Odeon software® v.9.22 both according to the project documentation, photos and dimensions taken in situ. Absorption properties of model surfaces were in both cases estimated and tuned based on measured

3.2.2. Simulation results

Distribution of the simulated Sound Pressure Level (SPL) at 1 kHz is shown in the Figure 7 left and in the Figure 8. In both cases Sound power level of the omnidirectional point source used in the simulation was 90 dB at 1 kHz. Values in the audience area from the given source placed in the stage of a virtual theatre have reached 65-71 dB in Český Krumlov and 60-70 dB in Drottningholm.

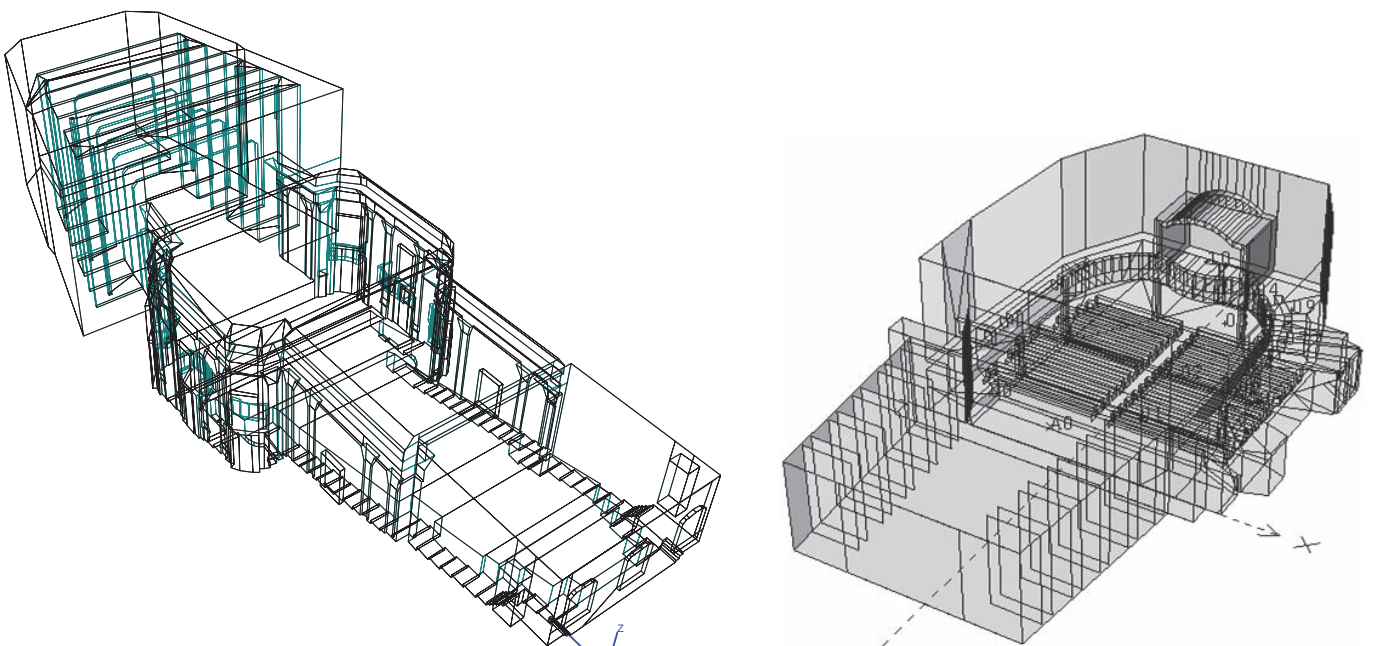


Figure 6. 3D model of Drottningholm theatre (left) and at theatre in Český Krumlov (right).

Clarity is a parameter that is based on the comparison between the early and late sound reflections and expresses how clear is a perceived sound. C_{80} in Český Krumlov has reached values from 2 to 7 dB, whereas in Drottningholm it has been between 0 and 3 dB in audience area. This can be considered a logical result, which can be explained by larger distances between the source and receiver in the Swedish theatre due to its basic shape. Results for both cases are displayed in colored “acoustical maps” in the figure 7 right and figure 9.

Speech intelligibility can be expressed by many different parameters such as Articulation index, Deutlichkeit or Articulation loss of consonants. Speech Transmission Index (STI) that is based on the modulation function calculations is also one of the commonly used quantities that describe speech understanding and it has been chosen for our comparisons too.

Simulated STI values in both case studies have been considered without background noise (BKG noise),

since both theatres have shown its very low values. Results were analyzed in the audience area part and have reached 60-65% in the Czech theatre and 50-60% in Swedish one.

Both theatres, that belong to national heritages of Bohemia and Sweden and are also on UNESCO's World Heritage list, have shown good acoustical properties. Simulation software made it possible to compare these places in more detail and to conclude their acoustical similarities.

4. ACKNOWLEDGMENTS

We would like to express our gratitude to Mr. Pavel Slavko for his kind help on preparation of the information about theatre in Český Krumlov and to Mr. Per Forsström for his kind support during our measurements in the Drottningholm theatre. This work was financed by the foundation of the baroque theatre and a company Studio D-akustika from Czech republic.

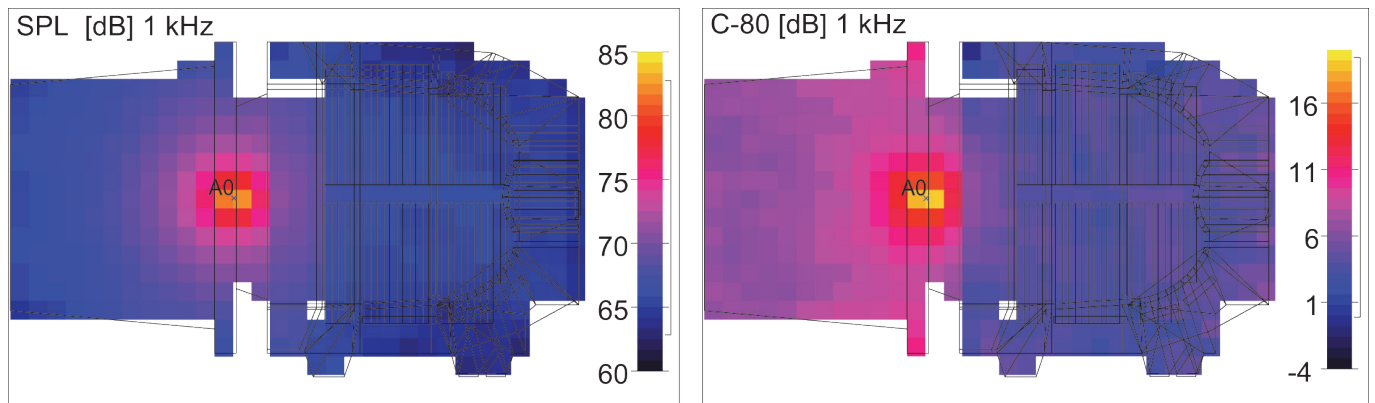


Figure 7. Distribution of Sound pressure level values SPL (left) and Clarity C_{80} (right) at 1kHz in the model of the Český Krumlov theatre (CATT acoustics®).

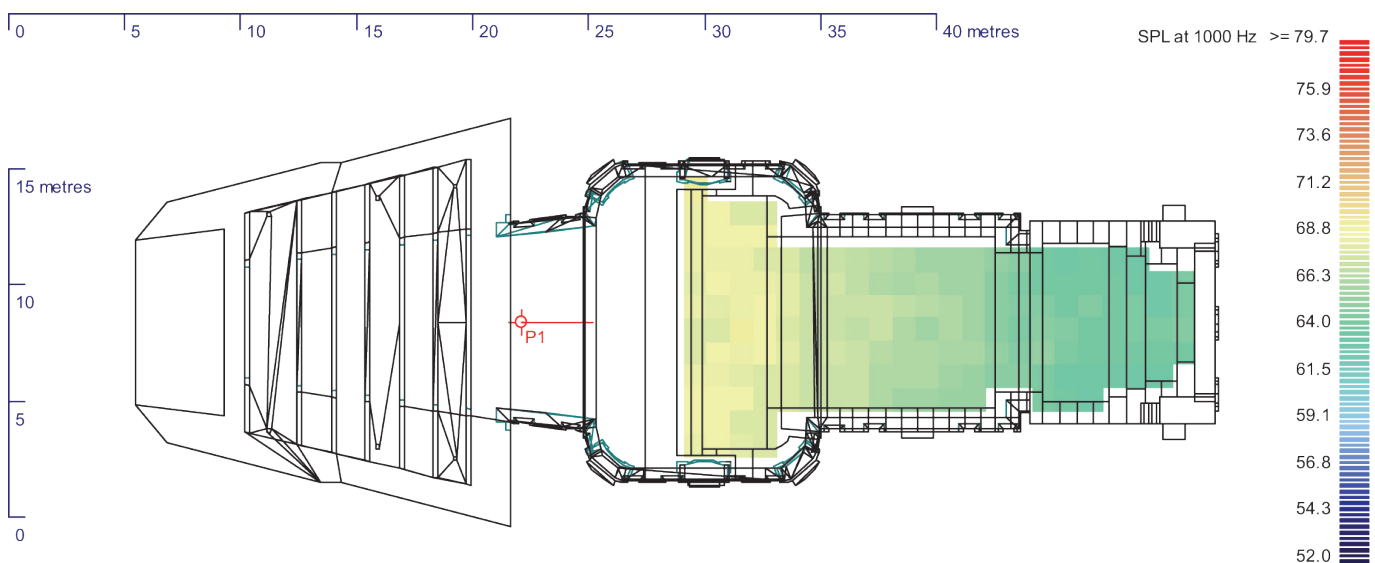


Figure 8. Distribution of Sound pressure level SPL (left) at 1 kHz in the model of the Drottningholm theatre (Odeon®).

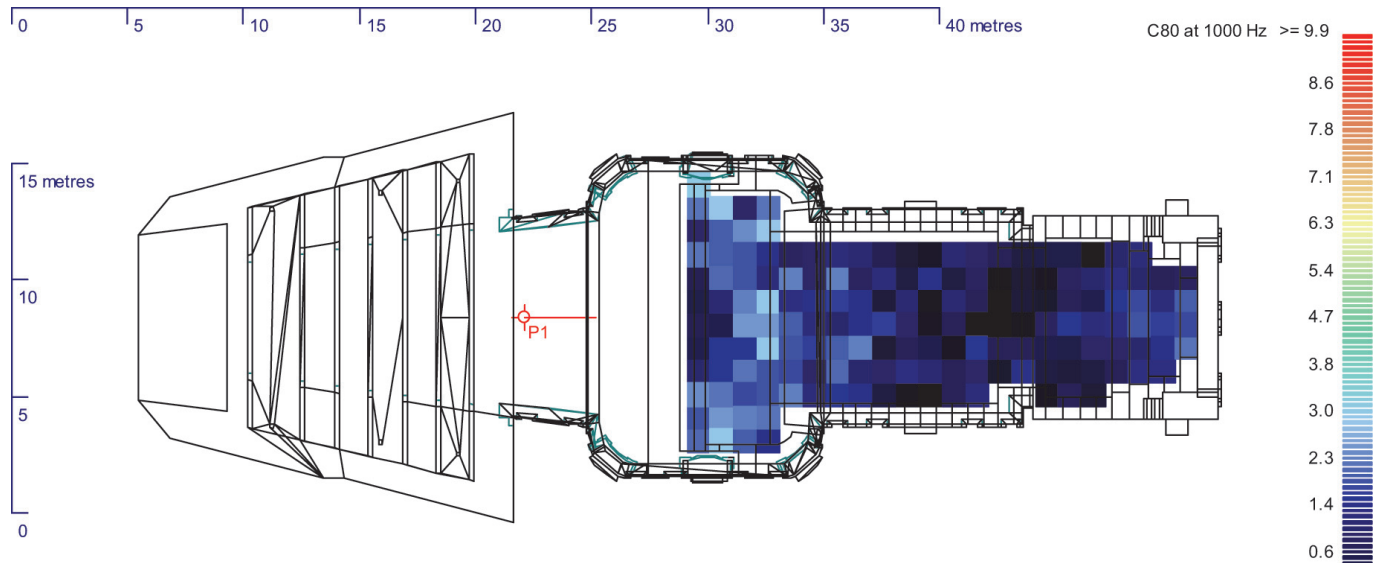
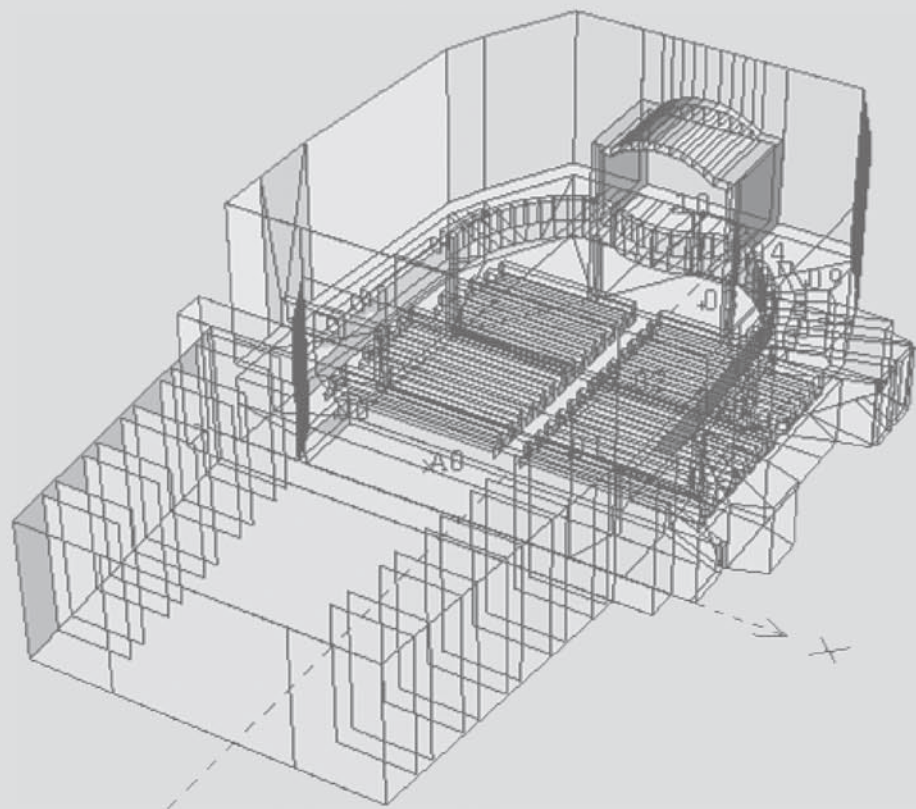
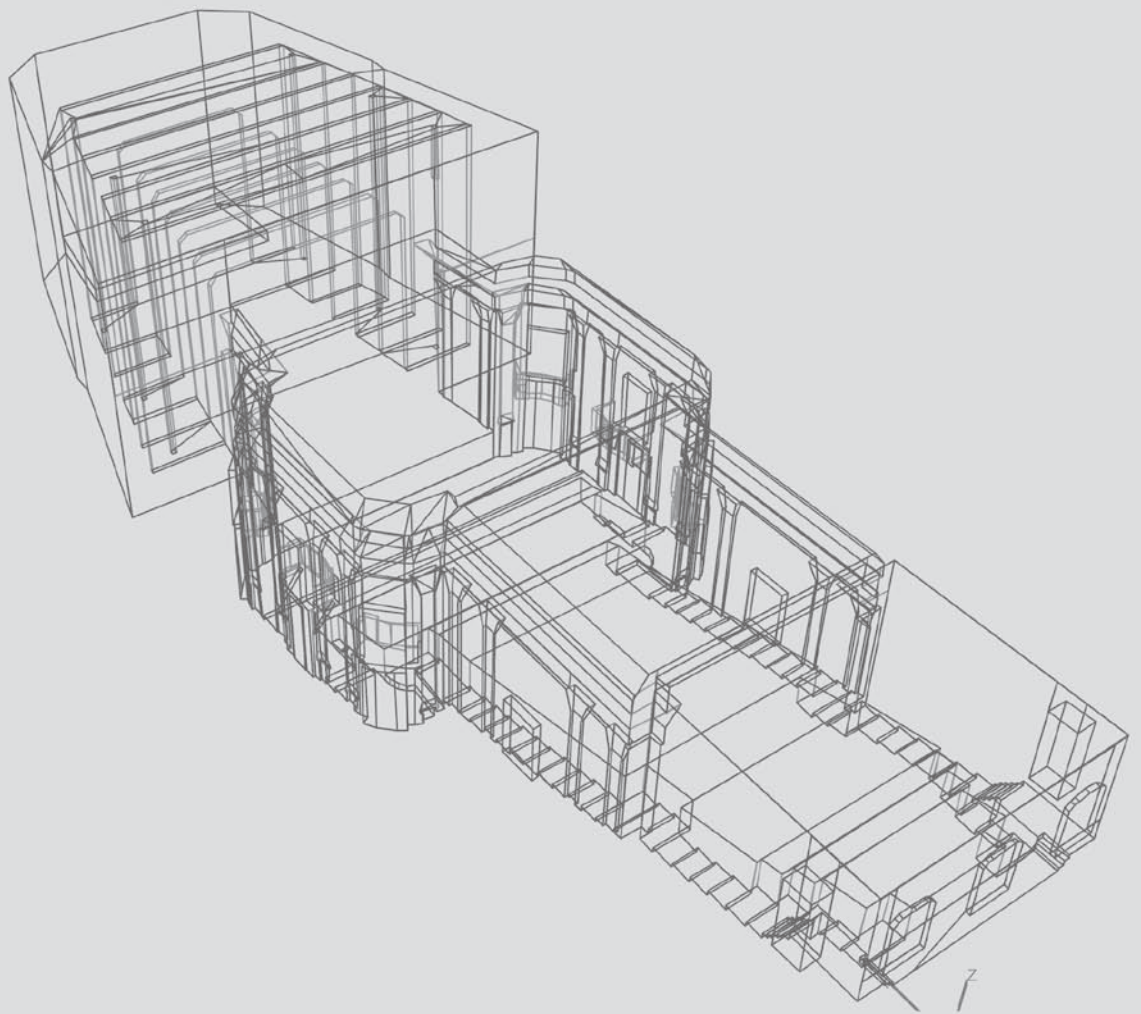


Figure 9. Distribution of C_{80} values in the model of the theatre in Drottningholm (Odeon®).

5. REFERENCES

- [1] Kitson, M.: *The Age of Baroque*. Landmarks of the World's Art. London: Hamlyn; New York: McGraw-Hill. 1966.
- [2] Dolejší, J.; Slavko, P.; Pouzar, L.; Rychtáriková, M.: Acoustics of Unique Baroque Theatre in Český Krumlov. *Akustika - odborný časopis o akustice a vibracích*, Vol. 9, Czech Republic, 2008, pp 2-15.
- [3] Dolejší, J.; Slavko, P.; Pouzar, L.; Rychtáriková, M.: Room acoustical properties of the Baroque theatre in Drottningholm. *Akustika - odborný časopis o akustice a vibracích*, Vol. 13, Czech Republic, 2010.
- [4] www.zamek-ceskykrumlov.eu
- [5] 3382-1:2009: Acoustics - Measurement of the reverberation time of rooms with reference to other acoustical parameters. International standard, 2009.
- [6] IEC 60268-16:2003: Sound system equipment – Part 16: Objective rating of speech intelligibility by speech transmission index, 2003.



Acoustic sound insulation measurements for the direct and flanking transmission of typical swiss timber constructions

Amabel Melián Hernández, Christoph Geyer, Andreas Müller, Ali Sanavi
Bern University of Applied Sciences

PACS: 43.55.-n

ABSTRACT

For multi storey buildings a high quality of the building acoustic performance is an important subject.

Therefore it is crucial for consultants and timber industry to plan and to deliver buildings which achieve a high level of sound insulation. Both need values of the airborne and impact sound insulation of the different construction elements as input parameters for their calculation of the apparent sound insulation in timber buildings. To deliver these measurement results for timber lightweight buildings was the driving motivation to build the lightweight building test facility in Dübendorf, Switzerland.

The direct sound insulation of timber floors and the flanking sound insulation of walls for airborne and impact sound has been measured including a variety of constructions.

The results presented indicate the presence of timber construction systems available for the separating and flanking elements that can achieve a high level of acoustic insulation even at low frequencies.

Keywords: Building Acoustic, Sound Insulation, Acoustic Measurement, Timber Construction, Flanking Transmissions

1. INTRODUCTION

Lightweight timber construction in multi-storey buildings is a fast growing market in Switzerland. Residents of these buildings expect a high level of sound insulation, as well as the high acoustic Swiss requirements [1] between dwellings, where the minimum airborne sound insulation is set up at $D'_{nT} + C \geq 52$ dB and the maximum impact sound level $L'_{nT} + CI \leq 53$ dB for room volumes below 200 m³.

Therefore it is very important for the construction sector to predict the airborne and impact sound insulation between rooms in lightweight buildings with a high extent of accuracy within the design stage.

To achieve this high accuracy of prediction, the availability of a data base with the direct and flanking sound insulation rates of the building elements is important, which will be necessary as input data for the future sound insulation prediction models in lightweight construction. Some of these measurements have been performed during the last years and its results have been presented in several papers [2, 3, 4] and some others are still running.

2. OBJECTIVES

The airborne and impact sound insulation of several hollow box timber floors have been measured. Choosing one of these floors as separation element of the construction, the contribution of the flanking transmissions from diverse timber stud test walls has been evaluated.

In this paper the direct and flanking sound insulation of timber floors and timber stud walls in the vertical direction are reported.

3. MEASUREMENT PRINCIPLE

To carry out the measurements, firstly the vertical direct transmission of the timber floor will be measured with different types of timber floors. To do it, it has to be ensured that the flanking sound transmissions in these measurements are much lower than the direct one. To achieve this requirement, the massive walls of the test facility are covered with high quality acoustic linings and the lightweight test walls of both rooms are built up with lightweight timber elements, the so called Default Elements, which minimize the flanking sound transmission within the construction.

The airborne sound insulation between the two test rooms is presented as the normalized level difference D'_n , which is defined as:

$$D'_n = L_1 - L_2 - 10 \log\left(\frac{A}{A_0}\right) \text{ in dB} \quad (1)$$

In which,

- L_1 is the average sound pressure level in the source room in dB;
- L_2 is the average sound pressure level in the receiving room in dB;
- A is the equivalent sound absorption area in the receiving room, in m^2 ;
- A_0 is the reference equivalent sound absorption area, $A_0 = 10 \text{ m}^2$.

The impact sound insulation between the two test rooms is presented as the normalized impact sound pressure level, $L'_{n,i}$, which is given as:

$$L'_{n,i} = L_2 + 10 \log\left(\frac{A}{A_0}\right) \text{ in dB} \quad (2)$$

The measurements of the direct sound insulation are carried out in accordance with EN ISO 10140-2 [5] and EN ISO 10140-3 [6] for airborne and impact sound respectively.

For a second measurement, two Default Elements are replaced by test specimen walls. For this setup, the airborne and impact sound insulation between the two test rooms are measured again. The sound pressure level in the receiving room of the second measurement is given as the sum of the direct sound transmission of the timber floor and the flanking sound transmission via the flanking test specimen wall.

To extract the flanking sound transmission out of the two measurements, the direct sound transmission (determined in the first measurement) has to be subtracted from the second measurement.

3.1. Direct sound insulation

At first, normalized sound level difference, $D'_{n,1}$, and impact sound pressure level, $L'_{n,1}$, are measured between the two rooms in the vertical direction when flanking transmission is at its minimum, applying the Default Elements within the laboratory flanking paths.

Assuming that the flanking sound transmission is much lower than the direct sound transmission, the direct airborne and impact sound insulation of the separating

test floor, D_n and L_n are determined with the first measurement. Thus:

$$D_n \approx D'_{n,1} \quad (3)$$

$$L_n \approx L'_{n,1} \quad (4)$$

3.2. Flanking transmission

The physical quantities, which describe the airborne and impact sound insulation of a flanking construction element, are the flanking normalized level difference $D_{n,f}$ and the normalized flanking impact sound pressure level $L_{n,f}$, according to the international standard EN ISO 10848-1 [7].

In this standard, the flanking normalized level difference $D_{n,f}$ is defined as:

$$D_{n,f} = L_1 - L_2 - 10 \log\left(\frac{A}{A_0}\right) \text{ in dB} \quad (5)$$

In which,

- L_1 is the average sound pressure level in the source room, in dB;
- L_2 is the average sound pressure level in the receiving room, in dB;
- A is the equivalent sound absorption area in the receiving room, in m^2 ;
- A_0 is the reference equivalent sound absorption area, $A_0 = 10 \text{ m}^2$.

The formula for the normalized flanking impact sound pressure level $L_{n,f}$ is given as:

$$L_{n,f} = L_2 + 10 \log\left(\frac{A}{A_0}\right) \text{ in dB} \quad (6)$$

Where:

- L_2 is the average sound pressure level in the receiving room, in dB;
- A is the equivalent sound absorption area in the receiving room, in m^2 ;
- A_0 is the reference equivalent sound absorption area, $A_0 = 10 \text{ m}^2$.

For the flanking transmission measurement, two of the Default Elements, one from the top and one from the bottom room (both on the same side of the laboratory) are replaced by the test specimen wall. With this configuration, the normalized level

difference, $D'_{n,2}$, and the normalized impact sound pressure level, $L'_{n,2}$, between the two rooms are measured.

This second measurement contains both, the direct sound transmission of the separating floor and the flanking sound transmission of the test wall.

To isolate the flanking airborne and impact sound insulation of the test specimen wall from the direct sound transmission (determined in the first measurement), the direct transmission has to be subtracted from this measurement result.

Thus, the flanking normalized level difference D_{nf} is calculated from the two measurements of the sound insulation between the rooms, $D'_{n,1}$ and $D'_{n,2}$, according to the following equation:

$$D_{nf} = \begin{cases} D'_{n,2} & \text{for } D'_{n,1} - D'_{n,2} \geq 15 \text{ dB} \\ -10 \log \left(10^{\frac{-D'_{n,2}}{10 \text{ dB}}} - 10^{\frac{-D'_{n,1}}{10 \text{ dB}}} \right) & \text{for } 6 \text{ dB} < D'_{n,1} - D'_{n,2} < 15 \text{ dB} \\ D'_{n,2} + 1.3 \text{ dB} & \text{for } D'_{n,1} - D'_{n,2} \leq 6 \text{ dB} \end{cases} \quad (7)$$

Where:

- D_{nf} is the flanking normalized level difference of the test specimen wall
- $D'_{n,1}$ is the normalized level difference between the two rooms, measured with the Default Elements.
- $D'_{n,2}$ is the normalized level difference between the two rooms with the test specimen wall.

The corresponding equation for the impact sound is:

$$L_{nf} = \begin{cases} L'_{n,2} & \text{for } L'_{n,2} - L'_{n,1} \geq 15 \text{ dB} \\ 10 \log \left(10^{\frac{L'_{n,2}}{10 \text{ dB}}} - 10^{\frac{L'_{n,1}}{10 \text{ dB}}} \right) & \text{for } 6 \text{ dB} < L'_{n,2} - L'_{n,1} < 15 \text{ dB} \\ L'_{n,2} - 1.3 \text{ dB} & \text{for } L'_{n,2} - L'_{n,1} \leq 6 \text{ dB} \end{cases} \quad (8)$$

Where:

- L_{nf} is the normalized flanking impact sound pressure level of the test specimen wall
- $L'_{n,1}$ is the normalized impact sound pressure level between the two rooms, measured with the Default Elements.
- $L'_{n,2}$ is the normalized impact sound pressure level between the two rooms with the test specimen wall.

4. METHODOLOGY

The direct sound transmission of four hollow box timber floors have been measured with the Default Elements as walls.

To measure the same acoustic parameter including the flanking transmissions, D'_{n2} and L'_{n2} , the Defaults Elements in the laboratory have been replaced by six different lightweight timber stud walls. The chosen floor for the evaluation of the flanking transmissions was the floor 3.

The sound pressure level in the source room for the airborne noise measurements was generated with pink noise by placing a dodecahedron loudspeaker at two positions in the source room. The sound pressure levels were taken by a rotating microphone at two positions in each room.

These measurements of the airborne sound insulation of the timber floor in the vertical direction have been taken in both ways, from the upper room to the bottom one and vice versa. The final results for the airborne sound insulation are calculated as the arithmetic average of both ways.

For the impact sound measurement, the sound pressure level was generated by placing a standard tapping machine on the floor in six different positions at fixed and randomly distributed locations. The sound pressure level in the receiving room was measured with a rotating microphone at two positions as well.

For the calculation of the needed acoustic parameters, the reverberation time and the background noise were also measured. The frequency range of the measurements covers all the one third octave bands from 50 Hz to 5.000 Hz.

With this data, named as D'_{n1} and D'_{n2} and L'_{n1} and L'_{n2} for the airborne and impact noise respectively, the flanking transmissions D_{nf} and L_{nf} can be calculated using the equations 7 and 8.

If the difference between the two measurements, D'_{n1} and D'_{n2} for the airborne noise and L'_{n1} and L'_{n2} for impact noise, is less than 6 dB the comparison of the two measurements gives only a lower limit for the flanking airborne sound insulation of $D_{nf} > D'_{n,2} + 1.3 \text{ dB}$ and an upper limit of the flanking impact sound insulation of $L_{nf} < L'_{n,2} - 1.3 \text{ dB}$ (e.g. for walls 2 and 3). In this case the flanking airborne sound transmission can be measured with an intensity probe in order to measure the flanking path without any other influence. These measurements were carried out by the Swiss Federal Laboratories for Materials Science and

Technology with the intensity method, following the standard EN ISO 15186-1 [8], generating the sound field in the source room with the dodecahedron loudspeaker, as described in the standard 10140-2 [5], and measuring the intensity level with the intensity probe with a spacer of 12 mm and 100 mm depending on the frequency (12 mm for frequencies above 400 Hz and 100 mm for frequencies below or equal to 400 Hz).

5. FACILITIES AND TEST SPECIMENS DESCRIPTION

5.1. Test facility

The lightweight construction test facility is a collaboration project between Swiss Federal Laboratories for Materials Science and Technology (EMPA) and Bern University of Applied Sciences (BFH). It is situated in Dübendorf, Switzerland. The skeleton of the test facility consists of two massive concrete walls and a massive concrete plate. Within this massive frame of the laboratory (5,4 m x 13,2 m x 7,0 m), a maximum of 4 rooms can be built with lightweight construction elements, one above or side by side the other, to investigate the sound propagation in the horizontal, vertical and diagonal direction. The dimensions of each room vary slightly in order of the thickness of the installed elements.

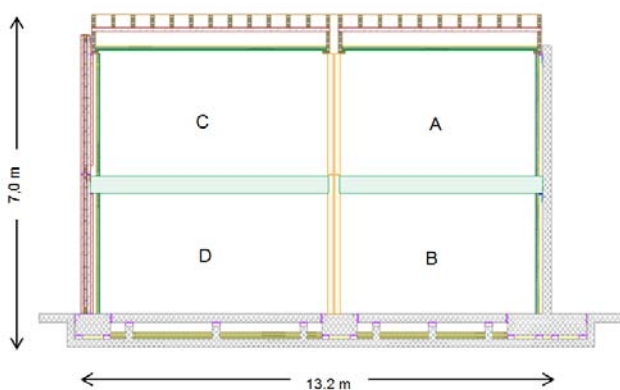


Figure 1: Vertical cut of the test facility with four rooms. The massive elements are grey shaded. The separating test walls are marked in brown and the separating lightweight floor in green. The external walls at the left side are the Default Elements. The massive and the Default Elements are covered by acoustical linings (green). The joists between the elements are inked purple.

For the measurements reported in this document only two rooms (room A and B), one above the other, are build up. The following Table summarizes the geometrical quantities of the test device.

Table 1. Geometry of the test rooms in the laboratory.

Geometry	
Volume of the upper room A	65 m ³
Volume of the lower room B	62 m ³
Area of the separating floor S	22.6 m ²
Length of the flanking test specimen wall	4.2 m

Using this geometrical quantities the apparent sound reduction index R' can be calculated from the normalized sound level difference $D'n$ by the following equation:

(9)

Where S is the area of the separating floor.

5.2. Default Elements

As explained in chapter 3, the Default Elements are used to ensure the minimum flanking transmission to measure just the direct sound transmission path. These elements consist on double walls with massive timber plates and an acoustical lining at the inner side, which are described in Table 2.

Table 2. Construction build-up of the Default Elements from outside to inside the test room.

Description of the Default Element	
80 mm	Solid wood board
100 mm	Cavity filled with mineral wool
2 x 80 mm	Solid wood board
175 mm	Cavity of the acoustic lining with sub construction and 100 mm mineral wool
2 x 12.5 mm	Gypsum fibre board

5.3. Separating timber floors

The separating floor consists of a hollow box timber construction with timber beams and plates, as described in Table 3. This is a common timber floor construction system in Switzerland.

Table 3. Description of the basic floor construction from top to bottom.

Description of the Default Element	
80 mm	Solid wood board
100 mm	Cavity filled with mineral wool
2 x 80 mm	Solid wood board
175 mm	Cavity of the acoustic lining with sub construction and 100 mm mineral wool
2 x 12.5 mm	Gypsum fibre board

Table 4 presents the specifications of the different timber floor constructions. Starting from the basic floor (Floor 1)

some additional linings and suspended ceilings were added to improve the sound insulation of the basic floor.

The flanking sound transmission of these walls was studied in combination with the Floor 3.

5.4. Flanking timber walls

The following timber walls are, as well as the floors, typical timber stud wall constructions in Switzerland.

The following table describes the specifications of each wall construction.

Table 4. Description of the different timber floors with the added construction elements from top to button.

Floor 1		
484 mm	Hollow Box timber floor with a floating floor	
15 mm	Gypsum fibre board	
Floor 2		
499 mm	Floor 1	
55 mm	Suspended ceiling with a stiff sub construction consisting of 40 mm wooden laths and single cladding of 15 mm gypsum fibre boards	
Floor 3		
499 mm	Floor 1	
135 mm	Suspended ceiling with elastic fixings: • 120 mm cavity with an 80 mm thick layer of mineral wool inside the cavity • 15 mm gypsum fibre board	
Floor 4		
634 mm	Floor 3	
15 mm	Gypsum fibre board as a second cladding	

Table 5. Construction specifications for the timber stud walls from outer face to inner face.

Description		
Wall 1		
15 mm	Oriented strand board	
240 mm	Timber stud (240 x 60 mm) in a distance of 625 mm, cavity filled with mineral wool	
15 mm	Oriented strand board	
Wall 2		
270 mm	Wall 1	
15 mm	Second cladding of the timber stud wall with a gypsum fibre board	
Wall 3		
285 mm	Wall 2	
75 mm	Rigid fixed acoustical lining with a single cladding, consisting of: <ul style="list-style-type: none"> • 60 mm sub construction with 60 mm x 40 mm wooden laths, cavity filled with mineral wool • 15 mm Cladding of gypsum fibre board 	
Wall 4		
360 mm	Wall 3	
15 mm	Second cladding of the acoustic lining with a gypsum fibre board	
Wall 5		
270 mm	Wall 1	
56 mm	Elastic fixings with a single cladding consisting of: <ul style="list-style-type: none"> • 41 mm sub construction of 24 mm x 48 mm wooden laths, cavity filled with mineral wool • 15 mm Cladding of gypsum fibre board 	
Wall 6		
326 mm	Wall 5	
15 mm	Second cladding of the acoustic lining with a gypsum fibre board	

6. RESULTS

The following table summarizes the acoustic measurement results of the direct airborne and impact sound insulation of the different timber floors. The

results are presented in terms of single number ratings, the weighted normalized sound level difference, $D_{n,w}$, and the weighted normalized impact sound pressure level, $L_{n,w}$ and the corresponding spectrum adaptation terms according to EN ISO 717 part 1 and 2 [9, 10].

Table 6. Results of the direct airborne and impact sound insulation of each floor.

Reference	Airborne Sound Dn, w (C; C50-5000)	Impact Sound Ln, w (CI, CI,50-2500)
Floor 1	72 (-6; -13) dB	47 (0; 8) dB
Floor 2	75 (-7; -19) dB	43 (3; 15) dB
Floor 3	82 (-4; -19) dB	28 (6; 27) dB
Floor 4	80 (-3; -13) dB	23 (3; 27) dB

The figures below show the sound insulation of the different floors in third octave bands for airborne noise (Figure 2) and for impact noise (Figure 3). Regarding to this curves, the influence of the suspended ceiling onto the sound insulation of the floor (Floors 3 and 4) is easy to see, even at low frequencies.

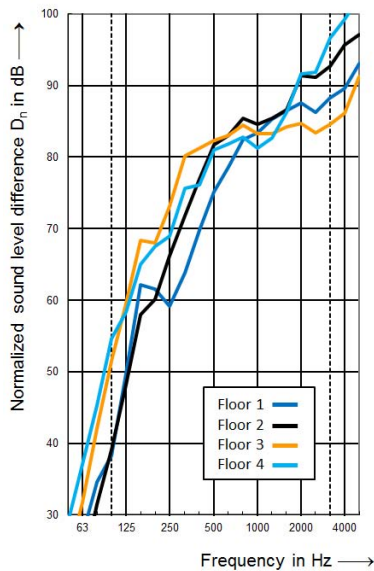


Figure 2: Comparison of the normalized sound level differences of the different floors in third octave bands.

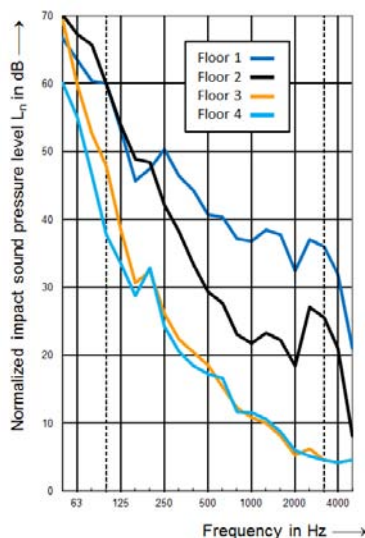


Figure 3: Comparison of the impact sound pressure levels of the different floors in third octave bands.

Table 7 shows the measurement results of the flanking sound transmission of the different walls in combination with Floor 3. The measurement results are given in terms of single number values, the weighted normalized flanking level difference, $D_{nf,w}$, the weighted normalized flanking impact sound pressure level, $L_{nf,w}$ and the corresponding spectrum adaptation terms for each of them.

Table 7. Single number values and the corresponding spectrum adaptation terms of the flanking airborne and impact sound insulation of the flanking timber walls.

Reference	Airborne Sound Dnf, w (C; C50-5000)	Impact Sound Lnf, w (CI, CI,50-2500)
Wall 1	≥ 60 (-2; -31) dB	≤ 37 (-3; 18) dB 1
Wall 2	≥ 69 (-4; -7) dB 1	≤ 32 (1; 22) dB 1
Wall 3	73 (-2; -7) dB 2	≤ 35 (1, 20) dB 1
Wall 4	76 (-2; -8) dB 2	≤ 34 (2; 21) dB 1
Wall 5	87 (-5; -18) dB 2	≤ 28 (4; 26) dB 1
Wall 6	91 (-7; -22) dB 2	≤ 27 (4; 28) dB 1

¹⁾ upper and lower limit because the difference between the two measurements is lower than 6 dB
²⁾ Measurements using the intensity probe.

7. CONCLUSIONS

The measurement results of the sound insulation of Swiss timber hollow box floors and timber stud walls, shown in the tables 6 and 7, indicate that the airborne and impact sound insulation of these constructions are high enough to assemble multi storey timber construction buildings with them, ensuring a high performance of airborne and impact sound insulation.

The results of the flanking transmissions shown in Table 7 reveal that the walls under study reach a high level of airborne and impact sound insulation. Moreover, the acoustic insulation at low frequencies (for airborne and impact noise) tends to be higher than the direct sound insulation of the timber floor.

The measurements are going on to determine the airborne and impact sound insulation of different types of timber constructions used in Switzerland. In the future, all the measurement results will be included in a web based database to provide input parameters which are required for predicting the sound insulation in lightweight timber buildings.

8. ACKNOWLEDGMENT

The measurements are performed as a part of the research program Forschungsschwerpunkt Schallschutz im Holzbau, a joint project of Bern University of applied

Sciences and Lignum Timber Industry Switzerland. We like to thank the Swiss Federal Office for the Environment FOEN for the funding within the framework Aktionsplan Holz and a couple of industrial partners and associations for the support and assistance of the project.

9. REFERENCES

- [1] Schweizer Norm SIA 181: 2006- Schallschutz im Hochbau
- [2] C. Geyer, R. Bütikofer, A. Müller, B. Schuppisser, A. Sanavi ; The acoustical performance of Swiss timber constructions; Internoise 2013, Innsbruck.
- [3] A. Sanavi, C. Geyer, A. Müller, B. Schuppisser, U. Gerhafer, H.J. Strehler; Development of wall-floor junctions in timber buildings with resilient layers to reduce flanking sound transmission.
- [4] A. Melián Hernández, C. Geyer, A. Müller, A. Sanavi; Measurements of airborne and impact flanking sound insulation of Swiss timber constructions; Tecniacustica 2013, Valladolid.
- [5] EN ISO 10140-2: 2010 Acoustics – Laboratory measurement of sound insulation of building elements – Part 2: Measurement of airborne sound insulation
- [6] EN ISO 10140-3: 2010 Acoustics – Laboratory measurement of sound insulation of building elements – Part 2: Measurement of impact sound insulation
- [7] EN ISO 10848-1: 2006 Acoustics – Laboratory measurement of the flanking transmission of airborne and impact sound between adjoining rooms- Part 1: frame document.
- [8] EN ISO 15186-1: 2000 Acoustics – Measurement of sound insulation in buildings and of building elements using sound intensity – Part 1: Laboratory measurements
- [9] EN ISO 717-1: 1997 Acoustics – Rating of sound insulation in buildings and of building elements – Part 1: Airborne sound insulation
- [10] EN ISO 717-2: 1997 Acoustics – Rating of sound insulation in buildings and of building elements – Part 2: Impact sound insulation

Localization Experiments with two Different Configurations in an Artificial Water Depository

Panagiotis Papadakis I. and George Piperakis S.

Foundation for Research and Technology – HELLAS. Institute of Applied and Computational Mathematics (IACM).
Iraklion Crete, GREECE

Corresponding author: panos@iacm.forth.gr, piperak@iacm.forth.gr

PACS numbers: 43.20.Ei, 43.20.Gp, 43.30.Es

ABSTRACT

The Laboratory for Underwater Acoustic Measurements of the Institute of Applied and Computational Mathematics conducted shallow water experiments in an artificial water depository. The purpose of these experiments was to test standard acoustic instruments in the field (under partially controlled conditions as a step from tank testing to open sea use), to verify their good operation and then to analyze the data collected using two different experimental configurations. The instruments used in the experiments were hydrophones, array of hydrophones, pingers, transducers, data acquisition cards etc. Some of the acoustic instruments were placed in fixed positions inside the water column while others changed position during the experiments. In this work the setup and planning of the experiments will be presented, the experimental procedures will be explained and the analysis of the data collected, for estimating the position of the fixed instruments will be presented. An acoustical localization method based on the identification of arrival times using signal processing will be presented. Then an attempt was made to estimate the position of the moving instrument (pinger or transponder). Since the exact position of the instruments was unknown the results were compared with GPS measurements and the maximum difference between them was of the order of 2-3%.

1. INTRODUCTION

The Laboratory of Underwater Acoustic Measurements of the Institute of Applied and Computational mathematics has several acoustic instruments that can be used in the open sea. These instruments have been tested in the small size (5m x1.5m x 1.3m) water tank of the laboratory. As a second step before these instruments deploy in the open see was to test them in a larger body of water under partially controlled conditions. An artificial water depository was chosen for this purpose. Two experiments took place during May and June of 2009. These experiments are presented in this work.

The main idea of the first set of experiments (after validating the trouble-free operation of the instruments) was the following: Using two transponders, fixed in the water column in two positions, a source (pinger) moving inside the water and a single hydrophone (also fixed in the water column), to estimate the distances between the fixed instruments and to estimate the position of the moving source.

There is extensive literature on single hydrophone localization methods (for example [1,2]), and the researchers on our Institute have recently developed several localization methods [3,4]. However, these methods either assume more than one hydrophones, or use not only the signal arriving directly from the source to the hydrophone but also its reflections. These methods cannot be used in our case, since the small dimensions of the water body result in the fact that the direct and reflected pulses are not separable.

During the second set of experiments different instruments were tested and used. A towed array (consisting of a flexible oil filled plastic tube) with two hydrophones, a pinger positioned next to one of the array hydrophones and a transponder positioned in different places inside the lake were used. The data of the experiment were once more analyzed in order to estimate the position of the transponder.

We will first describe the instruments, the location, and the setup of the first experiment. We will then present a method for estimating the position of the fixed instruments and for locating the moving source for the first experiment. Then the second set of experiments will be discussed and the procedure used to estimate the position of the moving source will be presented. A detailed description of the first experiment was presented by the authors in [5]

2. FIRST SET OF EXPERIMENTS

2.1. The instruments used in the experiments.

The following scientific instruments were used in the first set of experiments:

- 2 TDR's. (Temperature and depth loggers)
- 2 transponders (receivers and emitters of acoustic pulses) and 1 pinger (emitter of acoustic pulses)
- 1 omnidirectional hydrophone (1Hz to 120 kHz)
- 1 data acquisition card (100 kHz sampling rate), a signal amplifier and a low pass filter at 50kHz.
- A digital oscilloscope and a portable PC

Other instruments used were: a GPS navigator, a laser distance meter, a depth finder, a UPS inverter, batteries, a small boat, cables, weights etc.

2.2. The location of the experiment

Both experiments took place in an artificial water depository near the village Gergeri, 40 km from the city of Iraklion Crete. A picture of the depository is shown in Figure 1. In Figure 2 a Google Earth picture of the lake is shown. The area of the lake is about 41 km², and its maximum capacity is 244077 m³. The maximum depth near its center is about 14m.

The depository is used during the summer months to water the crops of the area. A pump used for removing water from the depository was turned off during the experiments. There were no other noises except the physical noises (birds, frogs, wind etc.). There were no fish in the lake.



Figure1: A photo of the depository.

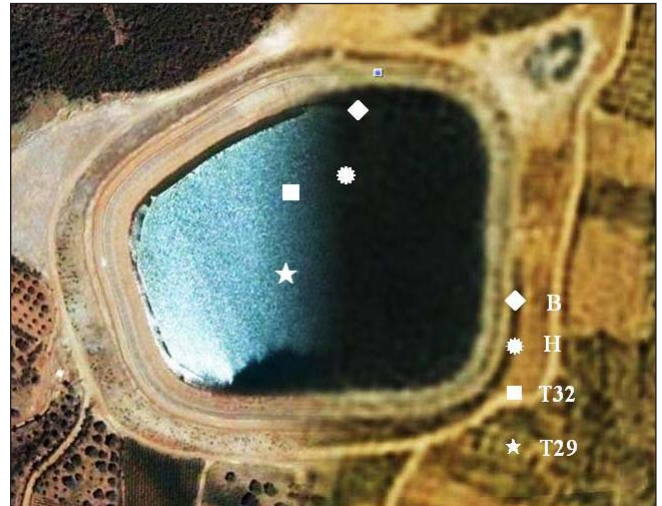


Figure 2. The lake from Google Earth with the positions of the base (B), the hydrophone (H) and the transducers (T32 and T29).

2.3. Experimental setup

All instruments were first moved to a platform (base B on Figure 2) on the lake's shore. There the PC, oscilloscope, batteries etc. were placed. The TDR's are autonomous devices logging the temperature and the depth during a time period. The time period and the logging time steps are adjustable by the user. One of the TDR's was put 10 cm above the hydrophone with a time step of 1 minute and the other was put next to the pinger with a time step of 1 second. The hydrophone (H) was deployed near the base and was connected with a 50 m cable to the amplifier, filter and data acquisition card which was connected to the PC. The two transponders (manufactured by Benthos) were put in two unknown position inside the lake. The transponders are autonomous acoustic instruments both emitters and receivers. They were set to emit an acoustic pulse, one of them in 29 kHz (called T29) and the other at 32 kHz (T32), 20 msec after they receive an acoustic pulse of 26 kHz. The pinger is only an emitter and was set up to emit an acoustic pulse (4 msec long) at 26 kHz, every 2.048 seconds.

The approximate positions of these instruments can be seen in Fig. 2. A schematic of the instruments put in fixed positions inside the water is shown in Fig. 3. A photo of the positioning of transponder T32 is shown in Fig. 4. The pinger (with the second TDR attached next to it) was placed in the water column under the small dinghy and was moving inside the lake. As the dinghy was moving in the lake, it stopped at a few points and the pinger with the second TDR attached was slowly lowered to the sea floor and raised to the surface. This was done in order to get measurements of the temperature at many points of the water column. These measurements were then used to calculate the sound speed in the water.

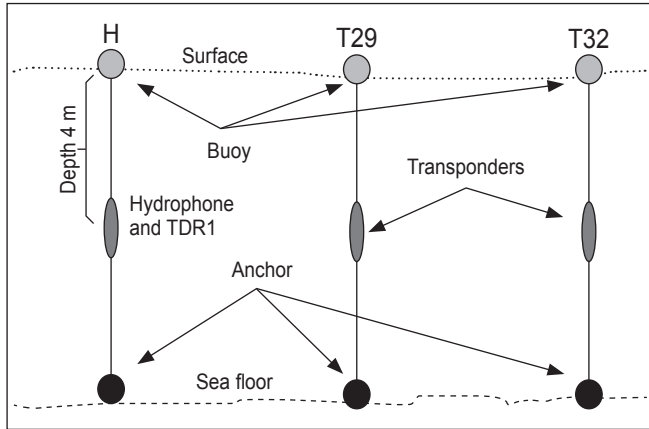


Figure 3. The anchoring of the fixed instruments in the water column.



Figure 4. The positioning of first transponder (T32) in the small red circle. The position of the hydrophone is shown as a larger red circle on the left of the photo.

During the experiment the pinger was continuously emitting pulses every 2.048 seconds. The signal received in the hydrophone was recorded by the data acquisition card and saved in the portable PC. Several 2 minute recordings were made for different positions of the pinger. The sampling acquisition rate was 100 kHz. The filter at 50 kHz was ensuring that no antialiasing phenomena were present in the recorded signal. GPS measurements were also made at the position of the hydrophone (H) and at the two transducers (T32 and T29).

2.4. Estimation of the sound speed in the water

Using the TDR measurements, temperature versus depth can be calculated. The results can be seen in Figure 5 (left) where the red line is the average profile in the lake. The temperature values can then be used to calculate the sound speed profile in the lake (Figure 6 right) and to calculate the way the sound propagates in the water column.

Figure 6 presents the acoustic rays (top) according to ray theory and the transmission loss (bottom). The seafloor was unknown but a soft bottom was used for the calculations of the rays. The sound speed calculated

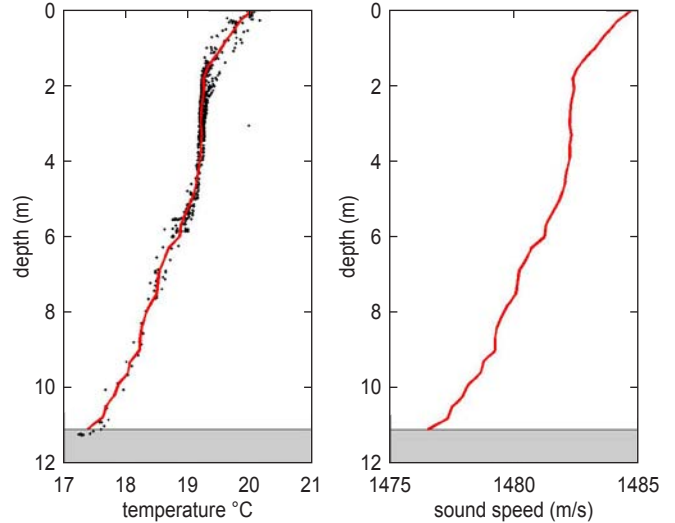


Figure 5. Left: Temperature measurements (black dots) and the average temperature profile (red line). Right: Sound speed profile produced by the temperature measurements.

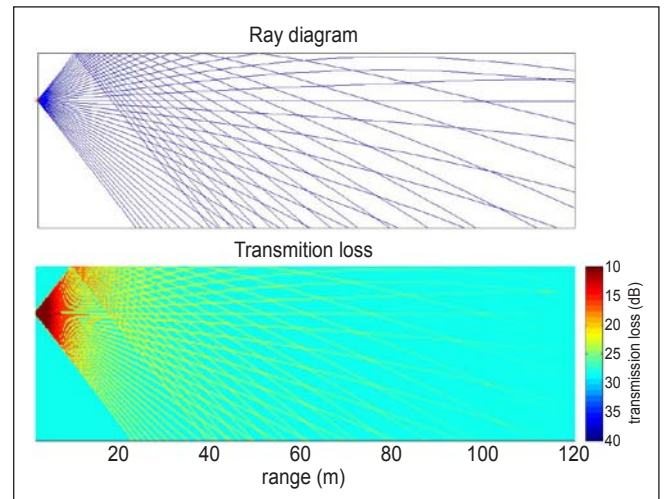


Figure 6. The acoustic rays (top) and the transmission loss (bottom) in the lake.

from these measurements was 1483.2 m/sec for a depth of 4 m. This value was used in the analysis of the arrival times presented in the following section since all our fixed instruments were put in about 4 meters depth.

2.5. Estimation of the position of the fixed instruments

The next step was to process the recorded data in order to estimate the position of the hydrophone (H), and the transponders (T29 and T32). All instruments were positioned at 4 meters depth. Our purpose was to estimate the distance between H, T29 and T32 α_1 , α_2 and α_3 respectively (see Figure 7). If τ_1 , τ_2 , and τ_3 are the corresponding sound travel times between the three instruments and since the sound speed is known, it is enough to estimate the travel times.

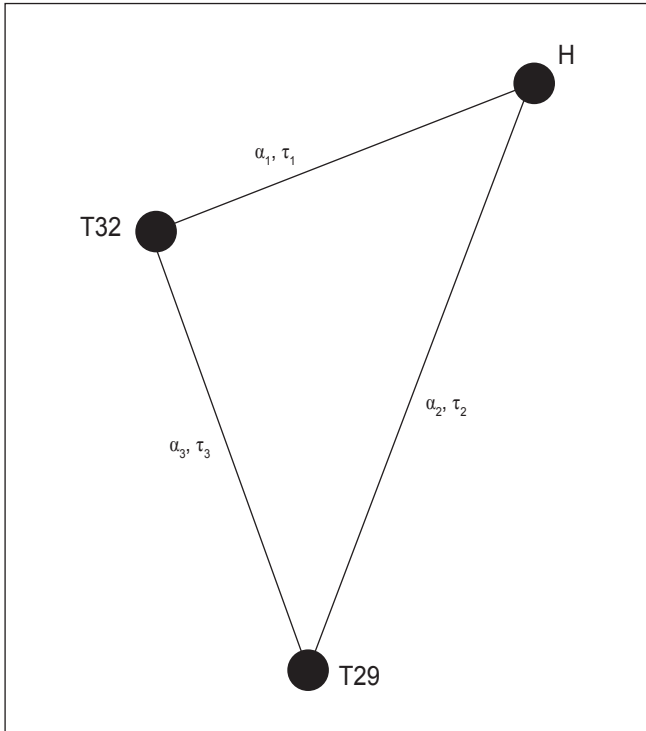


Figure 7. The distance and travel times between the three instruments.

The travel times were estimated using the signals when the pinger was next to the hydrophone and when it was next to T32 as follows:

2.6. Calculation of the travel times

In Figure 8a, a 0.5 second window of the signal recorded with the pinger next to the hydrophone is shown. The pulse from the pinger can be easily seen in this picture. However the pulses from the two transponders are not

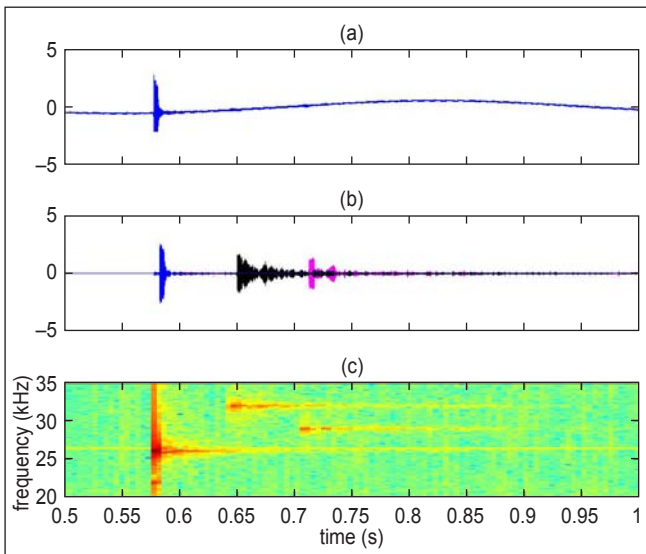


Figure 8. The recorded signal (a), the signal after application of the filter method (b) and the spectrogram of the signal (c).

visible. These pulses were emitted 20 msec after the transponders received the pulse from the pinger. In order to be able to find the time position of these pulses the noise must be somehow removed from the signal. The following filter method was used for this:

A passband filter around the frequencies 26 kHz, 29 kHz and 32 kHz was applied to the signal. The filtered signal is shown in Figure 8b. The blue signal (first pulse) is the 26 kHz component, the black (second pulse) is the 32 kHz and the pink (third pulse) the 29 kHz component. The amplitude of the black and pink component was increased in order for the pulse to be visible. Finding the time of the maximum of each component, we can calculate the difference in time between the arrival times of each pulse. Let dt_1 be the time difference between the first and second pulse (H and T32) and dt_2 the difference between the first and third pulse (H and T29). We can thus estimate the travel times as follows:

$$\tau_1 = (dt_1 - 0.02) / 2 \text{ and } \tau_2 = (dt_2 - 0.02) / 2$$

A second method based in the time-frequency analysis of the signals was also used. A Fast Fourier Transform was applied in a moving time window and the frequency content is obtained. Figure 8c presents the result (spectrogram) of such an analysis. The time position of the maximum at the frequencies 26, 29 and 32 were estimated and used to calculate the dt_1 and dt_2 . We then proceed as in the first method. This method produced similar results and it is presented in [5].

2.7. Estimation of the distances

Since the travel times τ_1 and τ_2 were calculated the distances can also be calculated by:

$$a_1 = c \cdot \tau_1, a_2 = c \cdot \tau_2 \text{ with } c = 1483.2 \text{ m/sec}$$

The recorded signal contained 20 pulses and so this procedure was repeated for all pulses obtaining 20 values for the distances a_1 and a_2 . In order to calculate τ_3 and the corresponding a_3 the signal recorded when the pinger was next to the transducer T32 was used. The method previously presented was also applied for this signal and the third distance was estimated. In this case 31 pulses were present in the signal giving 31 values for a_3 . Their average values and standard deviations were calculated and shown in Table 1. The last column of table 1 contains the values of the distances obtained using the GPS measurements at the location of each instrument. The difference between the GPS data and our estimated values is less than 2%.

Table 1. The results of the data analysis.

	Filter method		GPS
	Mean value(m)	Standard deviation(m)	(m)
α_1	36.83	3	37.72
α_2	82.15	1	83.43
α_3	60.42	4	62.79

2.8. Estimation of the position of the pinger in the water

2.8.1. Calculation of the position

Now that the distances between the fixed instruments are known it is examined if it will be possible to estimate the position of the pinger in the lake at any point different that the position of H, T29 and T32. Figure 9 describes the problem. Let the pinger be at some point P in the water. The pinger was put at 4 meters depth as the rest of the instruments. From this point it emits a pulse and the signal is recorded in the hydrophone located in H. It is also recorded there the pulse emitted by T29 and T32, 20 msec after they “listen” to the pinger pulse.

Let x, y and z the distances from P to H, T32 and T29 respectively. Can these distances be estimated? The problem would be trivial if the travel time t_1 from P to H was known. Then the distances x, y and z are given by:

$$x = c \cdot t_1$$

$$y = x - a - c \cdot (dt_1 - 0.02)$$

$$z = x - \gamma - c \cdot (dt_2 - 0.02)$$

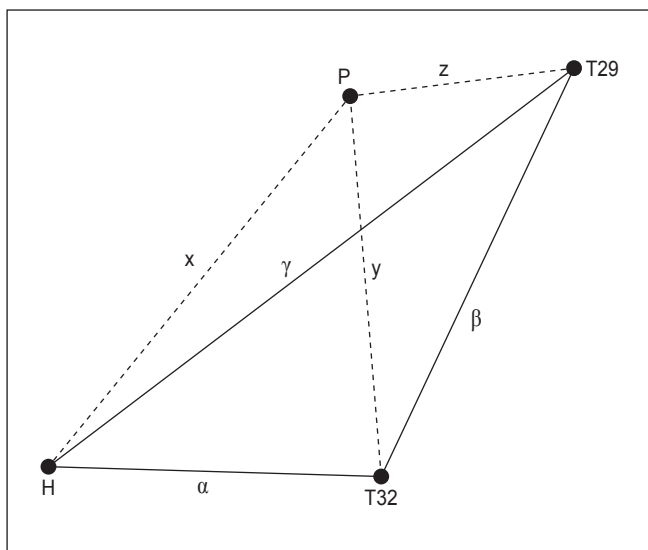


Figure 9. Schematic of the position of the fixed instruments and the pinger (P).

where dt_1 and dt_2 are the time differences between the pinger pulse and the pulse from T32 and T29 respectively.

However in our case the instruments were not synchronized and so the absolute travel time t_1 is unknown. The method used to overcome this problem was the following: Assume t_1 was known, then the point P would be located in the intersection of three circles with centers in H, T32 and T29 and with radii x, y and z respectively. However since all the travel times and distances were numerically calculated, they are not error free. So the three circles most likely will not intersect in one single point but they will form a curvilinear triangle (Figure 10). Let the area of this triangle be A. This was calculated using the method described in [6]. The method to find the appropriate t_1 is to define a time interval and a time step and for each time t in this interval to calculate x, y and z and then the area A of the triangle. The t with the minimum A will be chosen as the correct arrival time t_1 . Then from the three apexes of the triangle we choose the one that is closer to H, T29 and T32 at the same time. This will be taken as the position P of the pinger.

2.8.2. Application to recorded data

We applied the method of the previous section to three different recorded signals.

The first signal was recorded as the pinger was located in a point between H and T29, the other as the pinger was somewhere in the middle of the area between H, T29 and T32 and the third recording was done as the pinger was moving from H to T29. The first two cases

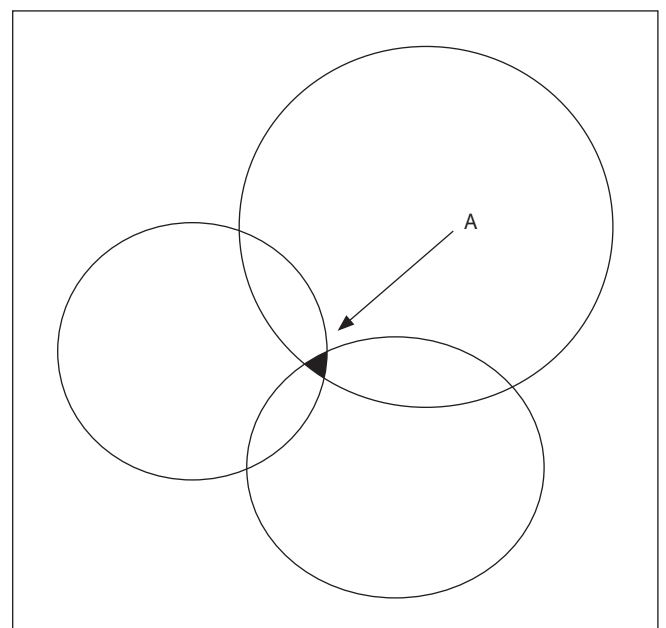


Figure 10. The intersection of three circles and the curvilinear triangle they form.

showed that the position of the pinger was estimated accurately enough ([5]). We will present here the results of the third case

The results of the analysis of the signals for the location of the pinger are shown in Figure 11. The black squares are the positions of the fixed instruments and the red circles the position of the moving pinger.

3. SECOND SET OF EXPERIMENTS

The purpose of the second experiment was to apply the localization technique discussed in the first experiment using a different experimental configuration with different instruments. The major change in this experiment was the use of a hydrophone array. The array is 10 meter oil filled flexible tube with three hydrophones inside and a 200 meters cable. The hydrophones inside the tube (H1, H2, H3) are shown in Figure 12. Either H1 and H2 or H1 and H3 can be used during an experiment. In our experiment we used hydrophones H1 and H3. Their distance - if the tube is straight - is 2.95 meters.

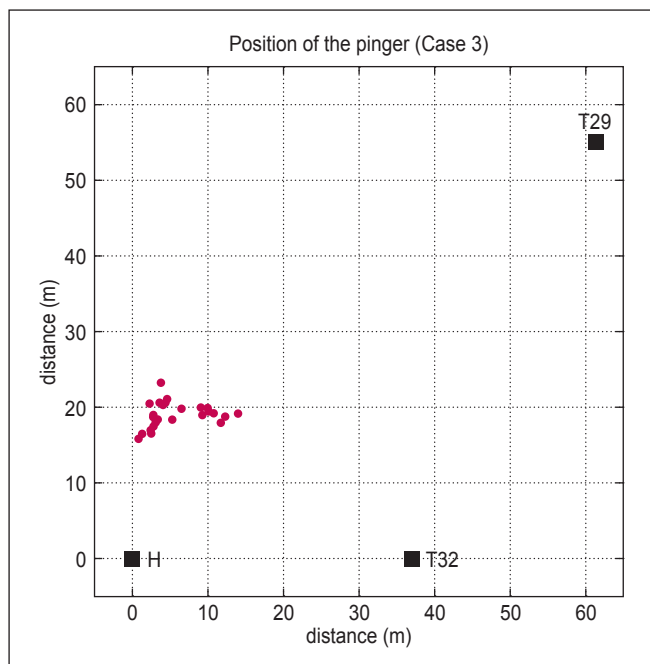


Figure 11. The position of the pinger P estimated by our method (red points) as the pinger was moving inside the lake (case 3).

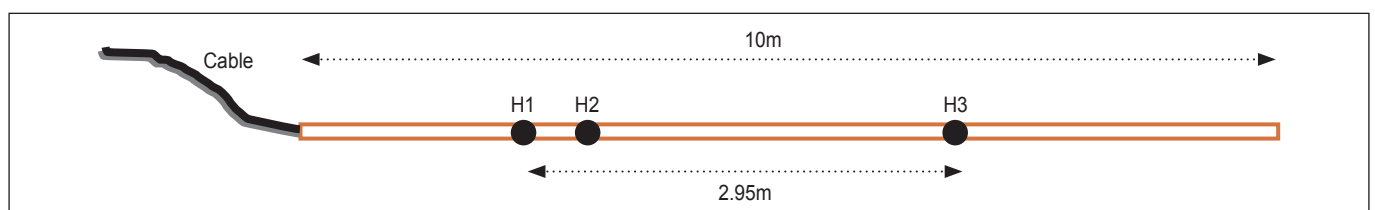


Figure 12. The hydrophone array with the approximate location of the three hydrophones.

3.1. The instruments used in the experiments.

The following scientific instruments were used in the second set of experiments:

- 2 TDR's. (Temperature and depth loggers) 1 transponder and 1 pinger
- 1 array of two omnidirectional hydrophones (1Hz to 120 kHz)
- 1 data acquisition card (100 kHz sampling rate) with a signal amplifier
- A digital oscilloscope and a portable PC

Other instruments used were: a GPS navigator, a laser distance meter, a depth finder, a UPS inverter, batteries, a small boat, cables, weights etc.

3.2. The location of the experiment

The location of the second experiment was the same as the one of the first experiment (section 2.2)

3.3. Experimental setup

All instruments were once again moved to a platform (base B on Figure 2) on the lake's shore. There the PC, oscilloscope, batteries etc. were placed. The pinger (P) was tied on the tube of the array at a position where hydrophone H3 was located (Figure 13).

Two floats were tied to the array (at the position of the hydrophones) with a 4m cable and two anchors were used (Figure 14). Then the array was put in the water 90 meters from the base near the center of the lake.

The transponder (T) was tied to a rope and the TDR was tied 10cm above the transponder and was programmed to log data with a time step of 1 second. Then the transponder was immersed in the water from the dinghy which was moving inside the lake at different positions. The depth of the transponder was 4 meters below the surface. The pinger emitted pulses 5msec



Figure 13. The hydrophone array with the pinger (black cylinder) tied on it.

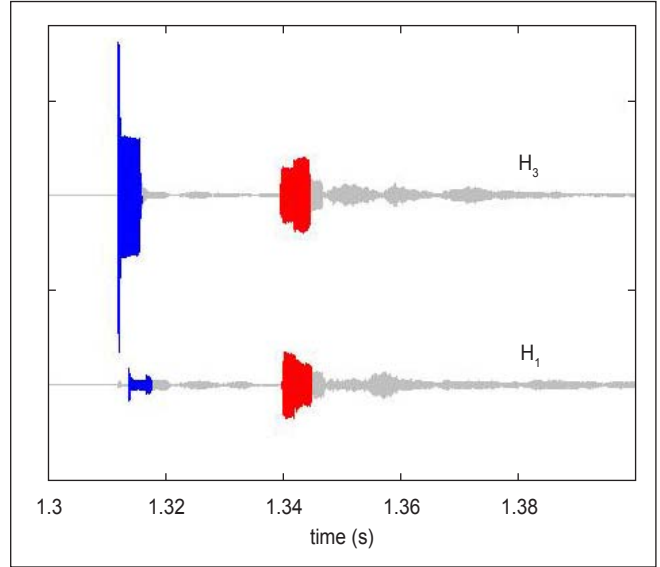


Figure 15. Examples of the signals recorded at the hydrophones H3(top) and H1(bottom). The blue signal is the pinger signal and the red the signal from the transponder.

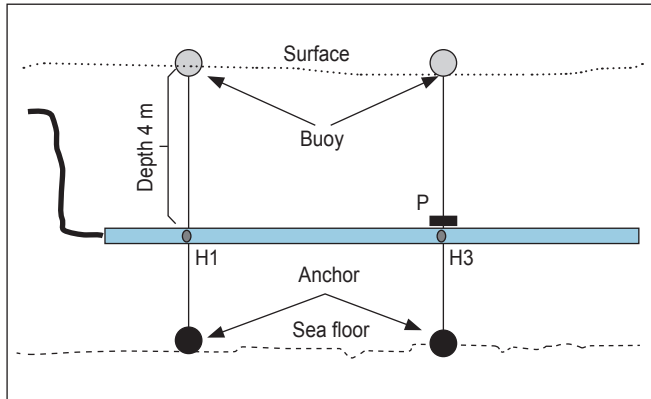


Figure 14. A schematic of the positioning of the array inside the lake.

long at 26 kHz every 2.048 msec and the transponder emitted a 4 msec pulse at 32 kHz after the arrival of the pinger signal at the transponder. The data from the two hydrophones were then recorded using the data acquisition card.

3.4. Estimation of the position of the transponder in the water

The recorded by the hydrophones signals were used to estimate the distance between the two hydrophones and the position of the transponder inside the lake. In Figure 15 two such signals are shown. The top signal is the one recorded from H3 and the one at the bottom from H1.

The signals in blue are the ones coming from the pinger and in red from the transponder. The rest of the signals in grey are either multiple reflection from the surface or the sea floor, or noise. From the two blue signals the distance between the two hydrophones can be obtained. The method used was the same as the first experiment. Using many such measurements the average distance

from H1 to H3 was calculated at 2.76 meters. This indicates that the tube was not straight but it was bended since the straight distance between them is 2.95 meters. Using the arrival times of the blue and red signals in both hydrophones the distance from the transponder to the hydrophones was estimated. The method used was similar to the method used in the first experiment. Now the absolute times from the emission of the signal from the pinger are known since the pinger was located next to the hydrophone H3. Knowing the distance between

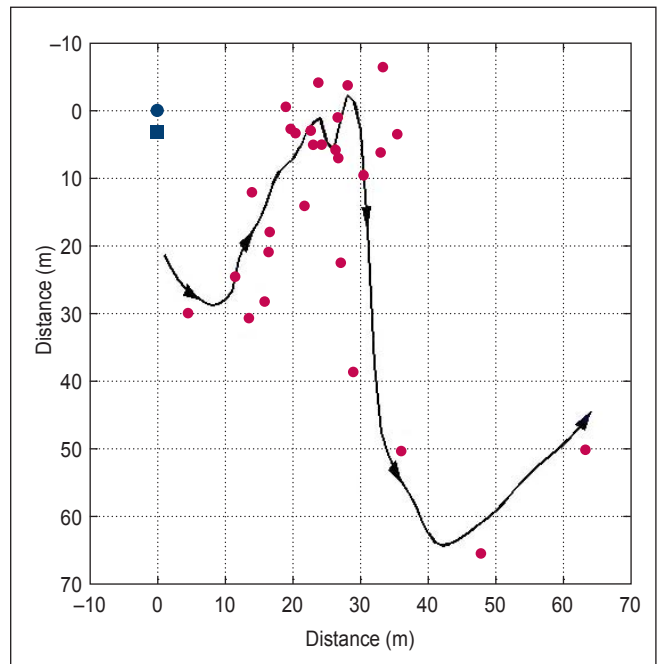


Figure 16. Analysis results: The blue square and circle are the position of the hydrophones, the red circles are the position of the transponder using the analysis of the acoustical data and the black line is the position of the dinghy calculated from the GPS data.

the transponder and the hydrophones its position can be estimated (with a left-right ambiguity) as the intersection points of two circles.

Figure 16 shows the position of the transponder as red circles using the method described above for a 30 seconds period. The blue circle is the position of H3 and the blue square the position of H1. The black curve is the position of the dinghy which was calculated by GPS measurements. The accuracy of the GPS position was about 4 meters. It is observed that the mean difference between the GPS data and the estimated values was 2.5%

4. CONCLUSIONS

The experiments in the artificial depository were done in order to verify that the instruments used will operate as expected and to identify any problems related to the deployment, operation and retrieval of the instruments before they can be used in the open sea.

At the same time the signals recorded were used to calculate several unknown parameters such as sound speed and distances between the instruments. Finally an attempt was made to track the moving source (pinger or transponder) for two different experimental configurations. The results were encouraging, verified with GPS measurements and they suggest that it is possible to measure distances with these experimental configuration.

Some problems related to the calculation of the arrival times need more investigation in order to avoid erroneous results.

5. REFERENCES

- [1] S. M. Jesus, M. B. Porter, Y. Stephan, X. Démoulin, O. Rodríguez, and E. Coelho, **Single hydrophone source localization** *IEEE J. Ocean Eng.* 25(3), 337–346 (2000).
- [2] L. Neil Frazer and P.I. Pecholcs, **Single-hydrophone localization**, *J. Acoust. Soc. Am.*, vol. 88(2), pp.995-1002, (1990).
- [3] E.K. Skarsoulis, M.A. Kalogerakis **Ray-theoretic localization of an impulsive source in a stratified ocean using two hydrophones** *J. Acoust. Soc. Am.* Volume 118, Issue 5, pp. 2934-2943 (2005).
- [4] E.K. Skarsoulis, G.S. Piperakis, **Use of acoustic navigation signals for simultaneous localization and sound-speed estimation** *J. Acoust. Soc. Am.*, Vol. 125, pp. 1384-1393, (2009).
- [5] Panagiotis Papadakis, George Piperakis, **Instrument testing and localization experiments in an artificial depository**. In Proceedings of the 10th European Conference on Underwater Acoustics 2010, pp. 1209-1216 (2010)
- [6] M.P. Fewell **Area of common overlap of three circles** Defense Science and Technology Organization Technical report DSTO-TN-0722, (2006).

Defining the Acoustic Environment of (semi-)open Plan Offices

Acoustic Measurements leading to Activity Based Design for retrofit Buildings

Sara Vellenga-Persoon, ir. Theodoor Höngens,
M+P consulting Engineers, Aalsmeer, The Netherlands
corresponding author: SaraVellenga@mp.nl

PACS: 43.55.-n

ABSTRACT

Before creating a new activity-based design in retrofit buildings projects the existing acoustic environment is carefully measured. Not only the acoustical qualities of the existing building and facilities are measured (according to NEN 5077 for sound insulation, ISO 3382 for room acoustics and ISO 3382-3:2012 for room acoustics in open plan offices), but also the actual behaviour of people is measured as well as this is a very important input for defining the acoustic environment. During a representative week of working hours, the sound levels are monitored at different locations in the open plan office. To gather information about the character of the sound, sound fragments are also recorded based on a trigger level.

Defining the acoustic environment of (semi-) open plan offices based on building measurements and noise level measurements provides a good starting point for redesigning a diversity of office environments. Often the new design leads to activity-based office plans, where the different activities are carefully projected in a (semi-) open plan office. Practical measurement data of office noise levels are presented and analysed.

1. INTRODUCTION

Working in an office environment includes many different activities. Communication on the phone, social interaction and meetings produce not only sound, but are also require good speech intelligibility and therefore need good room acoustics. Difficult performance tasks require different acoustic conditions. Areas with a quieter environment are needed so the level of distraction from surrounding activities is minimised. In the same office environment there is also a need for areas with a high level of interaction for the purpose of teamwork. Because the different activities ask for specific acoustic conditions, the existing acoustic environment is first mapped before creating a new office environment in an existing retrofit building.

2. NORMS AND RESEARCH

The ISO 3382-3 [1] norm provides guidelines for measuring building characteristics for open plan offices. An important statement is that concentration and privacy start to improve rapidly where the speech transmission index falls below 0,50. This statement is reinforced by Jahncke, Hongisto and Virjonen [2] where the effects of speech intelligibility have been studied for different office tasks. This work demonstrates that attempts to minimize speech intelligibility will yield increases in cognitive performance with a varying degree, depending on the type of focus task.

The corresponding distance for an STI below 0,50 is defined as the *distraction distance* r_D . This is the distance between the receiver and the speaker. The distraction distance is defined based on STI measurements combining the receiver levels of speech $L_{p,A,S}$ and the levels of background noise levels $L_{p,A,B}$. The built environment of the office without the existing background noise levels can be defined by the spatial decay rate of A-weighted SPL of speech $D_{2,S}$. The room acoustics can be defined by measurements as well as by predictions using computer modelling [3], [4]. Keränen and Hongisto [5] present a regression model for predicting the spatial decay. Their research has shown an acceptable prediction accuracy for most practical purposes.

However, the actual behaviour of people and how many people are talking at the same time is often not taken into account in defining the acoustic environment. The effects of unattended speech on



Figure 1. Open plan office (source www.bbc.com/news/magazine-23502251 "The decline of privacy in open-plan offices").

performance and subjective distraction have recently been studied by the Finnish Institute of Occupational Health and the University of Turku [6]. The speech conditions differed in terms of the degree of absorption, screen height, desk isolation and the level of masking sound. The actual sound level of the unattended speech is not taken in account as such, but can be regarded as varied in the distance to the receiver (2 to 6 metres). For all situations the distraction was rated higher for the nearby speech as opposed to the speech heard from a further distance. However, this result has to be seen as a combination of a level increase and an increase of intelligibility and cannot be used as an evaluation of purely the effect of the sound levels. In 2005 Chigot presented an overview of 11 abstracts on the topic of effects of sound in offices - subjective experience versus objective assessment [7]. Besides parameters as 'satisfaction with privacy' the sound level is often mentioned in relation to an increase of

subjective workload [8] and a decrease of cognitive performance in memory tasks [9]. As an important comment on the research of Tang [10], Chigot mentions that $L_{A,eq, 5 \text{ min}}$ correlates the best with human auditory sensation.

3. OFFICE NOISE LEVELS

In 1978, some interesting information was published about office noise levels in the Acoustical Designing in Architecture [12]. A comprehensive survey of the noise in several thousand locations was conducted by the Bell Telephone Laboratories in order to determine typical noise conditions indoors and outdoors. The noise levels are a combination of three broad classifications: people, machinery and outdoor sources. For 45 per cent of the business locations people were the predominant source of noise, followed by machinery in 25 per cent of the locations and outdoor sources in 30 per cent of the locations.

We have collected a lot of data of noise levels in our measurements in open plan offices floors. During a representative week of working hours, the noise levels have been measured in different buildings with different types of workplaces. All measurements were conducted in open plan offices (> 10 desks). Measured data are presented in Figure 2 that show a comparison of office sound levels through history. We conclude that the noise levels of modern day offices are substantially lower compared with those in the seventies of the twentieth century. The old fashioned loud typewriters and hard acoustic environments will probably have been a cause of this.

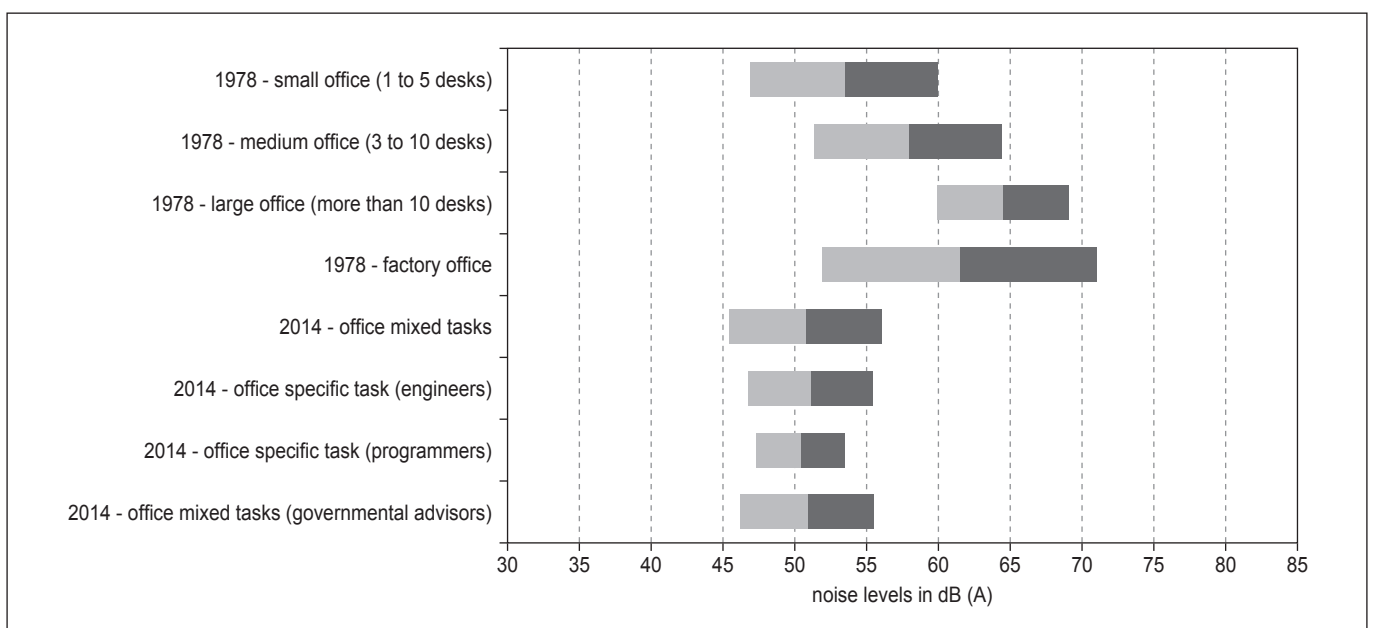


Figure 2. Noise level data (mean value \pm standard deviation), comparison data 1978, United States of America, D.F. Seacord [1] and data 2014, The Netherlands, M+P.

4. STATISTICS OF MODERN DAY NOISE LEVELS

In Figure 3 the noise levels in modern day offices in The Netherlands measured by M+P are presented in a histogram. The data for offices with mixed tasks were collected for one working week from 9 to 5 for 8 offices with 2 or 3 monitoring positions per office. The curve of the histogram shows the curve of a normal distribution. The remaining data in the histogram were collected from 1 or 2 buildings for the specific office tasks (engineering, programming, governmental advisors). The main characteristic is that all measurements have a mean value of 50 to 51 dB(A). The difference is especially noticed in the standard deviation. Specific office tasks like computer programming and engineering tasks show a smaller standard deviation (3-4 dB) compared with the mixed tasks (5 dB) as shown in figure 2 and 3 for modern day offices.

4. OFFICES TYPES AND DIMENSIONS AND PERFORMANCE

Modern day offices do not conform to a standard format with fixed workplaces in cellular offices. Because of new ways of working, based on more flexibility, new office environments are being realised in existing buildings as retrofit projects. These days it is seldom found that new offices are being built, so new office environments can seldom be created from scratch. In The Netherlands a lot of the existing office buildings are made ready for refurbishment within the retrofit building project. The pattern of the office lay-out and the use of workspaces is no longer set as a regular pattern with fixed working spaces within cellular offices.

De Croon, Sluiter, Kuijer and Frings-Dresen state in [13] that conventional and innovative office concepts can be described using three parameters: 1. the office location (e.g. telework office versus conventional office), 2. the

office lay-out (e.g. open lay-out versus cellular office), 3. the office use (e.g. fixed versus shared workplaces). A systematic review of literature between 1972 and 2004 provides strong evidence that working in open workplaces reduces privacy and job satisfaction. Limited evidence is available that working in open workplaces intensifies cognitive workload and worsens interpersonal relations. Close distances between workstations intensifies cognitive workload and reduces privacy and desk-sharing improves communication.

In 2009 the Finnish Institute of Occupational Health and the University of Turku in Finland performed a longitudinal study during relocation on the effects of the acoustic environment on work in private office rooms and open plan offices [13]. The aim was to determine how the perceived work environment –especially acoustic environment– and its effects differed in private office rooms as opposed to open-plan offices. Room descriptors showed a significant reduction in speech privacy after relocation. The noise level averaged over the whole working day did not change, but the variability of noise levels reduced significantly. Negative effects of the acoustic environment increased significantly, including increased distraction, reduced privacy, increased concentration difficulties and increased use of coping strategies. Self-rated loss of work performance because of noise doubled and cognitively demanding work and phone conversations were most distracted by noise. The article states that the results suggest that the open plan office is not recommended for professional workers.

5. (SEMI-)OPEN PLAN OFFICES AND ACTIVITY BASED DESIGN

It is important to define the existing office environment before starting a new office floor design. The variation can be found in office design, building acoustics and the activities of the workers. In Table 1 variations with

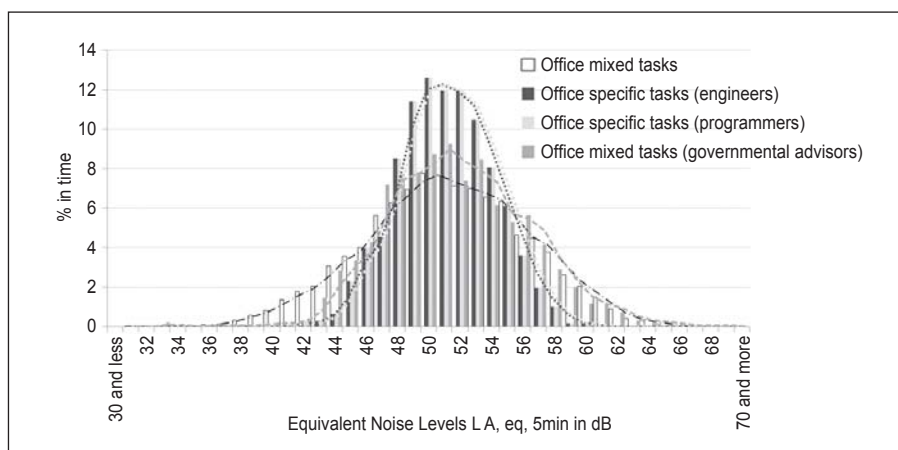


Figure 3. Histogram noise level in modern day offices measurement data M+P.

Table 1. Defining the variations with associated parameters for defining the (acoustical) environment

	Variation	Choices	Acoustical parameters
Office design	LAY-OUT	open / semi-open / closed	–
	USE	permanent versus flexible (desk-sharing)	–
	TYPE	mixed or activity based	–
Measurements building acoustics	ABSORPTION/ AVOID REFLECTIONS	ceilings, wall panels, furniture, interior elements	reverberation time T spatial decay $D_{2,S}$ STI
	ROOM INSULATION	walls, ceilings, floors, facades, doors, windows	sound insulation $D_{nT,A}$
	SCREENS	screens, walls, rooms, cabinets	spatial decay $D_{2,S}$ STI
	INSTALLATIONS	ventilation principles, masking systems	background noise $L_{p,A,B}$ STI/SNR
Measurement behavioural Acoustics	–	–	sound level (L_{max} , L_{eq}) recording wave-files (defining sound source, type of sound)

associated parameters and choices are stated for defining the (acoustic) environment.

Based on the measured noise levels in modern day office buildings, the required distances have been calculated for the design of new office environments. The assumptions are a background noise level of 40 dB(A), a signal to noise ratio for speech of 3 dB and a spatial decay of 8 dB. These values are set as quite representative for modern Dutch office design as seen as in Figure 4.

6. RECOMMENDATIONS

For open plan office environments we recommend a semi-open structure which provides some screening



Figure 4. Modern modern day office in The Netherlands (semi-open, activity based).

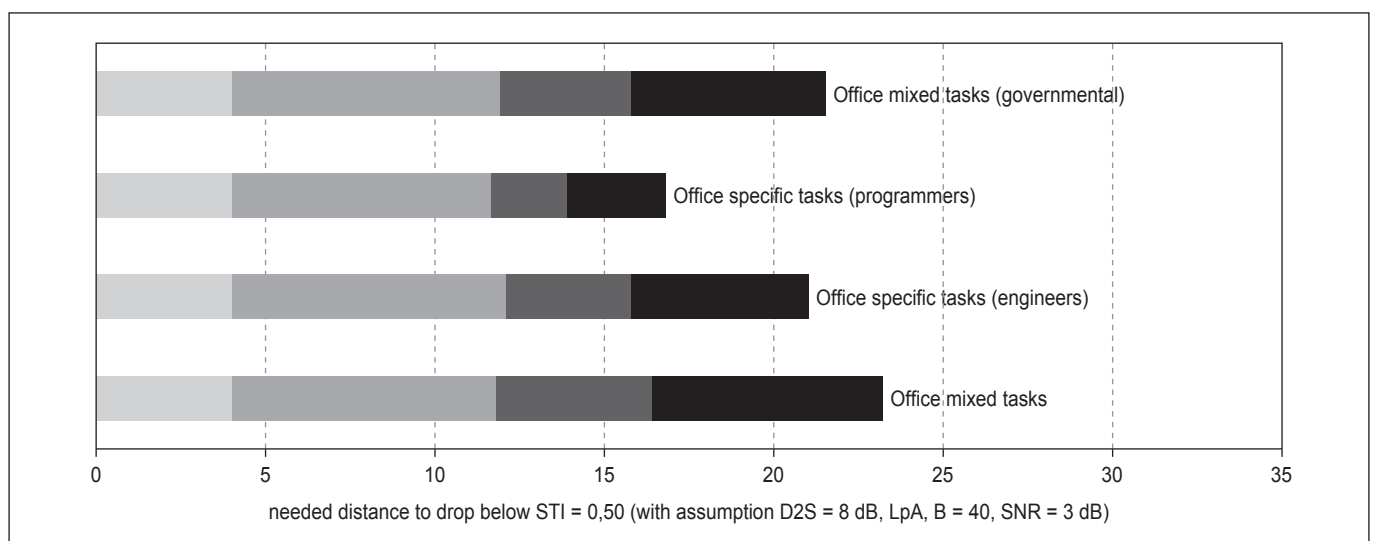
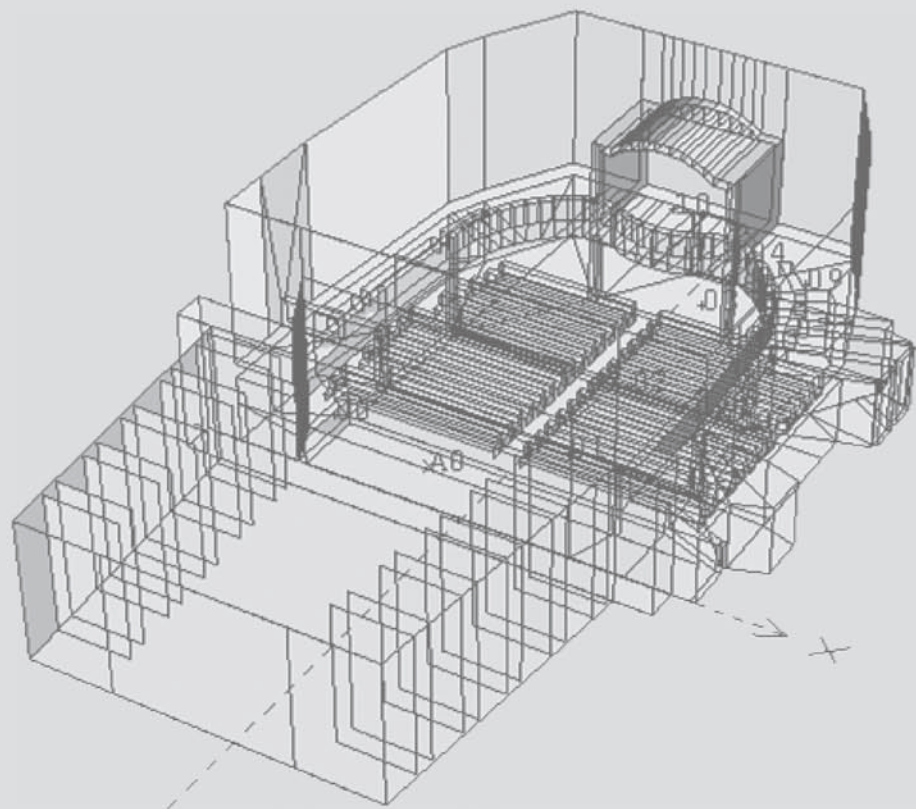
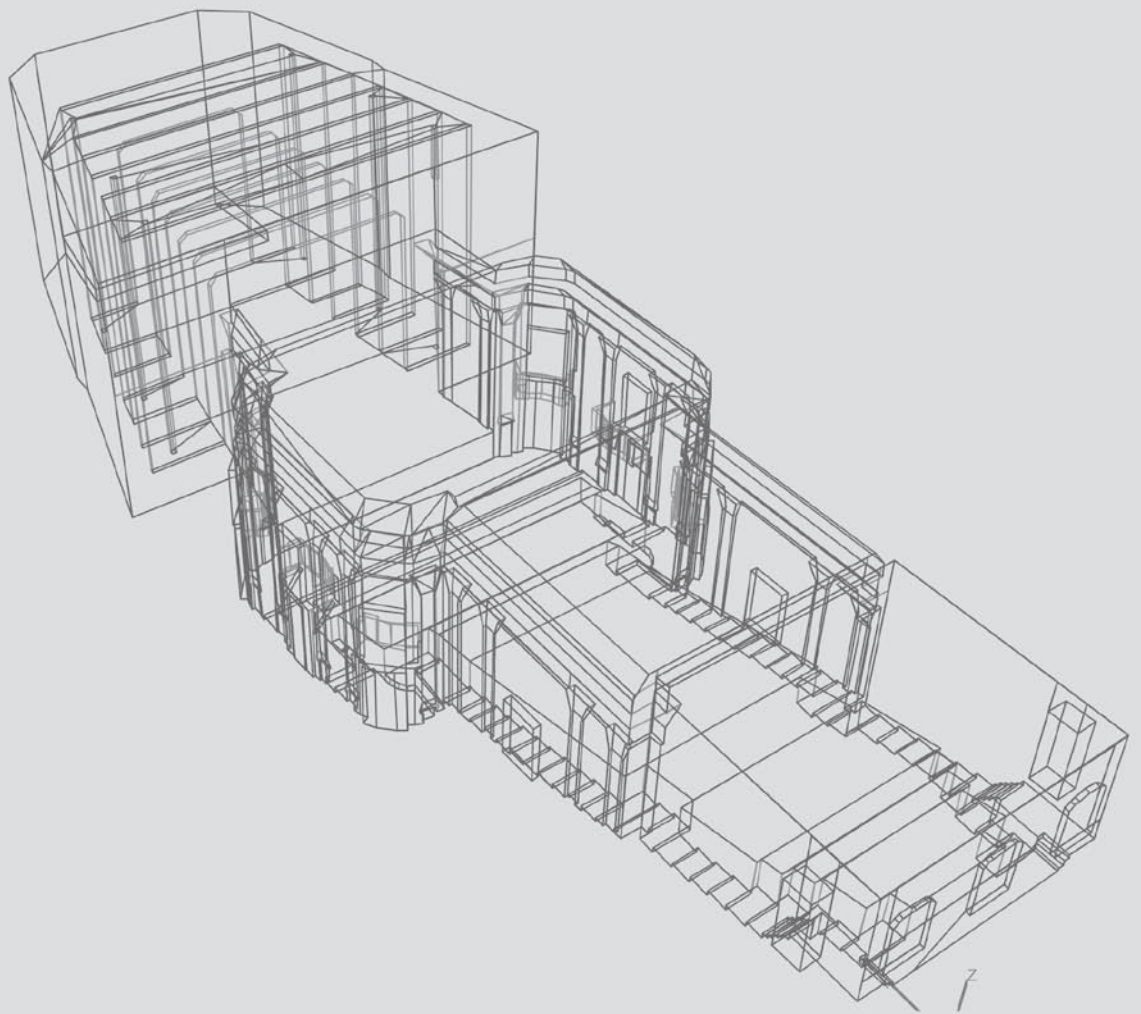


Figure 5. Required distance for STI to drop below 0,50 (distraction distance r_p) for different design criteria (98% of time corresponding to mean value+2*st.dev.. 85% of time corresponding to mean value+1*st.dev. or 50% of time corresponding to the mean value of measured noise levels).

and divides different areas in the working space. This results in a corresponding spatial decay of about 8 dB assuming that acoustic absorption is provided in ceiling and/or wall absorption. Another possibility is to create zones varying from silent to more interactive. Activity-based work provides the possibility of reducing the design distance between work departments (working groups) as seen in Figure 5. The bars corresponding to specific office tasks show a smaller standard deviation. Because of this a much smaller design distance is required. To achieve a distraction distance r_D (STI < 0.50 for 98% in time, a design distance is needed of about 23 metres in a mixed tasks office. In a specific task office this distance decreases to about 17 metres.

7. REFERENCES

- [1] International Organization for Standardization. ISO 3382-3:2012 Acoustics –Measurement of room acoustic parameters– Part 3: Open plan offices, Geneva, Switzerland.
- [2] Jahncke H., Hongisto V., Virjonen P. (2013). Cognitive performance during irrelevant speech: Effects of speech intelligibility and office-task characteristics, *Applied Acoustics* 74, 307-316, faculty of Engineering and Sustainable Development of University of Gävle, Gävle, Sweden, Finnish Institute of Occupational Health, department of Psychology of University of Turku, Turku, Finland.
- [3] Persoon S.A., Höngens Th. (2013). Modeling acoustics as a powerful design tool for open plan offices, proceedings IBPSA 2013, Aalsmeer, The Netherlands.
- [4] CATT 2012. CATT-Acoustic™ v9.0c, Gothenburg, Sweden.
- [5] Keränen J., Hongisto V. (2013). Prediction of the spatial decay of speech in open-plan offices, *Applied Acoustics* 74, 1315-1325, Indoor Environment Laboratory of Finnish Institute of Occupational Health, Turku, Finland.
- [6] Haapakangas A., Hongisto V., Hyönä J., Kokko J., Keränen J. (2014). Effects of unattended speech on performance and subjective distraction: The role of acoustic design in open-plan offices, *Applied Acoustics* 86, 1-16, Indoor Environment Laboratory of Finnish Institute of Occupational Health, department of Psychology of University of Turku, Turku, Finland.
- [7] Chigot, P. (2005). Effects of sound in offices – subjective experience vs. objective assessment, *Facilities*, Vol. 23 Iss: 3/4, 152-163, Ecophon, Hyllinge, Sweden.
- [8] Jackson T. S., Irrelevant speech, verbal task performance, and focused attention: A laboratory examination of the performance dynamics of open-plan offices. (1999), *The Sciences and Engineering*, Vol 60(6-B): 2997.
- [9] Kjellberg A., Landstroem U., Tesarz M., Soederberg, L. et-al (1996). The effects of nonphysical noise characteristics, ongoing task and noise sensitivity on annoyance and distraction due to noise at work, *Journal of Environmental Psychology*, Vol 16(2): 123-136.
- [10] Tang S. K. (1997). Performance of noise indices in air-conditioned landscaped office buildings, *Journal of the Acoustical Society of America*, Vol 102(3): 1657-1663.
- [11] Knudsen V.O., Harris C.M. (1978). Acoustical designing in architecture, *Acoustical Society of America*, United States of America.
- [12] De Croon E., Sluiter J., Kuijer P.P., Fings-Dresen M. (2005). The effect of office concepts on worker health and performance: a systematic review: a systematic review of the literature, *Ergonomics* 48:2, 119-134, Coronel Institute for Occupational and Environmental Health, Academic Medical Center, Research Institute Amsterdam for Health and Health Care Research (AmCOGG), Amsterdam, The Netherlands.
- [13] Kaarlela-Tuomaala A., Helenius R., Keskinen E., Hongisto V. (2009). Effects of acoustic environment on work in private office rooms and open-plan offices – longitudinal study during relocation, Indoor Environment Laboratory of Finnish Institute of Occupational Health, department of psychology of University of Turku, Turku, Finland.



The ballistic wave, from rifle bullet to Apollo command module

Jean Varnier and Frédéric Sourgen

ONERA, Dept. DSNA / Dept. DMAE, France

Corresponding Author: jean.varnier@onera.fr

PACS: 43.25.Cb, 43.28.Mw

ABSTRACT

The ballistic wave is a shaking generated by a solid body moving at supersonic velocity in the atmosphere. To human hearing, it is heard as a crack for small projectiles, as a detonation (sonic boom) for large-sized bodies. Their common signature is an N-shaped profile giving pressure in function of time, the formalism of which is known. But this formalism presents a practical difficulty, namely the calculation of a “volume function” for the mobile in question: we present an option for that calculation in the classical case of projectiles shot from small-calibre firearms (Camp Irwin, California, USA, 1944). Besides, that formalism has to be adapted for any object the diameter of which is bigger than length, which is the case of the Apollo Command Module during its reentry into the atmosphere above the Pacific Ocean. Measurements of sonic boom were carried out aboard US Navy ships during reentries of Apollo 15 and Apollo 16 Command Modules. These measurements constitute a very interesting data base in order to test, in cases of high altitude and high Mach number, the results given by a model of fluid mechanics and a model of nonlinear propagation in the one hand, by an analytical semi-empirical model on the other hand.

1. INTRODUCTION

The ballistic wave generated by a projectile moving at supersonic velocity was the subject of experimental studies from the end of 19th century and the beginning of 20th Century [1-2]. A semi-empirical theory enabling to calculate this shock wave was developed during World War II and after this war [3-6]. The theory was later extended to aircraft in order to foreknow the intensity of sonic boom, for instance when supersonic jets such as the French airliner *Concorde* or the USAF’s strategic reconnaissance plane SR-71 *Blackbird* were put into service [7-9]. However, small-calibre projectiles are the subject of recent studies, in mind for their operational detection and location [10-11]. On the other hand, the sonic boom generated by solid bodies entering the upper atmosphere was the subject of experimental studies [12-13]. In this case, classic physical models are on the very borderline of their application domain. We are interested in those uppermost cases that are in fact simulated by the same semi-empirical code. The study is completed by computations performed with the help of the ONERA’s CFD code CEDRE, giving pressure and velocity profiles around the Apollo Command Module moving at high altitude and at high Mach number.

2. BALLISTIC WAVE OF A PROJECTILE

2.1. Theory

For human hearing, the ballistic wave generated in the atmosphere by a body such as a rifle bullet moving at supersonic speed (Fig. 1) is perceived as a sharp snap similar to a whip crack when the projectile is passing by. The wave corresponds to a shock wave bordered with a sudden overpressure in front of the wave and a sudden underpressure at its rear part, hence the generic denomination “N-wave” given to the time signal (see Fig. 2, on the left). This profile can be characterized by two parameters: pressure amplitude ΔP and going past duration ΔT . Their values at a given distance from the projectile path can be calculated with the help of a semi-empirical formalism [4-6]. Dimensions and shape of the projectile are introduced by the Whitham function (also called “volume function”) the integral I_w of which, used in order to calculate ΔP and ΔT , is given by:

$$I_w = \int_0^L ds \frac{1}{2\pi} \int_0^s \frac{S''(x)}{\sqrt{s-x}} dx \quad (1)$$

where $S(x)$ is the cross-section of the mobile at abscissa x and L is its length (see Fig. 3), s being an integration parameter. It should be

noted that the complex formulas giving the values of ΔP and ΔT also refer to the Mach number of the mobile and to the ambient atmospheric conditions. In Ref. [11-12], Equation (1) is implicitly replaced by the following formula:

$$I_w = \frac{R^2}{\sqrt{L}} \tag{2}$$

where R is the projectile radius and L its overall length. A calculation of I_w performed at the ONERA with the parabolic shape of the nose cone shown in Figure 3 leads to the same formula, aside the fact that L is replaced by the length H of the ogival part of the bullet. Moreover the calculation shows that a sharp shape of the nose (similar to that of Fig. 1) generated by an arc of parabola, R and H remaining unchanged, increases the value of I_w given by Equation (2) only slightly.

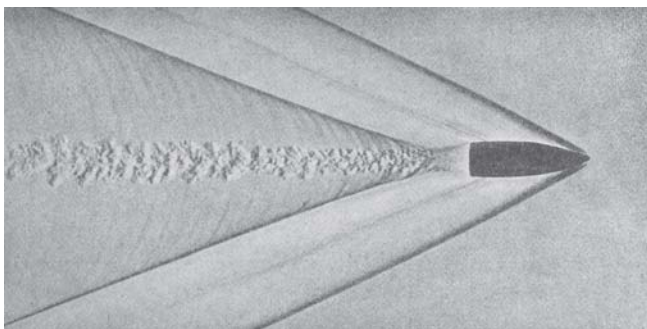


Figure 1. Shock wake from a rifle bullet [2].

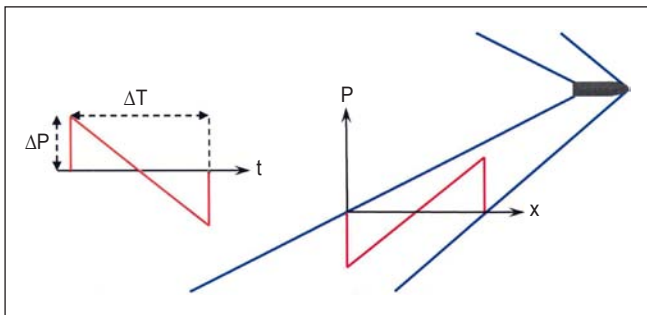


Figure 2. Time profile and space profile of the N-wave.

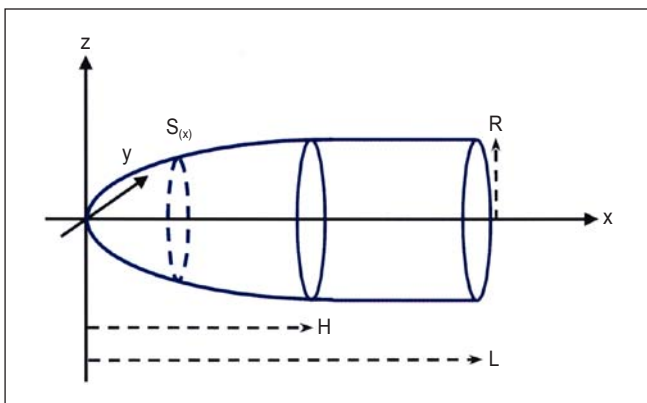


Figure 3. Geometry of a projectile to calculate the Whitham function.

2.2. Application

We refer to experimentations performed at Camp Irwin, California, in November 1944. They provided the data base used in Ref. [4]. The following calibres were tested: 7.62 mm (.30 inch), 12.7 mm (.50 inch), 20 mm and 40 mm. All these calibres were in standard service in U.S. Army at this time. Unhappily full test data are available for two calibres only, 12.7 mm and 40 mm. The study of corresponding firearms and ammunitions led us to consider the following initial velocities for projectiles: 880 m/s (Mach 2.58) for 12.7 mm calibre, 854 m/s (Mach 2.50) for 40 mm calibre. To perform the calculations, we have chosen the ambient pressure and temperature which correspond to the CIRA/COSPAR statistical atmosphere for the month of November, latitude 35° North, height 750 m over sea level. We have supposed that the fly-by speed of the projectiles during the experiments was roughly equal to their muzzle velocity.

The shapes of 12.7 mm bullet and of 40 mm shell are taken into account in order to calculate the values of integral (2) and of the theoretical parameters of the N-wave.

As experimental values of pressure peak ΔP and of fly-by duration ΔT of the ballistic wave, we adopt the averages determined by Du Mond et al. [4] out of several test shoots. It is important to notice that the amplitude ΔP is a datum less reliable than the duration ΔT for two reasons:

- at short distances, the nonlinear effects lead to an important decreasing in pressure according to the distance, a fact which is not reported by the far-field formalism used;
- Du Mond points out that there are sound reflection effects on the ground which are not quantified in his analysis.

These two types of effect tend to increase the amplitude of ballistic wave in comparison with theoretical calculation. In contrast, their influence on the ballistic wave duration seems to be negligible.

For the fly-by duration DT of the ballistic wave at various measurement distances, comparison of computed values to measured values (with use of the ONERA's code JAZZ that applies the Whitham's theory with some simplifications) is shown in Fig. 4 for two calibres, 12.7 mm and 40 mm. As a general rule, the similarity is very satisfactory, as it is also with calculations performed by Du Mond et al., who used a more or less similar formalism.

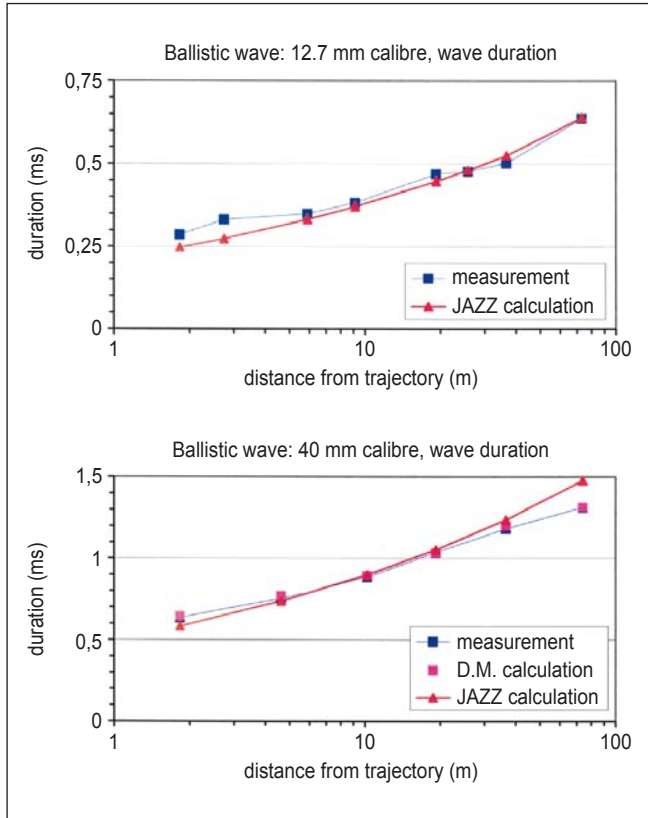


Figure 4. Comparison between computed and measured values for ΔT .

The same comparisons are done for the pressure peak ΔP in Fig. 5 - unhappily no reproduction of any actual recording is found in [4]. As expected, the differences between calculation and measurement are clearly greater, but we have to note that:

- these differences decrease when the distance increases;
- for the same distance, these differences are greater for the 40 mm calibre than for the 12.7 mm calibre.

The former remark is easy to explain by the decreasing of nonlinear effects, in particular decreasing of thermal dissipation, when we go away from the projectile path. The latter remark has the same cause, in relation with the calibre of projectiles to which the distances have to be related: thus 4 meters is equivalent to 315 calibres for the 12.7 mm bullet, but only to 100 calibres for the 40 mm shell.

We transferred to both Figures 5, linked up with calibres 12.7 mm and 40 mm respectively, the amplitudes calculated from the measured durations by the way of Equation (3) - so-called “reverse calculation”. Obviously, it gets closer to simulations, because this calculation cancels both nonlinear effects and effects of reflection on the ground at once. Note that the ratio $\Delta T/\Delta P$ removes the common factor $I_w^{1/2}$ in the formalism, and

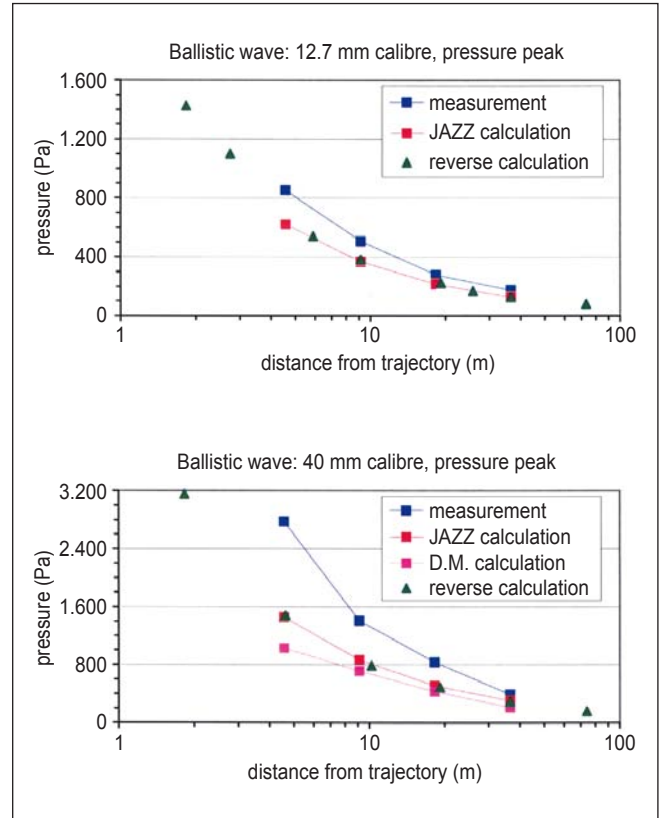


Figure 5. Comparison between computed and measured values for ΔP .

therefore is independent of the geometry of the projectile. We have indeed after simplification:

$$\frac{\Delta T}{\Delta P} = \frac{2}{P_0} \frac{\gamma + 1}{\gamma c_0} \frac{M}{\sqrt{M^2 - 1}} r \tag{3}$$

where r is the distance to the bullet trajectory, M is the Mach number, P_0 , c_0 and γ being ambient data (pressure, sound speed, air specific heat ratio).

3. SONIC BOOM OF APOLLO COMMAND MODULE

3.1. Simplified approach

The sonic boom of aircraft is a large-scale ballistic wave which is perceived as a violent detonation for human hearing, in particular if focusing occurs - do not confuse with the double-bang, the causes of which are different. The theory applied is identical to the theory of ballistic wave of projectiles, except the introduction of a “lift function” to take into account the effects of incidence, what increases the amplitude of the corresponding N-wave. Note that often a dissymmetry appears between the “positive” and “negative” parts of the amplitude: for instance, the Figure 6 shows the recording of a focused sonic boom due to the acceleration of an aircraft in horizontal flight [14].

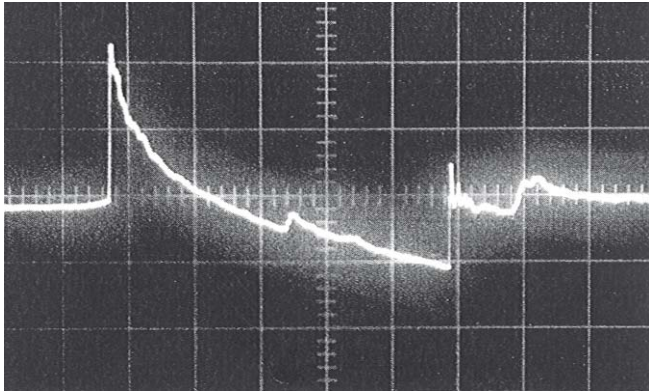


Figure 6. Sonic boom from a fighter Mirage III [14].

The case of sonic booms arisen from Apollo Command Modules during their reentry into the atmosphere above the Pacific Ocean [12-13] is different: indeed, velocities and altitudes have magnitude beyond usual limits of the model (Mach 3 at 26,000 m high at the most for SR-71), and a lift effect is generated by the incidence of the vehicle in reference to the velocity vector (about 20°). The problem that arises for the modelling is linked up to the particular shape of Apollo Command Module, a shape that has nothing in common with the one of a bullet or of an aircraft: 3.4 m high for 3.9 m in diameter (Fig. 7).

In order to calculate the Whitham's integral I_w for the heat shield, we suppose that its shape is generated by an arc of parabola: note that H replaces L in Equation (2).

On the other hand, some computations of fluid mechanics (ONERA's code ELSA) and of nonlinear propagation (NASA's code TRAPS [15]) concerning the influence of the length of a mobile on the N-wave duration DT showed that this duration had to be corrected by the following factor:

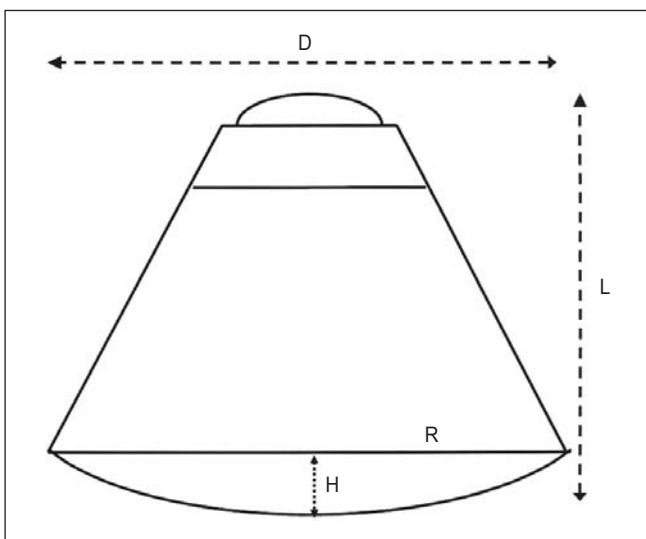


Figure 7. Apollo Command Module [12].

$$F_{(\Delta T)} = \left(\frac{L}{8D} \right)^{1/4} \quad (4)$$

where L is the overall length and D the diameter of the mobile.

Note that the value of this corrective factor would be close to one for the "slender body" which served as reference for the Whitham's theory [5], what can be accepted for firearm projectiles in general, because of the cap effect which widens the projectile wake (see Fig. 1).

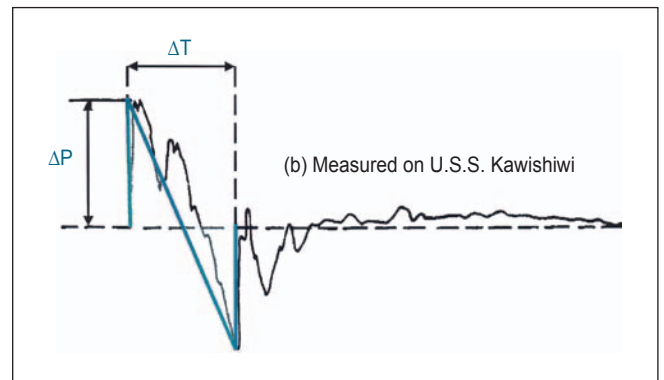


Figure 8. Recorded sonic boom signal [12], equivalent N-wave.

Moreover, a factor of reflected field equal to two has to be brought to amplitude ΔP when sensors are put on the ground, in this case the deck of US Navy's ships stationed under the reentry trajectory of the spacecraft.

The signals recorded on the ships have an irregular form very probably due to the reflection on the sea surface of the incident wave: see the double peak of "positive" and of "negative" pressure in Fig. 8. Following this hypothesis, parameters $[\Delta P, \Delta T]$ of an equivalent N-wave were correctly determined in the NASA's papers.

The Whitham's formalism is valid for a homogeneous atmosphere only (i.e. at a constant altitude), but the parameters of N-wave can be computed by taking into account ambient conditions of temperature and pressure prevailing in altitude and at sea level [16]. Table 1 shows the result of simulations from JAZZ code compared to measurements of sonic booms from Apollo 15 and Apollo 16 flights: for every flight point the altitude and Mach number of which are specified, we give the ratio ΔP computed to ΔP measured for amplitude, and the ratio ΔT computed to ΔT measured for duration.

We can see that the error does not exceed $\pm 30\%$ for the amplitude ΔP and $\pm 10\%$ for the duration ΔT , with mean ratios close to one, which can be considered as a good result for a semi-empirical code, considering

Table 1. Comparisons calculation-measurements for Apollo’s sonic booms.

US Navy ship	Altitude (m)	Mach number	Ratio of ΔPs	Ratio of ΔTs
USS Genesee	52,500	15.9	0.8	0.9
USS Ponchatoula	44,400	9.8	0.7	1.0
USS Kawishiwi	33,400	4.6	1.3	1.2
USS Okinawa	28,900	3.1	1.0	1.2
USS Ticonderoga	27,600	2.6	1.3	1.2
Average ratio			1.0	1.1

the simplifications carried out (neither incidence nor lift effect). Note that here the “short-body correction” of Equation (4) plays an important role in the calculation of the N-wave duration.

3.2. Numerical approach

Geometry of Apollo Command Module and considered flight points

The Command Modules CM112 and CM113 of Apollo flights 15 and 16 are identical, but their precise geometry was not published. The Apollo 6 Command Module - geometry available in [17], including the radius of curvature at the junction of the spherical cap with the conical part (see Fig. 9) - well reproduces the characteristics of CM112 (Apollo 15) and CM113 (Apollo 16). Possible differences, of the order of 1 millimeter or 0.5 degree, will not act upon Navier-Stokes computations focused on the wake.

Two points of flight corresponding to the recorded sonic booms have been selected:

- for Apollo 15: $z = 52.5$ km, $M = 16$, $T = 268$ K, $P = 58.4$ Pa;
- for Apollo 16: $z = 44.1$ km, $M = 9.6$, $T = 272$ K, $P = 186$ Pa.

For the reentry of Apollo 16 Command Module, some meteorological measurements from instrumentation carried aboard a sounding rocket are given in [13]. For the Apollo 15 mission, we have based our argument on the US 1976 Standard Atmosphere model.

Preliminary analysis

In order to run Navier-Stokes computations, the essential point is to know the gas thermochemical state

and the most appropriate physical model in order to describe such a state. According to the dissociation parameter, i.e. the product of upstream volumetric mass density ρ by reference length L_{ref} , one may foreknow that thermochemical state at the stagnation point by analogy with the study of R.N. Gupta et al. [18] about stagnation point on a sphere. Figure 10 shows the result of this analogy (the dissociation parameter is conserved): the studied cases Apollo 15 and 16 are both in a domain where the five chemical species are existing when the air is assumed in thermochemical equilibrium at the stagnation point.

Downstream, when the gaseous expansion is passing at the junction of the heat shield with the conical part and in the wake, these species can recombine occasionally, but the maximal number of species shall remain equal to five. However, it is not possible to assume that the flow remains at thermochemical

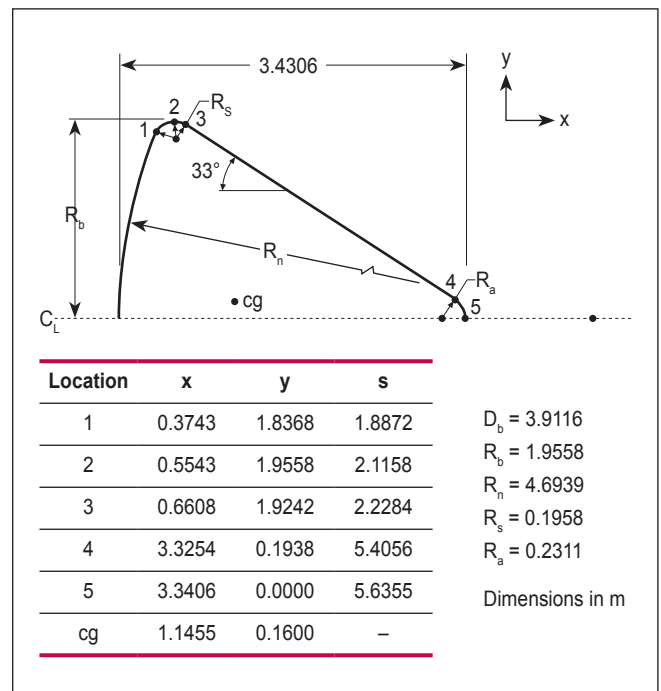


Figure 9. Geometry of the Apollo 6 Command Module [17].

equilibrium downstream, because kinetics of chemical recombination achieves finite values. However, a set of adapted chemical kinetics can be selected (Park's 5-species model).

Axisymmetrical analysis

Although both Command Modules were stabilized along their trajectories by a highly negative incidence (angle of attack included between -22° and -20° at the considered points of trajectory), an initial step to determine the best model for the thermochemical state of the gas consisted of doing a preliminary study supposing that the flow was axisymmetrical (i.e. without incidence).

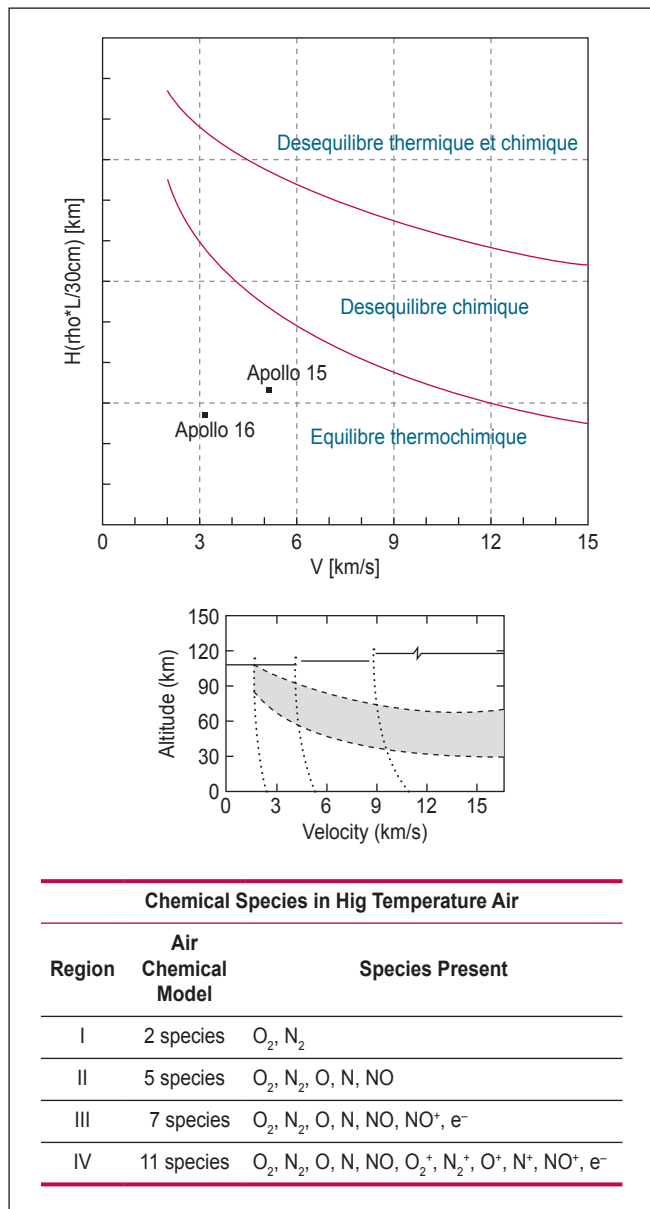


Figure 10. Thermochemical state of air at the stagnation point according to altitude, speed and aerodynamic parameters.

The results of the Apollo 15 case are shown in Figure 11. We compare Navier-Stokes computations assuming that the 5-species air mixture is either at chemical equilibrium or at chemical nonequilibrium (finite rate chemistry).

The stagnation region is noticed to achieve the chemical equilibrium with a good approximation. However we also observe, from the very start of the reduction in pressure and all along the central part of wake, that the temperature is clearly less high in case of computation in nonequilibrium state than in case of equilibrium assumption. From this observation we infer that the rates of chemical recombination (it releases energy to the air flow) cannot be considered as infinite. In particular, it has a consequence on the shape of shock and on the pressure field which is represented as cross-sections in Figure 12.

Note that the turbulence in the wake is taken into account by a model of Spalart and Allmaras. It modifies neither the shape of the shock nor pressure profiles, consequently the selection of the model does not matter much, but this selection is necessary to stabilize the flow in the central region of the wake (see

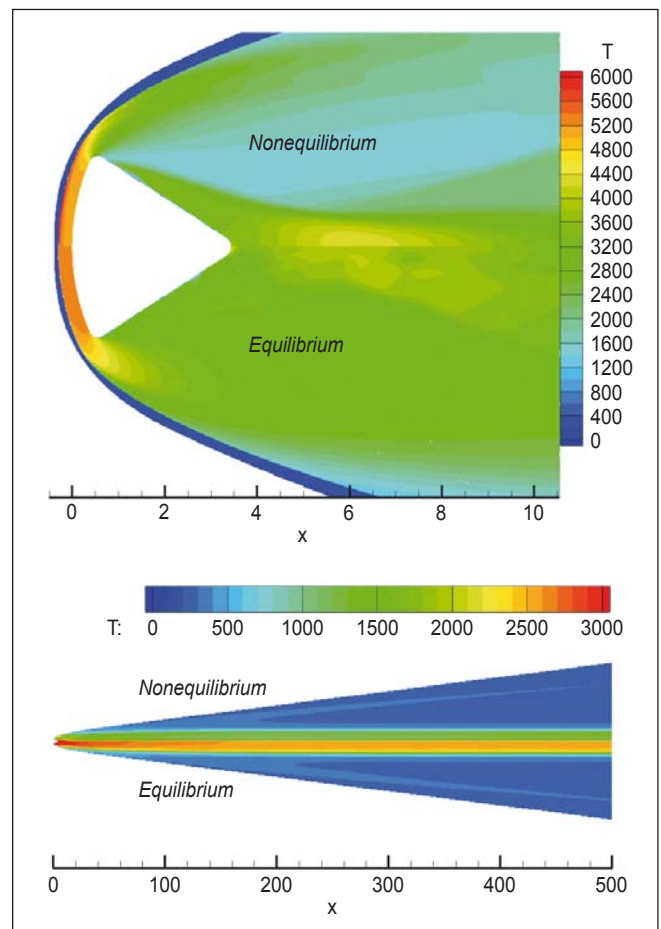


Figure 11. Comparison between Navier-Stokes computations (chemical equilibrium vs chemical nonequilibrium).

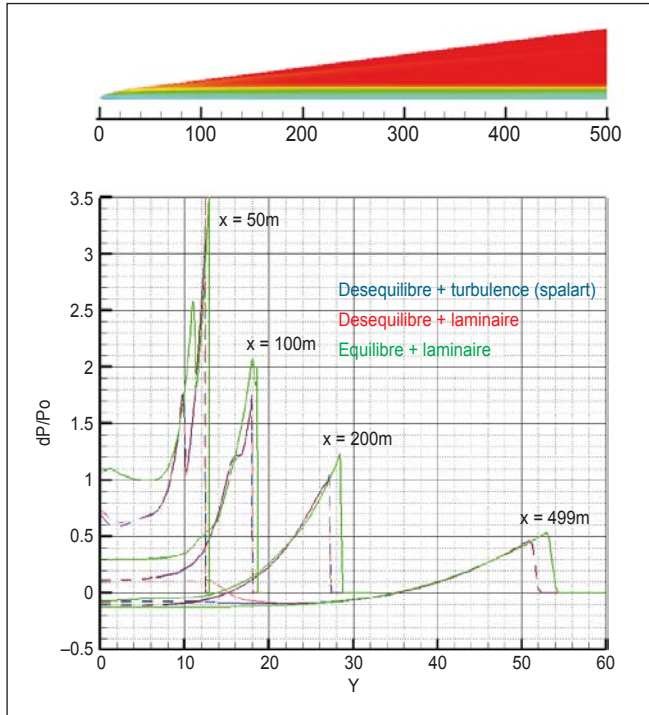


Figure 12. Vertical cross-sections of wake in pressure.

computation by half-wake in Figure 13). Moreover, Reynolds numbers achieved in the close and far wake increase sufficiently so as to admit, even considering a real gas hypersonic regime, there is established turbulence in this disturbed region. Note that the wake appears smoother in this case (Fig. 13, above).

Reconstructing of a sound source in 3D

The physical models selected could be identified in the cases of Apollo 15 and 16, as those of 5-species chemical equilibrium and 2-equations turbulence model. A 3D-mesh made up of parallelepipedic cells has been performed so as to catch the bow shock in the whole wake (for instance the location of the shock can be deduced by rotation from its position observed in axisymmetrical test case). Twenty six million cells

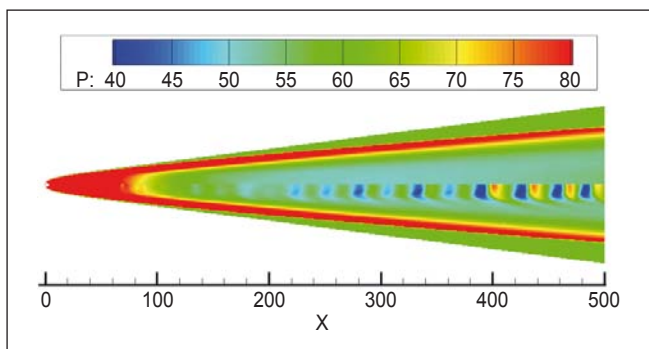


Figure 13. Navier-Stokes computation: half-wake in turbulent case (above), in laminar case (below).

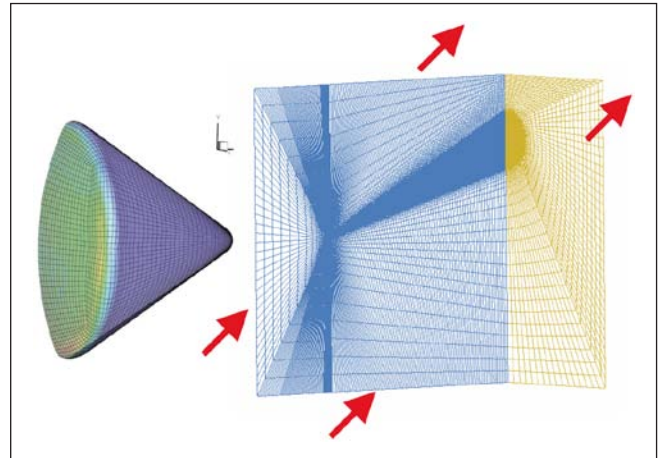


Figure 14. 3D mesh used for Navier-Stokes computations.

were necessary to catch the hypersonic flow field for three kilometers downstream from Apollo 15 Command Module. Actually, because the shock is highly tilted at hypersonic speeds, this distance is mandatory if the far field assumption has to be respected accordingly with a sound propagation computation. But a shorter wake (500 m long) was employed for the Apollo 16 case, due to a smaller Mach number at a lower height.

Such highly meshed computations are extremely unusual for real gas in the hypersonic domain, focusing mainly on the flow in the vicinity of the vehicle rather than in its far wake.

Longitudinal profiles of pressure extracted from 3D calculations and used as input data into the sound propagation computations are displayed in Fig. 16. A significant discrepancy is then observed between the usual supersonic N-wave profile and the present

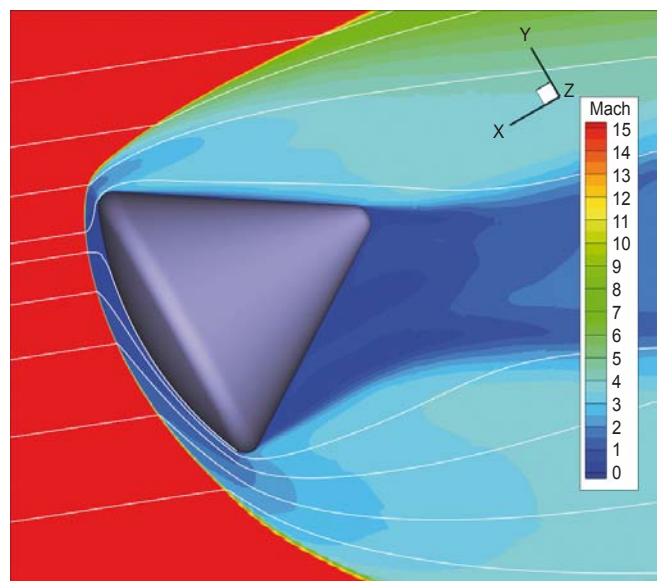


Figure 15. Navier-Stokes computation assuming both turbulent flow and chemical nonequilibrium.

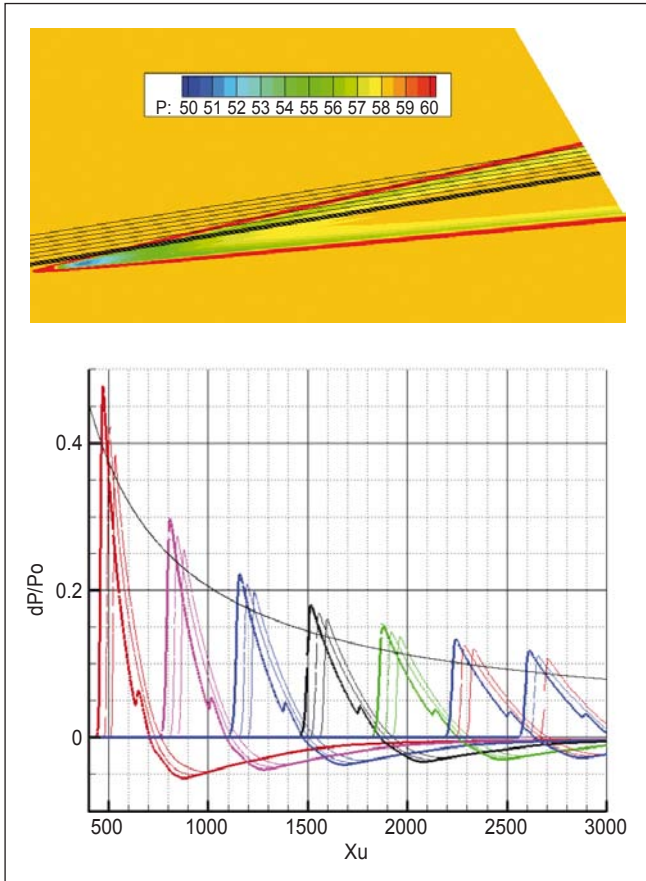


Figure 16. Apollo 15, longitudinal pressure profiles computation.

pressure profile, which tends towards the upstream value in an asymptotic way. Moreover, despite the high angle of attack and the expected 3D nature of the flow, the far-wake flow field is weakly asymmetrical regarding the pressure profiles.

Using the 20 m transversal profile (red curve in Figure 16) as input for the nonlinear propagation code TRAPS [15], we observe an intermediate shape of the propagated wave at first (Fig 17-1), then a return to the N-shape at sea level (Fig. 17-2). As a matter of fact, an intermediate shape was recorded actually (see Fig. 18), but this shape is also understandable by a wave reflected on the sea surface which arrives a small delay after the direct wave. The computation of Figure 17-2 provides the right global amplitude $[\Delta P^+ + \Delta P^-]$, but it clearly overestimates the duration of the observed N-wave. We can think that the nonlinear propagation used is not well adapted to the physics of high atmosphere.

In Fig. 19 is represented the result of the simulation by means of the semi-empirical model JAZZ (see Table 1, line USS “Genesee”), by adding to the calculated N-wave another N-wave reflected on the surface of the sea, of same duration but of amplitude one half: indeed the reflected wave arrives on the sensors with a grazing incidence. The delay has been calculated by

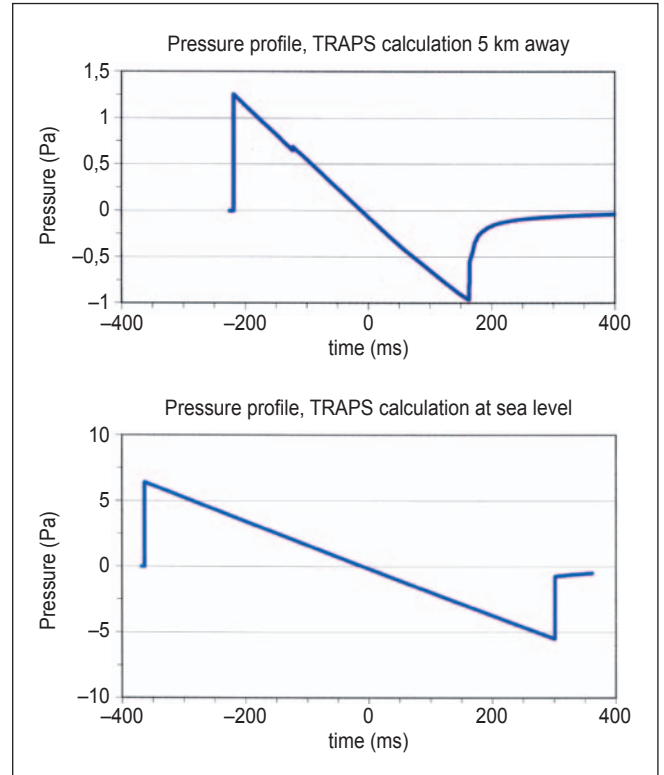


Figure 17. Computed N-waves by the NASA's code TRAPS [15] at 5250 m from the Command Module (above) and at sea level (below).

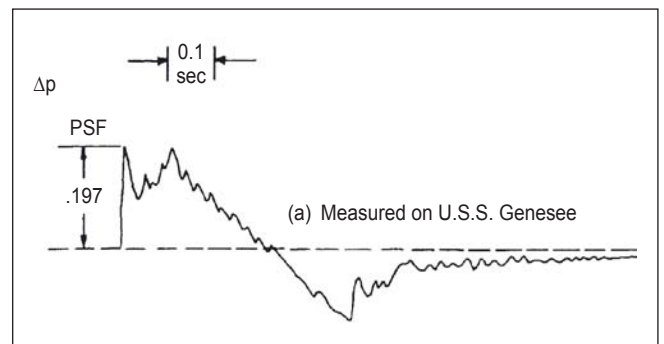


Figure 18. Sonic boom from Apollo 15 flying at 52 km in height recorded at sea level [12].

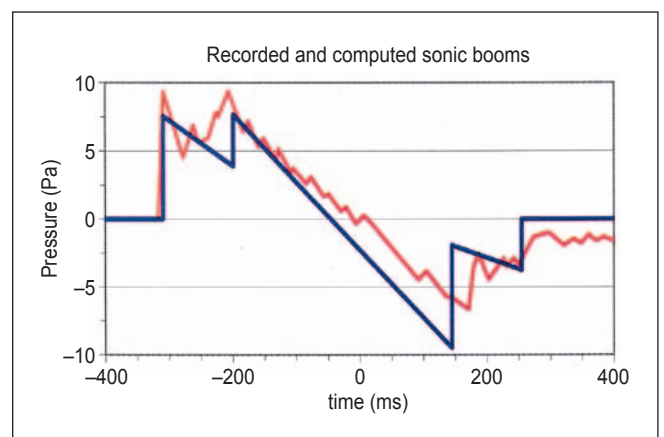


Figure 19. Simulation of the signal received aboard USS “Genesee”, by taking into account a sound reflection on the sea surface.

taking into account the height of the ship, knowing that the sensors are put on the deck.

4. CONCLUSION

We showed two possible approaches in order to calculate a ballistic wave and a sonic boom. Our former approach requires classic models of semi-empirical type, while the latter requires heavy computation codes of fluid mechanics (CEDRE code) and of sound propagation (TRAPS code). In the latter case, a thorough study was carried out in order to find the physical approach that is the best adapted to high altitude. In the vicinity of Apollo Command Module, the CFD code CEDRE does not give a classical N-wave, but a half-alternation followed by an asymptotic return to the ambient pressure. At sea level, a nonlinear propagation restored a classic N-shaped profile with a correct amplitude, the duration of signal observed being overvalued.

It is interesting to notice that the semi-empirical model JAZZ can be utilized with success in the Apollo case, in spite of unusual conditions of height and speed for this type of model. For the N-wave duration, we apply a “short-body correction” which does not appear in the Whitham’s theory. The simulation of the actual signal recorded at sea level can be improved by taking into account the sound reflection on the surface of the sea.

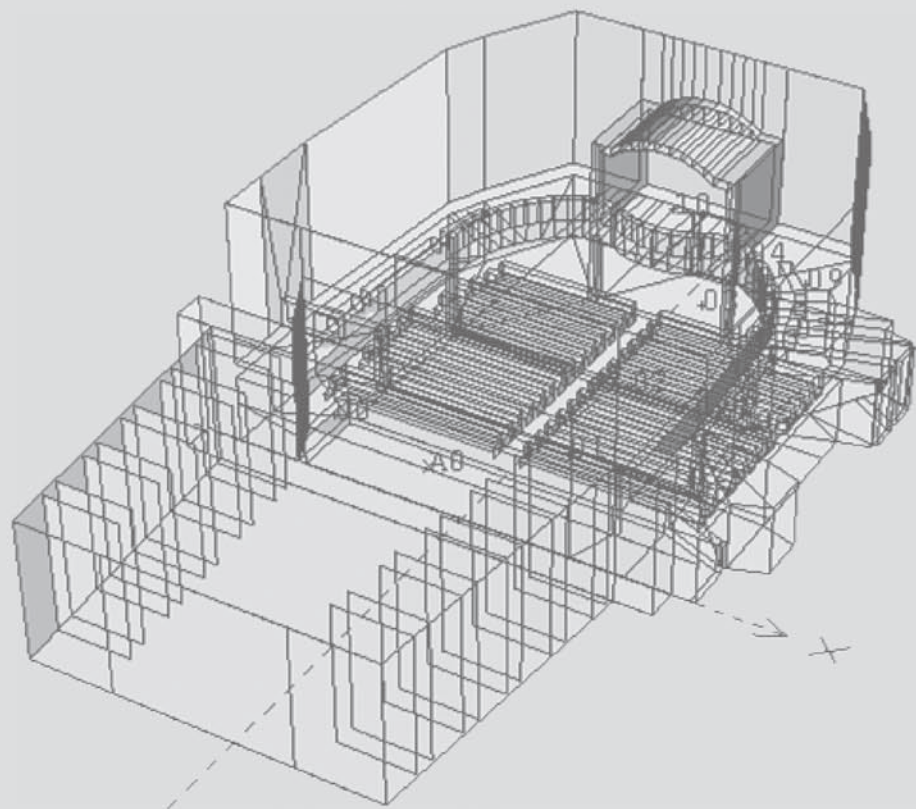
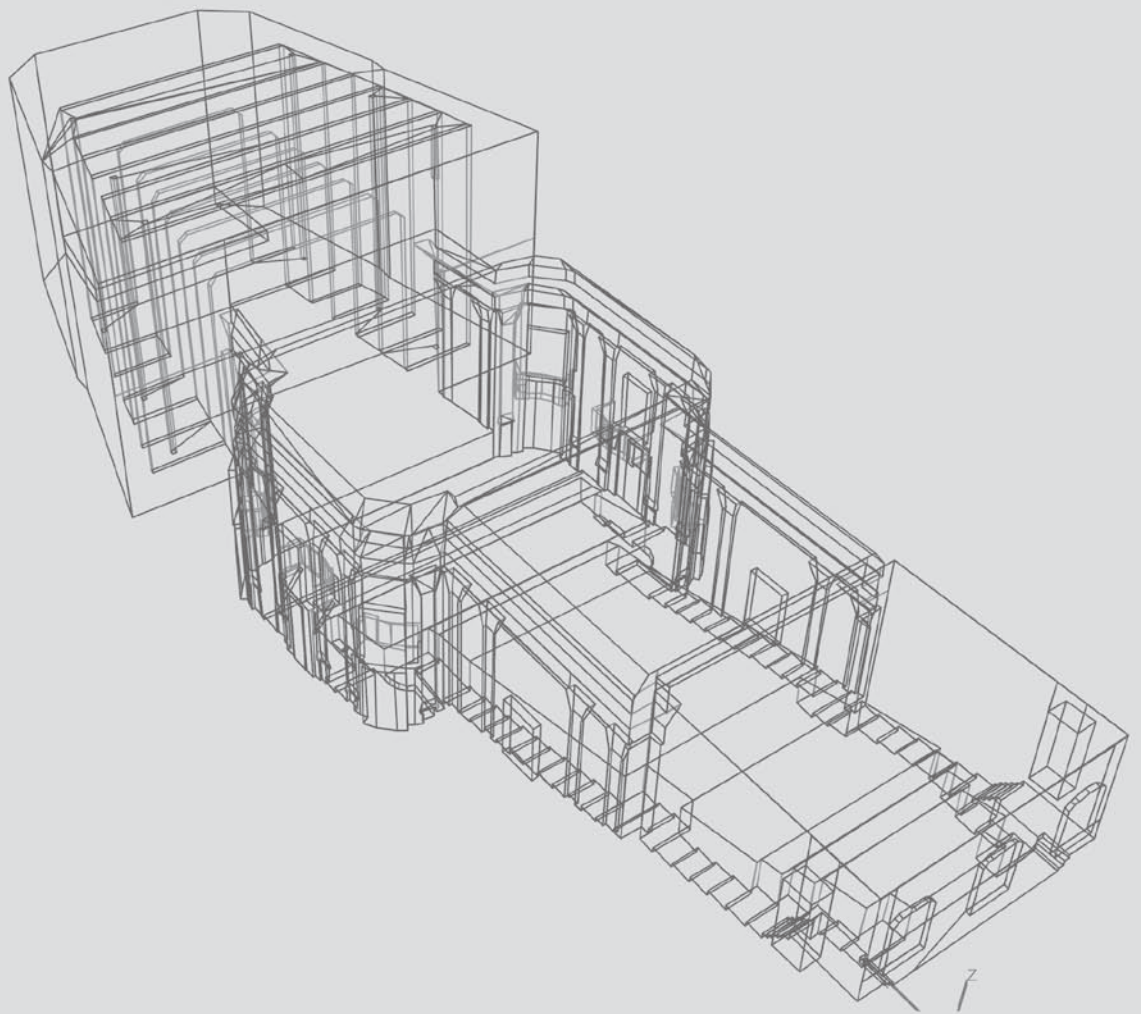
5. ACKNOWLEDGEMENTS

This work arises from the communication “L’onde balistique, de la balle de fusil au module Apollo” presented by J. Varnier and F. Sourgen (ONERA) during the French Congress of Acoustics CFA 2014, Poitiers, France, 22-25 April 2014.

The authors greatly appreciate Mr. Alexandre Alexieff, Consultant Engineer, for his helpful collaboration, as well as Dr. Jean-Luc Vérant, Head of Research Unit TACT, Dept. DMAE, ONERA, Toulouse, France.

6. BIBLIOGRAPHY

- [1] E. Mach, *Photographische Fixierung der durch Projectile in der Luft eingeleiteten Vorgänge*, Akademie der Künsten und Wissenschaften, Vienna, (1887).
- [2] P. Charbonnier, E. Esclangon, *Etude cinématique du champ acoustique d’un projectile. L’acoustique des canons et des projectiles*, Mémorial de l’Artillerie Française, tome IV, 3ème fascicule (1925).
- [3] L.D. Landau, *On shock waves*, J. Phys. Acad. Sciences URSS 6, pp. 229-301 (1942).
- [4] J.W.M. Du Mond, E.R. Cohen, W.K.H. Panofsky, and E. Deeds, *A determination of the wave forms and laws of propagation and dissipation of ballistic shock waves*, J. Acoust. Soc. Am., Vol. 18, No. 1, pp. 97-118 (1946).
- [5] G.B. Whitham, *The behaviour of supersonic flow past a body of revolution, far from the axis*, Proceedings of the Royal Society of London, Serie A, 201, pp. 89-109 (1950).
- [6] G.B. Whitham, *The flow pattern of a supersonic projectile*, Communications on pure and applied mathematics, Vol. V, No. 3, pp. 301-348, (1952).
- [7] M. Schaffar, G. Parmentier, A. Dancer, M. Froböse, *Revue et synthèse de l’ensemble des travaux effectués sur le bang sonique, en particulier à l’ISL 1961-1974*, Rapport 40/74, Institut Saint-Louis (1998).
- [8] S.R. Norris, E.A. Haering Jr., and J.E. Murray, *Ground-based sensors for the SR-71 sonic-boom propagation experiment*, NASA TM 104310 (1995).
- [9] L.G. Ivanteyeva, V.V. Kovalenko, E.V. Pavlyukov, L.L. Teperin, and R.G. Rackl, *Validation of sonic boom propagation codes using SR-71 flight test data*, J. Acoust. Soc. Am., Vol. 111, No. 1, pp. 554-561 (2002).
- [10] R. Stoughton R., *Measurements of small-caliber ballistic shock waves in air*, J. Acoust. Soc. Am., Vol. 102, No. 2, Part 1, pp. 781-787 (1997).
- [11] B.M. Sadler, T. Pham, L.C. Sadler, *Optimal and wavelet-based shock wave detection and estimation*, J. Acoust. Soc. Am., Vol. 104, No. 2, pp. 955-963 (1998).
- [12] D.A. Hilton, H.R. Henderson, and R. Mc Kinney, *Sonic-boom ground-pressure measurements from Apollo 15*, NASA TN D-6950 (1972).
- [13] H.R. Henderson and D.A. Hilton, *Sonic-boom ground-pressure measurements from the launch and reentry of Apollo 16*, NASA TN D-7606 (1974).
- [14] J. Vallée, *Opération Jéricho-Focalisation. Mesure de l’intensité des bangs soniques engendrés par un avion volant en palier accéléré*, Rapport d’études N° 272 du Centre d’Essais en Vol (1967).
- [15] A.D. Taylor, *The TRAPS sonic boom program*, NOAA TM ERL ARL-87, Air Resources Laboratories (1980)
- [16] J. Varnier, *Sonic boom, jet noise and Doppler effect*, Acoustics in practice, EAA, Vol. 1, No. 2, pp. 7-15, (2013).
- [17] *Apollo 6*, 9th AIAA/ASM Thermophysics and Heat Transfer Conference, San Francisco, CA (2006).
- [18] R.N. Gupta, J.M. Yos, and I.A. Thompson, *A Review of Reaction Rates and Thermodynamic and Transport Properties for the II-Species Air Model for Chemical and Thermal Nonequilibrium Calculations to 30,000 K*, NASA TM 101528 (1989).



Acoustics in Practice

The members of the initial editorial board are shown in the table below. New members will be added to the board to provide expertise in topic areas not sufficiently represented by the current members of the board. It is also hoped to widen the geographical spread of the board to include members from more EAA societies.

Editorial board

Name	Country	Topic
Colin English (Editor in Chief)	UK	Environmental noise and nuisance
Miguel Ausejo	Spain	Noise mapping
Arild Brekke	Norway	Building acoustics and railways
Jean-Pierre Clairbois	Belgium	Noise barriers
Victor Desarnaulds	Switzerland	Building and room acoustics
Klaus Genuit	Germany	Vehicle design
Laurent Gagliardini	France	Automotive vehicle NVH
Bart Ingelaere	Belgium	Standards for buildings
Janusz Kompala	Poland	Noise and vibration control
Maria Machimbarrena	Spain	Standards for buildings
Andrew McKenzie	UK	Environmental noise: Wind farms
Henrik Moller	Finland	Auditorium acoustics
Tønnes A. Ognedal	Norway	Offshore oil/HSE
Alexander Peiffer	Germany	Aircraft design
Patrick Van de Ponsele	Belgium	Product design and testing
Søren Rasmussen	Denmark	Environmental noise
Monika Rychtarikova	Slovakia	Building acoustics
Rui Riberio	Portugal	Industrial noise



European Acoustics Association – EAA

Comprising 33 national acoustical associations:

- Austria (AAA) • Belgium (ABAV) • Bulgaria (NSA) • Croatia (HAD) • Czech Republic (CAS)
- Denmark (DAS) • Finland (ASF) • France (SFA) • FYROM (MAA) • Germany (DEGA)
- Greece (HELINA) • Hungary (OPAKFI) • Iceland (IAA) • Israel (IAA) • Italy (AIA) • Latvia (LAA)
- Lithuania (LAS) • Morocco (MSA) • Norway (NAS) • Poland (PTA) • Portugal (SPA) • Romania (SRA)
- Russia (PAO) • Serbia (ASY) • Slovakia (SKAS) • Slovenia (SDA) • Spain (SEA) • Sweden (SAS)
- Switzerland (SGA-SSA) • The Netherlands (NAG) • Turkey (TAS) • Ukraine (UGA) • United Kingdom (IoA)

Serving more than 8500 individual members in Europe and beyond

The European Acoustics Association (EAA) is a non-profit entity established in 1992 that includes in its membership national acoustical societies interested in to promote development and progress of acoustics in its different aspects, its technologies and applications. The main objectives of the EAA are to:

- promote and spread the science of acoustics, its technologies and applications, throughout Europe and the entire world
- interface with associations whose activities are related to acoustics
- establish contacts across member associations and other public and private bodies
- promote the formation of national acoustical societies in European countries where these do not exist, and to support and strengthen activities of existing national associations, respecting the principle of subsidiarity
- publish a European journal on acoustics, in printed as well as in electronic format
- organize and promote congresses, publish books and monographs, and engage in all those activities that are connected with the diffusion, promotion and development of acoustics
- establish agreements for collaboration with European and international entities in order to better serve the objectives of EAA
- stimulate education activities and platforms in acoustics at all educational levels, both academic and professional
- promote and divulge the establishment and implementation of norms and recommendations in the various fields of acoustics

EAA is democratically organized (one vote per country) with a general assembly, a board and an executive council.

EAA web

www.euracoustics.org

EAA contact (General Secretary)

secretary@european-acoustics.net

EAA Board 2013-2016

President: *Michael Taroudakis*

Vice President: *Jean Kergomard*

Vice President: *Mats Åbom*

General Secretary: *Tapio Lokki*

Treasurer: *J. Salvador Santiago*

EAA Office

Antonio Perez-Lopez

c/o: Spanish Acoustical Society (SEA)

Serrano 144, ES-28006 Madrid, Spain

office@european-acoustics.net

Technical Committees

EAA has 7 technical committees which, at different level, are in charge of organizing specific activities (technical reports, round robin tests, structured session organization at congresses, symposia, etc.). They are open to all individual members of EAA member societies and are coordinated by a Chairman:

- CA, Computational Acoustics • HYD, Hydroacoustics • MUS, Musical Acoustics • NOI, Noise • PPA, Psychological and Physiological Acoustics • RBA, Room and Building Acoustics • ULT, Ultrasound

EAA is an Affiliate Member of the International Commission for Acoustics (ICA)



and Member of the Initiative of Science in Europe (ISE)



EAA Products

ACTA ACUSTICA united with ACUSTICA

Product Manager and Editor in chief: *Jean Kergomard*

Acta Acustica united with Acustica is an international, peer-reviewed journal on acoustics. It is the journal of the

EAA. It is published by S. Hirzel Verlag • Stuttgart.
See www.acta-acustica-united-with-acustica.com for more information.

EAA members receive Acta Acustica united with Acustica online as part of their membership.

NUNTIUS ACUSTICUS-EAA NEWSLETTER

Product Manager: *Kristian Jambrošić*

Nuntius Acusticus is the “acoustic messenger” of EAA to vitalize communication between and in the European acoustical societies on a variety of topics. It is published monthly in electronic format and distributed via e-mail to all EAA members.

DOCUMENTA ACUSTICA

Product Manager: *Sergio Luzzi*

Documenta Acustica is the literature distribution system of the EAA. It distributes conference and symposia proceedings as well as books, reports and theses.

FENESTRA

Product Manager: *Olivier Dazel*

Fenestra Acustica is the website of EAA. Fenestra provides information on the association and its members (products, technical committees, organisational structure and policies, contact information), up-to-date news, upcoming events, links to other no-profit organisations in acoustics, a job market and much more.

SCHOLA

Product manager: *Malte Kob*

Schola is an online platform for education in acoustics in Europe: <https://www.euracoustics.org/activities/schola>. Through Fenestra, it offers information on university acoustics courses in Europe at different levels (Bachelor, Master, Ph.D.).

ACOUSTICS IN PRACTICE

Product manager: *Colin English*

This new technical journal will be written by practitioners for practitioners and other professions: a new link between all members of all EAA societies. The journal will be published four times a year in electronic form only.

YOUNG ACOUSTICIANS NETWORK

Contact person: *Xavier Valero*

This network is a non-profit initiative within the European Acoustics Association (EAA) with the primary goal is to

establish a community for young researchers and young professionals in the field of Acoustics; to connect them and to provide support. It organises events at conferences and provide services that contribute to the community, such as a monthly newsletter and many communication channels to enable networking.

FORUM ACUSTICUM

Forum Acusticum is the triennial international convention organised by a national acoustical society on behalf of EAA. It is, in effect, a forum comprising a variety of different activities: high-quality scientific congress with invited plenary lectures, structured sessions, invited and contributed papers, an exhibition that includes commercial firms, laboratories and agencies, social meetings of acousticians with receptions, visits and awards.

EURONOISE

Euronoise is the European Conference and Exhibition on Noise Control, coordinated by the EAA Technical Committee Noise and organised by a national acoustical society on behalf of EAA.

EUROREGIO

Euroregio is an expression of EAA support for traditional regional events organized by groups of countries. Where and when appropriate, the regional events can be extended towards a full European and international scale.

EAA SYMPOSIA

EAA symposia are scientific meetings under the aegis of the EAA with a focus on specialised fields. They are typically organized by one or more member societies of EAA in conjunction with the Technical Committee of EAA.

YOUNG RESEARCHER AND STUDENT PROGRAM

EAA supports with grants and best paper and presentation awards the active participation of students and young researchers at EAA major events (Forum Acusticum, Euronoise, Euroregio).

EAA SUMMER AND WINTER SCHOOLS

The EAA Summer and Winter Schools are conceptualized as events where Master and PhD students of acoustics, as well as other young acousticians, can learn about a variety of new accomplishments in the field of acoustics in half day or full day courses.



European Acoustics Association (EAA)
secretary@european-acoustics.net
office@european-acoustics.net

www.euracoustics.org